A UNITED STATES DEPARTMENT OF COMMERCE PUBLICATION

OF MICHIGAN
DEC 28 1971
ENGINEERING

SECTION C

# JOURNAL OF RESEARCH

## of the NATIONAL BUREAU OF STANDARDS

U.S. National Bureau of Standards

Volume 75C, Number 2 April-June 1971

# Engineering and Instrumentation

U.S. DEPARTMENT OF COMMERCE
National Bureau of Standards

# Journal of Research

of the

National Bureau of Standards

C. Engineering and Instrumentation

April-June • 1971

VOLUME • 75C

NUMBER • 2

Editor: Martin Greenspan

Associate Editors: G. F. Montgomery, R. V. Smith, A. F. Schmidt

Publication dates: Feb. 15, May 15, Aug. 15, Nov. 15, 1971

J. Res. Nat. Bur. Stand. (U.S.), C
CODEN: JNBCA 75C (2) 69-143 (1971)


JOURNAL OF RESEARCH

The National Bureau of Standards Journal of Research reports research and development in the field of activity shown at right. Also included from time to time are survey articles on topics closely related to the Bureau's scientific and technical program.

The Journal is published in three separate sections as follows:

A. Physics and Chemistry

Contains papers of interest primarily to scientists working in these fields. Issued six times a year. Annual subscription: domestic, $9.50; foreign, $11.75. Single copy, varies.

B. Mathematical Sciences

Presents studies and compilations designed mainly for the mathematician and the theoretical physicist. Issued quarterly. Annual subscription: domestic, $5.00; foreign, $6.25. Single copy, $1.25.

C. Engineering and Instrumentation

Reports research and development results of interest chiefly to the engineer and the applied scientist. Issued quarterly. Annual subscription: domestic, $5.00; foreign, $6.25. Single copy, $1.25.

The National Bureau of Standards[1] was established by an act of Congress March 3, 1901. The Bureau's overall goal is to strengthen and advance the Nation's science and technology and facilitate their effective application for public benefit. To this end, the Bureau conducts research and provides: (1) a basis for the Nation's physical measurement system, (2) scientific and technological services for industry and government, (3) a technical basis for equity in trade, and (4) technical services to promote public safety. The Bureau consists of the Institute for Basic Standards, the Institute for Materials Research, the Institute for Applied Technology, the Center for Computer Sciences and Technology, and the Office for Information Programs.

**THE INSTITUTE FOR BASIC STANDARDS** provides the central basis within the United States of a complete and consistent system of physical measurement; coordinates that system with measurement systems of other nations; and furnishes essential services leading to accurate and uniform physical measurements throughout the Nation's scientific community, industry, and commerce. The Institute consists of a Center for Radiation Research, an Office of Measurement Services and the following divisions:

Applied Mathematics—Electricity—Heat—Mechanics—Optical Physics—Linac Radiation[2]—Nuclear Radiation[2]—Applied Radiation[2]—Quantum Electronics[3]—Electromagnetics[3]—Time and Frequency[3]—Laboratory Astrophysics[3]—Cryogenics[3].

**THE INSTITUTE FOR MATERIALS RESEARCH** conducts materials research leading to improved methods of measurement, standards, and data on the properties of well-characterized materials needed by industry, commerce, educational institutions, and Government; provides advisory and research services to other Government agencies; and develops, produces, and distributes standard reference materials. The Institute consists of the Office of Standard Reference Materials and the following divisions:

Analytical Chemistry—Polymers—Metallurgy—Inorganic Materials—Reactor Radiation—Physical Chemistry.

**THE INSTITUTE FOR APPLIED TECHNOLOGY** provides technical services to promote the use of available technology and to facilitate technological innovation in industry and Government; cooperates with public and private organizations leading to the development of technological standards (including mandatory safety standards), codes and methods of test; and provides technical advice and services to Government agencies upon request. The Institute also monitors NBS engineering standards activities and provides liaison between NBS and national and international engineering standards bodies. The Institute consists of the following technical divisions and offices:

Engineering Standards Services—Weights and Measures—Flammable Fabrics—Invention and Innovation—Vehicle Systems Research—Product Evaluation Technology—Building Research—Electronic Technology—Technical Analysis—Measurement Engineering.

**THE CENTER FOR COMPUTER SCIENCES AND TECHNOLOGY** conducts research and provides technical services designed to aid Government agencies in improving cost effectiveness in the conduct of their programs through the selection, acquisition, and effective utilization of automatic data processing equipment; and serves as the principal focus within the executive branch for the development of Federal standards for automatic data processing equipment, techniques, and computer languages. The Center consists of the following offices and divisions:

Information Processing Standards—Computer Information—Computer Services—Systems Development—Information Processing Technology.

**THE OFFICE FOR INFORMATION PROGRAMS** promotes optimum dissemination and accessibility of scientific information generated within NBS and other agencies of the Federal Government; promotes the development of the National Standard Reference Data System and a system of information analysis centers dealing with the broader aspects of the National Measurement System; provides appropriate services to ensure that the NBS staff has optimum accessibility to the scientific information of the world, and directs the public information activities of the Bureau. The Office consists of the following organizational units:

Office of Standard Reference Data—Office of Technical Information and Publications—Library—Office of Public Information—Office of International Relations.

---

[1] Headquarters and Laboratories at Gaithersburg, Maryland, unless otherwise noted; mailing address Washington, D.C. 20234.
[2] Part of the Center for Radiation Research.
[3] Located at Boulder, Colorado 80302.


U.S. DEPARTMENT OF COMMERCE
Maurice H. Stans, Secretary
NATIONAL BUREAU OF STANDARDS
Lewis M. Branscomb, Director

Order all publications from the Superintendent of Documents
U.S. Government Printing Office, Washington, D.C. 20402.

Use of funds for printing this publication approved by the Director of the Bureau of the Budget (June 22, 1966).

JOURNAL OF RESEARCH of the National Bureau of Standards—C. Engineering and Instrumentation
Vol. 75C, No. 2, April-June 1971

# Heated Air Adiabatic Saturation Psychrometer

**Lewis Greenspan**

**Institute for Basic Standards, National Bureau of Standards, Washington, D.C. 20234**

(December 29, 1970)

A portable self-contained heated-air adiabatic saturation psychrometer intended as a field and laboratory instrument has been developed and constructed. The instrument measures the humidity of air in the range from 0 to 50 grams of water vapor per kilogram of dry air over an ambient temperature range of −5 to 40 °C. It samples a test gas at the rate of 4 liters per minute.

The psychrometer was compared with the NBS pressure humidity generator over the mixing ratio range of 2.5 to 19 grams of water per kilogram of dry air (equivalent to a dew-point range of −5.4 to 24 °C at atmospheric pressure). The mixing ratio indicated by the psychrometer was higher than that produced by the generator by 0.025 g/kg + 0.24 percent of the reading with a standard deviation of 0.024 g/kg; that is, it was higher by 1.24 percent to 0.37 percent of the reading as the measured mixing ratio increased from 2.5 to 19 g/kg. In equivalent terms of dew point, the psychrometer reading was higher by 0.16 deg C to 0.06 deg C as the measured dew point increased from −5.4 to 24.0 °C. The results are approximately those which would be expected based on an analysis of estimated errors in individual measurements.

Key words: Adiabatic saturation; dew point temperature; humidity; hygrometer; mixing ratio; moist gas; psychrometer; vapor pressure.

## 1. Introduction

Although the psychrometer is one of the oldest and most common instruments used to measure the humidity of air, no theory adequately predicts its performance. Empirical and semiempirical formulas exist which describe, under limited conditions, the performance of psychrometers of particular dimensions and configurations.

In 1967, we developed and constructed a laboratory model of an adiabatic saturation psychrometer [1][1] the performance of which is specified by means of an equation. This instrument differed from other psychrometers in that it was designed to utilize a steady-flow adiabatic isobaric saturation process, whereas other psychrometers, even under steady-state conditions, are an open system undergoing a nonequilibrium process which cannot be described completely by classical thermodynamics. It was tested with various fluids and gases under conditions of zero vapor content. Because the results agreed with an equation derived from classical thermodynamics to within the limits of the experimental uncertainties associated with the conducted tests, it was concluded that the equation did indeed predict the behavior of this adiabatic saturation psychrometer. This was particularly significant in the tests with vapor-gas systems other than water-air where other psychrometers give results which differ markedly from those derived from the postulates of classical thermodynamics.

The adiabatic saturation psychrometer has been developed further into a portable and self-contained instrument, intended for both laboratory and field use. In order to permit its employment at low ambient dry-bulb temperatures of meteorological interest without freezing of the wet-bulb water supply and wicking, provision was made for heating the test air to a fixed elevated temperature.

It appeared to us that the heated-air adiabatic saturation psychrometer could be used to investigate more fully the validity of our earlier conclusion that the instrument performed in accordance with the derived equation. It had been suggested that because the original tests had been made only under conditions of zero vapor content, the equation had been validated only under this unique condition and that the use of the relationship at other humidities could not be accepted with complete certainty.

We believed that the condition of zero vapor content was a unique condition only in that it represented the most severe condition under which to test the behavior of a psychrometer, and that the instrument would behave in accordance with the derived equation at all vapor contents. The availability in our laboratory of a highly accurate humidity generator [2] made it feasible for us to perform an extensive series of tests over a wide range of humidities.

The general design and operational features, as well as the test results, of the heated-air adiabatic saturation psychrometer are the subjects of this paper.

## 2. Theory

When a quantity of liquid or solid water at pressure $P$ and temperature $T_w$ is evaporated into a vapor-gas mixture at pressure $P$, temperature $T$ and mixing ratio $r$ to bring the gas adiabatically to saturation at pressure $P$, temperature $T_w$ and mixing ratio $r_w$, the sum of the enthalpies of the various phases are conserved. Thus the

[1] Figures in brackets indicate the literature references at the end of this paper.

initial and final enthalpies are equal, leading to the following equation:

$$h(P,T,r) + (r_w - r)\, h'_w\,(P,T_w) = h\,(P,T_w,r_w) \quad (1)$$

where

$h(P,T,r)$ = the enthalpy per gram of dry (vapor-free) gas of the initial vapor-gas mixture at pressure $P$, temperature $T$ and mixing ratio $r$;

$h(P,T_w,r_w)$ = the enthalpy per gram of dry gas of the final vapor-gas mixture at pressure $P$, temperature $T_w$ and mixing ratio $r_w$;

$h'_w\ (P,T_w)$ = the enthalpy per gram of liquid or solid water at pressure $P$ and temperature $T_w$.

$r$ = the mixing ratio of the initial vapor-gas mixture in grams of vapor per gram of associated dry gas.

$r_w$ = the saturation mixing ratio of the final vapor gas mixture in grams of vapor per gram of associated dry gas.

Since $r_w$ is a function of only $T_w$ and $P$, $r$ may be determined by means of (1) from a knowledge of $P$, $T$, $T_w$ and other available data for the gas, vapor and liquid or solid involved.

We have built an instrument which approaches a steady-state adiabatic saturation flow process and, to which eq (1) may be applied. It consists of a well insulated enclosure where a gas is saturated and liquid at exit temperature, sufficient for evaporation, is provided, as well as means for measuring entrance and exit temperatures and pressure. In accordance with the terminology usually used in psychrometry, the entrance and exit temperature also will be called the dry-bulb and wet-bulb temperatures in this paper. In a conventional psychrometer, the wet-bulb temperature is the temperature of a wetted thermometer whereas in this psychrometer, the wet-bulb temperature is the temperature of the exit gas.

Equation (1) describes an ideal system which the instrument is not. Among the deviations from ideality are the following: (1) The instrument is not isobaric but has a pressure drop of the order of ½ percent of the total pressure; (2) The velocity of gas changes in the instrument due to its change in pressure and temperature as well as changes in cross-sectional area and the addition of vapor to the gas; (3) The enclosure is not a perfect adiabatic enclosure; (4) The liquid may not enter the instrument at precisely the gas exit temperature; (5) The gas may not be precisely saturated at exit. No attempt was made to evaluate these various effects individually in this instrument. An analysis of the overall performance of the instrument was utilized to determine the overall effect of these deviations from ideality. In addition, equation (1) refers only to an equilibrium condition and is not applicable when inlet temperature or humidity are changing or shortly after a change.

The instrument is modified in one important respect: the entrance gas is heated. This does not affect eq (1) since the entrance temperature is measured subsequent to the heating and it is this elevated temperature which enters into the computations. The range of the instrument is increased by this heating since it ensures exit temperatures above freezing regardless of the conditions of temperature and humidity of the test gas prior to heating.

## 3. Description

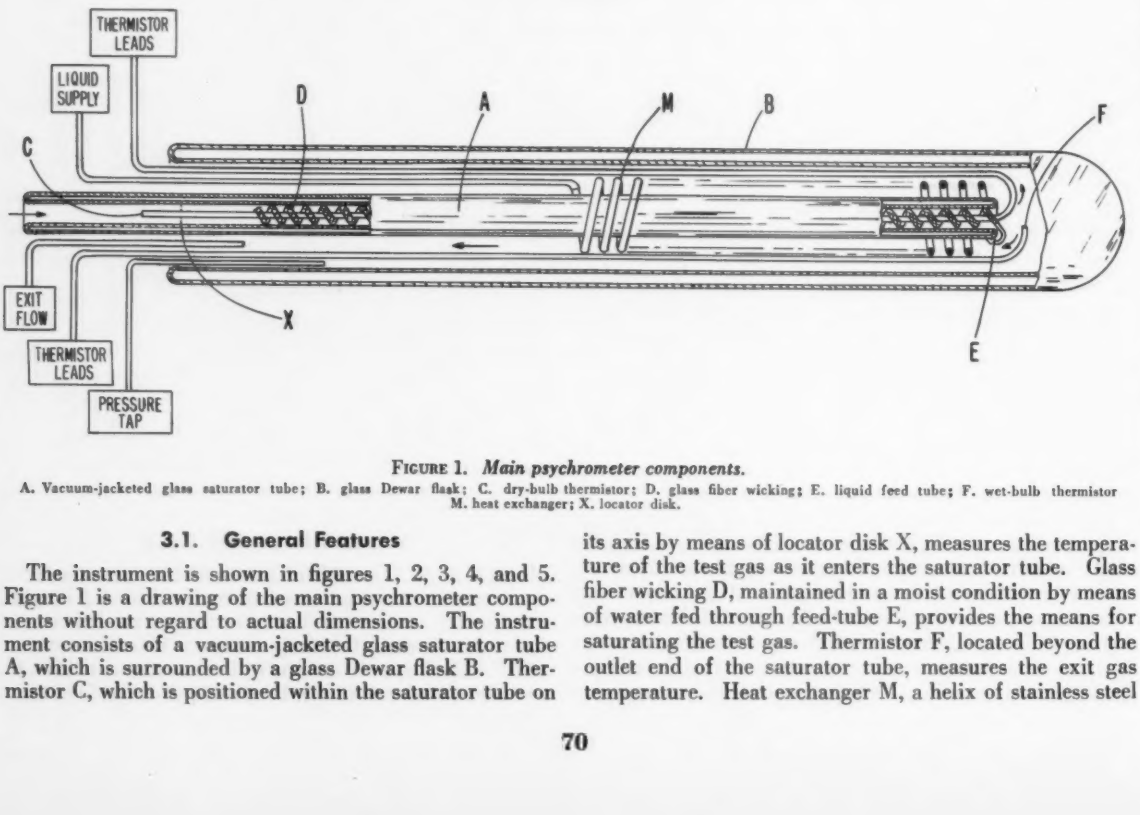


FIGURE 1. *Main psychrometer components.*

A. Vacuum-jacketed glass saturator tube; B. glass Dewar flask; C. dry-bulb thermistor; D. glass fiber wicking; E. liquid feed tube; F. wet-bulb thermistor M. heat exchanger; X. locator disk.

### 3.1. General Features

The instrument is shown in figures 1, 2, 3, 4, and 5. Figure 1 is a drawing of the main psychrometer components without regard to actual dimensions. The instrument consists of a vacuum-jacketed glass saturator tube A, which is surrounded by a glass Dewar flask B. Thermistor C, which is positioned within the saturator tube on its axis by means of locator disk X, measures the temperature of the test gas as it enters the saturator tube. Glass fiber wicking D, maintained in a moist condition by means of water fed through feed-tube E, provides the means for saturating the test gas. Thermistor F, located beyond the outlet end of the saturator tube, measures the exit gas temperature. Heat exchanger M, a helix of stainless steel

capillary tubing surrounding the saturator tube, controls the temperature of the water moistening the wicking D. Exiting from the Dewar flask are the thermistor leads, a pressure tap, a plastic water-fed tube (through which water enters from a liquid supply) and a gas-flow exit tube.

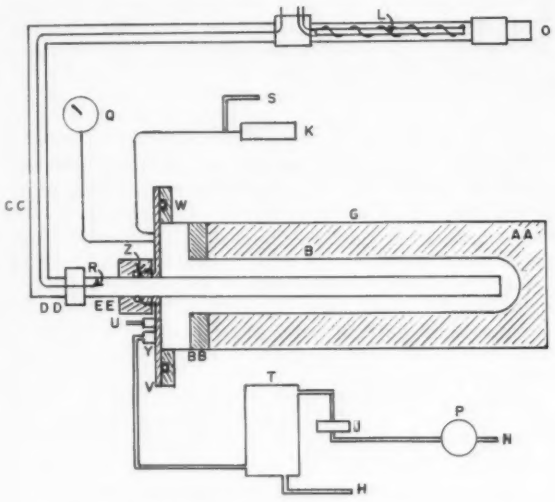


FIGURE 2. *Schematic diagram of auxiliary components.*

B. Glass Dewar flask; G. brass cylinder; H. trap drain; J. critical nozzle flow controller; K. syringe pump; L. nickel-chrome heater coil; N. flow exit; O. flow entrance; P. vacuum pump; Q. differential pressure gage; R. control thermistor; S. liquid filler tube; T. liquid trap; U. thermistor leads; V. cylinder cap; W. "O" ring; Y. compression seal; Z. "O" ring; AA. polystyrene foam packing; BB. rubber stopper; CC. insulated polytetrafluoroethylene tubing; DD. saturator tube connector; EE. cap seal assembly; FF. pressure signal tubing; HH. polytetrafluoroethylene liquid flow tubing.

Figure 2 is a schematic representation of all hydraulic and pneumatic components not shown in figure 1. A brass cylinder G surrounds the Dewar flask B shown in figure 1. Flask B is held rigidly in place on the axis of G by means of polystyrene foam packing, AA. Cap V is sealed to saturator tube A by means of "O" ring Z within assembly EE, and to cylinder G by means of "O" ring W. In addition to providing the means for sealing, cap V supports and locates saturator tube A coaxially within Dewar flask B. Insulated polytetrafluoroethylene tubing CC connects to the saturator tube. The thermistor leads, pressure tap, plastic water-feed tube and gas flow exit tube pass through compression seals in cap V. Test gas enters the instrument at O, is heated by the nickel-chrome heater coil L, flows through tubing CC and enters the saturator tube. After passing over the moist wicking it leaves the psychrometric section at Y and passes through trap T, where entrained water is separated from the gas stream. The trap is drained through tube H. The gas then passes through the critical nozzle flow controller J and on through vacuum pump P, and exits at N. Differential pressure gage Q measures the pressure difference between flask B and atmospheric pressure. Syringe pump K forces liquid into the instrument at a constant rate of flow. The syringe is refilled through tube S. The temperature of the air entering the saturator tube is sensed by thermistor R, which in conjunction with a proportional heat controller (not shown) controls the voltage supplied to heater L, thereby regulating the temperature of the air entering the saturator tube to 41¾ °C. ± ¾ °C.

Figure 3 is a circuit diagram of the two Wheatstone bridges, power supply and galvanometer circuit. The Wheatstone bridges and galvanometer measure the entrance (dry-bulb) and exit (wet-bulb) thermistor resistances. In addition, there are two temperature control circuits (not shown) operating from mechanical thermostats. One of the temperature control circuits regulates the air temperature surrounding the Wheatstone bridge and the other prevents the section of the instrument which contains water from falling to freezing temperature.

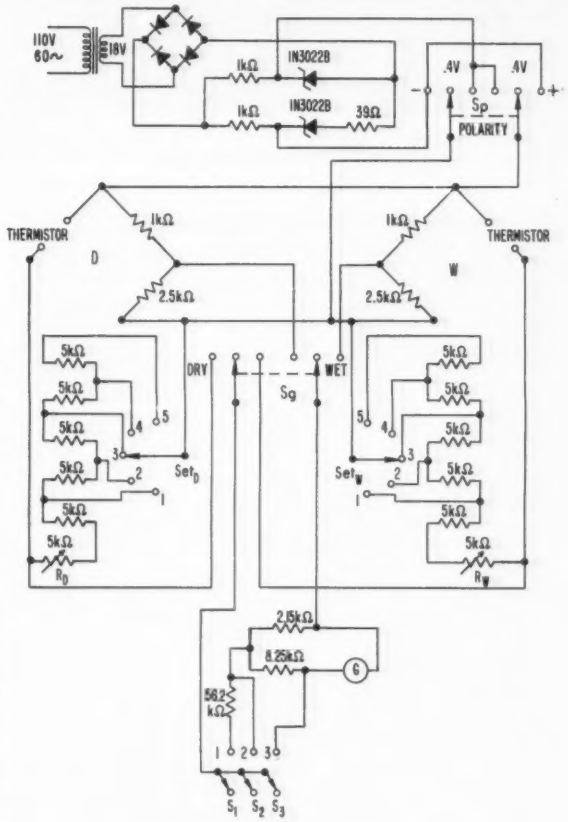


FIGURE 3. *Temperature measurement circuit.*

D. Dry-bulb temperature bridge; W. wet-bulb temperature bridge; G. galvanometer; $R_D$. dry-bulb heliopot; $R_W$. wet-bulb heliopot; $Set_D$. dry-bulb step switch; $Set_W$. wet-bulb step switch; $S_P$. polarity reversing switch; $S_G$. wet-bulb or dry-bulb selector switch; $S_1$. low sensitivity galvometer switch; $S_2$. medium sensitivity galvanometer switch; $S_3$. high sensitivity galvanometer switch.

Figure 4 is a top view photograph of the instrument assembled and ready for operation. The instrument is 23-in long, 16-in wide and 13-in high, and weighs 77½ pounds.

Figure 5 is a photograph of the section where the water is drained and the syringe refilled, taken with the side panel removed and lying in front of the instrument.

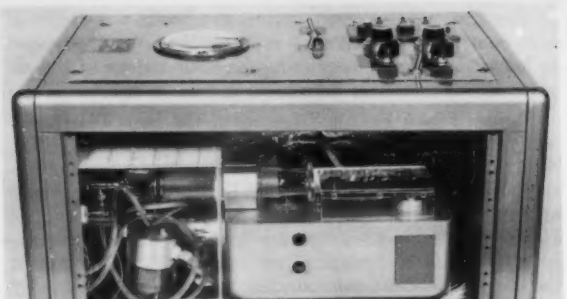

FIGURE 4. *Psychrometer top view.*

FIGURE 5. *Psychrometer side view.*

### 3.2. Saturator Assembly

The saturator tube is a straight double-walled glass tube, 18-in long, with an i.d. of ¼ in and an o.d. of ⅝ in. The space between the walls is evacuated and the glass surface within this space is silvered.

The saturating element is a helix with a fiber glass surface. It was made by covering 7 ft of polytetrafluoroethylene tubing, having an i.d. of about 0.022 in and an o.d. from 0.042–0.050 in, with number 22-gage fiber glass spaghetti. The fiber glass spaghetti extends beyond the upstream end of the polytetrafluoroethylene tubing and is tied off with linen thread. The tubing was wound into a helix of ¼-in o.d. and placed in boiling water for 1 hr. This had the effect of cleaning the fiber glass spaghetti and setting the polytetrafluoroethylene into a quasi-permanent helical shape.

### 3.3 Water Heat-Exchanger

Eight feet of stainless steel tubing with an o.d. of 0.0355 in and an i.d. of 0.023 in, wound into a ¾-in helix, serves as the water heat-exchanger. This exchanger surrounds the saturator tube and is joined at one end to the polytetrafluoroethylene tubing of the saturating element and at the other end to a polytetrafluoroethylene tube which is fed through a pressure seal in cap V to the water-feed pump. At the normally used water flow-rate of 10 $cm^3/h$, there is a 4 min supply of water within the heat exchanger.

The heat exchanger is surrounded by a Dewar flask with an i.d. of ⅞ in. and a straight section of 14 in. This flask reduces heat losses from the region around the heat exchanger.

### 3.4. Outer Case

In order to protect the glass elements and to seal the saturator tube so that the test gas flows as desired, a brass cylinder 17 in long, with an o.d. of 3 in and a wall thickness of ⅛ in, closed at one end, surrounds the Dewar flask. The space between the flask and the brass cylinder is filled with foamed polystyrene and a rubber stopper, permanently positioning the flask within the cylinder along its axis. At the open end of the cylinder is a flange which mates with cap V and seals to the cap by means of a 3-in i.d. "O" ring. The cap is held to the cylinder with screws.

The cap has four openings within it. At its center is an opening through which the saturator tube protrudes. By means of an "O" ring seal, the cap is sealed to the outer surface of the saturator tube and positions this tube within the Dewar flask.

Two of the other openings in the cap are polytetrafluoroethylene packing-gland compression seals. One of the seals holds the pressure tap and water-feed tube, and the other serves as a pass-through for the two thermistor leads. The remaining opening in the cap serves as a flow exit for the test gas.

### 3.5. Air Heater

The test gas heater L is formed by winding 25 ft of bare nickel-chrome wire on a 1-ft long, ¼-in diam, polytetrafluoroethylene rod. The rod has a few longitudinal grooves for the lead wire and to expose more of the wire to the air flow. The heater is contained within a ⅜-in polytetrafluoroethylene tube which is surrounded with rubber foam insulation. The small diameter bare wire has a low thermal lag.

### 3.6. Temperature Regulator

The inlet test gas temperature is controlled by a proportional electronic temperature controller. The sensor R which activates the controller is placed in the test gas flow stream just at the inlet to the saturator tube.

### 3.7. Temperature Measuring Circuit

The temperature measuring circuit is shown in figure 3. It consists of two separate Wheatstone bridges D and W, each connected to a thermistor encased in polyethylene tubing. One of the thermistors is held in place at the entrance end of the saturator tube by means of a polytetrafluoroethylene disk containing many holes, while the other thermistor is secured along the axis at the exit of the saturator tube by means of a small diameter wire. The bridge circuit is powered by 0.4 V from the power supply and the voltage is continuously supplied to each bridge circuit, including thermistor, whenever the psychrometer is in operation, in order to maintain constant self-heating of thermistors. A selector switch Sg allows the reflecting galvanometer G to be connected to either of the bridge circuits as desired. A switch Sp provides for a reversal of voltage polarity to the bridges in order to obtain an electrical zero in the balancing of the bridges. The polarity switch also removes the voltage from the bridge circuits whenever it is placed in its center position. There are three buttons, S1, S2, S3, which connect the galvanometer into the circuit, each having resistance circuits which provide for three different galvanometer sensitivities. The power supply is supplied with 18 V from a transformer.

The bridge circuits, power supply and galvanometer are contained in a separate enclosure within the instrument cabinet which is temperature regulated. Temperature in the enclosure is maintained by means of a 44-W heater and a miniature thermoswitch preset to 40 °C. A miniature blower within the enclosure operates continuously, and a panel light on the top of the psychrometer indicates whenever the heater is on.

### 3.8. Flow System

Flow is drawn through the psychrometer by means of a moisture-resistant vacuum pump, P. Upstream of the vacuum pump is a nozzle assembly J which limits the flow to approximately four ambient liters per/minute. Upstream of the nozzle assembly is a water trap T which separates liquid from the exit gas. The level of liquid in the trap is determined visually, and the trap is drained by means of a plastic tube H connected to the trap.

### 3.9. Water-Feed System

When operating, water is pumped into the psychrometer at the rate of 10 $cm^3$ per hour by means of a syringe pump K. A motor drives the plunger of a 100 $cm^3$ glass syringe. An "O" ring fits into a groove on the piston to provide a leak-free seal in the syringe. Connected to the syringe is a two-way automatic valve which allows for filling of the syringe without disconnecting it or disassembly. A plastic filler tube S remain connected to the two-way valve at one tap. Attached to the other tap of the two-way valve is a hypodermic needle to which, in turn, is connected the tubing HH that goes through the pressure seal in the cap V of the brass case G to the heat exchanger M in Dewar flask B.

In the region around the syringe K and liquid trap T are located three 15-W miniature light bulbs connected in parallel. These are connected, in turn, through an adjustable liquid-bellows type thermoswitch, directly to the power cord to the instrument, and constitute the freeze-protection circuit.

### 3.10. Pressure Measurements

A plastic tube connects the pressure tap in the psychrometer to a differential pressure gage Q, having a range of 0 to 20-in of water. The gage is mounted at the top of the instrument. The gage pressure, when subtracted from the ambient pressure (independently determined), gives the pressure $P$ in the psychrometer. If the pressure of the test gas is not at atmospheric pressure but is known, another plastic tube can be connected to the reference port of the differential pressure gage Q and connected to the test gas source. The psychrometer pressure $P$ is then the source pressure less the gage pressure.

### 3.11. Thermistor Calibration

It was desirable to have an equation for temperature in terms of bridge switch positions and potentiometer readings. Since the resistance of the thermistors is an exponential function of temperature, a least squares fit to an equation of the following form was made:

$$T = A + B \ln x + C (\ln x)^2 \text{ °C} \qquad (2)$$

where

$x = 0.9847\ \text{Set}_D + 0.001\ R_D$ for the inlet thermistor

and

$x = 0.9846\ \text{Set}_W + 0.001\ R_W$ for the outlet thermistor.

$\text{Set}_D$ and $\text{Set}_W$ are indicated switch positions from 1 to 5 and represent nominal bridge resistances of 5,000 Ω per unit. $R_D$ and $R_W$ are helipot readings from 0 to 1,000 and represent nominal bridge resistances of 5 Ω per unit. The values 0.9847 and 0.9846 are the ratios of the mean of the step resistances to the maximum variable resistance in the corresponding bridge. The bridge has a ratio of 2.5 to 1 and therefore the resistance of the thermistors is approximately 2,000 $x$. The thermistors were simultaneously calibrated at 34 different temperatures against a calibrated platinum resistance thermometer. Two of the calibration points were eliminated from both calibrations and one other from the outlet thermistor calibration for statistical reasons. Fits were then obtained as follows:

$$T_D = 67.09652 - 32.43244 \ln x + 2.109868 (\ln x)^2 \text{ °C} \qquad (3)$$

$$T_W = 61.16210 - 32.65236 \ln x + 2.230575 (\ln x)^2 \text{ °C}. \qquad (4)$$

The residual standard deviation for $T_D$ was 0.01 °C and for $T_W$ it was 0.007 °C.

## 4. Calibration

The psychrometer was operated with a continuous sample of humid air supplied by the NBS pressure humidity generator [3] over a range of mixing ratios from 2.5 to 19 grams of water vapor per kilogram of dry air. The mixing ratio, $r$, obtained by measurements with the psychrometer was calculated by computer on the basis of eq (1). Expressions for the enthalpies of moist air in terms of IT calories per gram of dry air were obtained from the equation given on page 334 of the Smithsonian Meteorological Tables [4] which when inserted into equation (1) yielded the following equation:

$$r = \frac{-0.2405095\,\Delta T + 0.4408952\,r_w\,(T_w + 1354.74) - 0.0049 - r_w\,h'_w}{0.4408952\,(T_w + 1354.74) - h'_w} \qquad (5)$$

where

$h'_w = h'_w\,(P, T_w)$ at atmospheric pressure and was obtained by interpolation from a table given by Goff [5] in terms of BTU/lb. These values were divided by 1.8 to obtain IT calories per gram.

$$r_w = \frac{0.62198\,f_w\,e_w}{P - f_w\,e_w} \text{ grams/gram [6]}$$

$$f_w = \exp\left[\alpha\,(T_w) \times \left(1 - \frac{e_w}{p}\right) + \beta\,(T_w) \times \left(\frac{p}{e_w} - 1\right)\right]$$

dimensionless quantity [5]

$\alpha\,(T_w)$ = dimensionless coefficient obtained for values of $T_w$ by interpolation from a table given by Goff [5].

$\beta\,(T_w)$ = dimensionless coefficient obtained for values of $T_w$ by interpolation from a table given by Goff [5].

$P$ = Total pressure at the psychrometer outlet in atmospheres.

$e_w$ = saturation vapor pressure in atmospheres, obtained by solving equation given by Goff [5].

$\Delta T = T_D - T_W$ °C.

The results of the calibration are given in table 1 and indicate that there is a mean difference in mixing ratio $r$ of + 0.047 g/kg between the generator and this instrument. The largest difference measured is 0.119 g/kg.

The results are also given in terms of the partial pressure of vapor and dew-point that would exist in air of the same mixing ratio at ambient pressure [4].

It was found that the differences were well represented by a linear relationship with respect to the instrument indications, but that points 4, 6, and 40 deviated from this curve by an amount greater than that which should be expected in 52 measurements (standardized residual[2] greater than 2.34). We therefore, eliminated points 4, 6, and 40 on the basis that they were not statistically representative of the calibration and refitted the remaining 49 points to a linear equation, which we shall consider an error curve: Error = 0.025 + 0.24 percent of indication in grams of water per kilogram of dry air.

[2] The standardized residual is the deviation of the point from the fitted curve divided by its own standard deviation.

The estimate of the standard deviation of this error is 0.024 g/kg.

## 5. Error Analysis

As was mentioned above, one of the purposes of the calibration of this instrument was to determine whether this instrument performed as an adiabatic saturation instrument. We propose to accomplish this by comparing the differences between the pressure humidity generator and this instrument with the uncertainties associated with these two instruments. Whereas assignment of random uncertainties can often be done with reasonable accuracy by statistical analysis, assignments of systematic uncertainties are usually more subjective and arbitrary. The most we can hope to come up with are reasonable estimates of these systematic uncertainties.

We estimate the maximum systematic uncertainty in our ambient pressure measurement to be 0.1 mm Hg and the maximum systematic uncertainty in our pressure difference measurements to be 0.2 in of water. For our temperature measurements we have taken three residual standard deviations of our fitted curve and have added to these 0.002 °C, our estimate of the systematic uncertainty in our resistance thermometer temperature measurement. This amounts to 0.031 °C for our entrance temperature measurement and 0.023 °C for our exit temperature measurement. Our final estimate of systematic uncertainty is for our pressure humidity generator [3] which we estimate to be 0.05 percent of indication.

We have likewise assigned random uncertainties to the same parameters as follows: 0.05 mm Hg. in ambient pressure, 0.2 in of water in pressure difference, 0.010 °C in inlet temperature, 0.007 °C in outlet temperature and 0.1 percent of indication for the pressure humidity generator. The random uncertainties assigned to the temperatures are the estimates of one residual standard deviation for the temperature equation used.

In order to determine the maximum total systematic uncertainty to be expected from the psychrometer at each calibration point, we reevaluated eq (5) for each of the calibration points with each parameter changed by the amount of the systematic uncertainty for that parameter and assigned signs to these uncertainties such that they would maximize the difference. In order to determine the random uncertainty of the instrument, we changed one parameter at a time by an amount equal to the estimate of the random uncertainty in that parameter and calculated the difference in mixing ratio this would cause by means of eq (5). We applied the propagation of error formula [8] at each calibration point to obtain an estimate of the one sigma random uncertainty. For the pressure humidity generator, we applied the pertinent estimated percentage uncertainties to the indicated value of mixing ratio. We added the two estimated systematic uncertainties together to obtain an overall estimate of the predicted maximum systematic difference between the two instruments and the root mean square of the two random uncertainties was used as the estimate of the predicted one sigma random difference to be expected. Table 2 gives these values along with the measured mixing ratio and the measured difference.

As was mentioned in the calibration section, the mea-

TABLE 1. *Calibration results*

| No. | Ambient pressure mb Pa | Generated | | | Difference (Measured-Generated) | | |
|---|---|---|---|---|---|---|---|
| | | Mixing ratio g/kg *r* | Partial pressure vapor mb[a] *e* | Dew point °C[b] | Mixing ratio g/kg | Partial pressure vapor mb | Dew point °C |
| 1. | 995.86 | 2.566 | 4.092 | −5.447 | 0.044 | 0.070 | 0.224 |
| 2. | 995.66 | 2.835 | 4.518 | −4.135 | .056 | .089 | .260 |
| 3. | 995.78 | 3.153 | 5.022 | −2.721 | .043 | .068 | .183 |
| 4. | 995.78 | 3.538 | 5.632 | −1.168 | −.042 | −.066 | −.160 |
| 5. | 995.72 | 4.437 | 7.053 | 1.938 | .048 | .076 | .149 |
| 6. | 995.91 | 4.006 | 6.373 | 0.528 | −.064 | −.101 | −.221 |
| 7. | 996.12 | 4.806 | 7.638 | 3.058 | .034 | .054 | .099 |
| 8. | 996.27 | 5.984 | 9.494 | 6.166 | .036 | .056 | .086 |
| 9. | 1,006.83 | 5.960 | 9.556 | 6.260 | .035 | .055 | .084 |
| 10. | 1,006.65 | 5.243 | 8.415 | 4.432 | .030 | .048 | .081 |
| 11. | 1,006.46 | 6.401 | 10.252 | 8.282 | .003 | .005 | .007 |
| 12. | 1,006.14 | 7.769 | 12.412 | 10.106 | .027 | .043 | .052 |
| 13. | 1,005.92 | 9.211 | 14.679 | 12.637 | .046 | .073 | .075 |
| 14. | 1,005.87 | 10.700 | 17.011 | 14.904 | .034 | .053 | .048 |
| 15. | 1,005.69 | 12.200 | 19.347 | 16.916 | .036 | .056 | .045 |
| 16. | 1,005.42 | 14.100 | 22.287 | 19.164 | .046 | .071 | .052 |
| 17. | 1,005.10 | 15.760 | 24.838 | 20.914 | .057 | .088 | .057 |
| 18. | 1,004.80 | 17.260 | 27.130 | 22.357 | .068 | .104 | .063 |
| 19. | 1,004.25 | 18.160 | 28.489 | 23.162 | .059 | .090 | .053 |
| 20. | 1,003.95 | 17.600 | 27.627 | 22.655 | .050 | .077 | .046 |
| 21. | 1,003.75 | 16.380 | 25.756 | 21.505 | .075 | .114 | .073 |
| 22. | 1,003.72 | 15.870 | 24.973 | 21.002 | .104 | .159 | .103 |
| 23. | 1,003.56 | 14.540 | 22.925 | 19.618 | .106 | .163 | .114 |
| 24. | 1,003.16 | 12.660 | 20.011 | 17.449 | .119 | .185 | .145 |
| 25. | 1,002.71 | 11.410 | 18.063 | 15.838 | .102 | .158 | .137 |
| 26. | 1,007.67 | 3.699 | 5.957 | −0.401 | −.009 | −.014 | −.032 |
| 27. | 1,007.34 | 6.374 | 10.218 | 7.234 | .021 | .034 | .048 |
| 28. | 1,006.90 | 9.506 | 15.157 | 13.126 | .051 | .081 | .081 |
| 29. | 1,005.09 | 3.722 | 5.979 | −0.351 | .056 | .089 | .204 |
| 30. | 1,004.78 | 6.346 | 10.148 | 7.134 | .037 | .059 | .084 |
| 31. | 1,004.50 | 9.647 | 15.342 | 13.312 | .071 | .111 | .111 |
| 32. | 1,004.00 | 14.620 | 23.058 | 19.711 | .062 | .096 | .066 |
| 33. | 1,003.74 | 18.510 | 29.008 | 23.461 | .056 | .085 | .049 |
| 34. | 1,005.60 | 3.704 | 5.953 | −0.411 | .056 | .089 | .204 |
| 35. | 1,005.36 | 6.527 | 10.441 | 7.549 | .026 | .042 | .058 |
| 36. | 1,005.12 | 9.886 | 15.725 | 13.691 | .049 | .077 | .075 |
| 37. | 1,004.61 | 15.040 | 23.718 | 20.167 | .045 | .069 | .047 |
| 38. | 1,003.74 | 18.919 | 29.630 | 23.813 | .060 | .092 | .051 |
| 39. | 1,003.17 | 6.505 | 10.383 | 7.468 | .086 | .136 | .190 |
| 40. | 1,002.33 | 3.769 | 6.037 | −0.218 | .105 | .167 | .375 |
| 41. | 1,008.78 | 3.756 | 6.055 | −0.177 | −.012 | −.020 | −.045 |
| 42. | 1,008.75 | 6.517 | 10.460 | 7.576 | .001 | −.001 | −.002 |
| 43. | 1,007.79 | 6.490 | 10.407 | 7.501 | .037 | .058 | .082 |
| 44. | 1,007.50 | 9.862 | 15.725 | 13.690 | .037 | .057 | .056 |
| 45. | 1,007.35 | 14.980 | 23.691 | 20.148 | .053 | .081 | .055 |
| 46. | 1,007.14 | 19.010 | 29.869 | 23.947 | .060 | .091 | .051 |
| 47. | 1,007.07 | 19.050 | 29.928 | 23.980 | .057 | .086 | .048 |
| 48. | 1,006.88 | 15.040 | 23.772 | 20.203 | .075 | .115 | .079 |
| 49. | 1,006.85 | 9.904 | 15.781 | 13.745 | .079 | .123 | .120 |
| 50. | 1,006.74 | 6.499 | 10.411 | 7.507 | .043 | .068 | .095 |
| 51. | 1,006.66 | 6.499 | 10.410 | 7.506 | .033 | .053 | .073 |
| 52. | 1,006.70 | 3.766 | 6.059 | −0.168 | .061 | .097 | .219 |
| Mean | | | | | .047 | .073 | .083 |
| Excluding Points 4, 6, and 40 Mean | | | | | .050 | .078 | .088 |

[a] $e = \frac{r\,\mathrm{Pa}}{0.62198 + r}$ with respect to ambient pressure (*r* in grams per gram) [4].

[b] The temperature at which the saturation mixing ratio at ambient pressure equals the generated mixing ratio.

TABLE 2. *Error analysis*

| No. | Measured mixing ratio g/kg | Measured difference psychrometer-generator g/kg | Estimated systematic error | | Estimated random error | | Estimated differences | |
|---|---|---|---|---|---|---|---|---|
| | | | Psychrometer[a] g/kg | Generator g/kg | Psychrometer[a] g/kg | Generator g/kg | Systematic g/kg | Random g/kg |
| 1. | 2.610 | 0.044 | 0.048 | 0.001 | 0.011 | 0.003 | 0.049 | 0.011 |
| 2. | 2.891 | .056 | .049 | .001 | .012 | .003 | .050 | .012 |
| 3. | 3.196 | .043 | .049 | .002 | .012 | .003 | .051 | .012 |
| 4. | 3.496 | −.042 | .050 | .002 | .012 | .003 | .052 | .012 |
| 5. | 4.485 | .048 | .051 | .002 | .012 | .004 | .053 | .013 |
| 6. | 3.942 | −.064 | .050 | .002 | .012 | .004 | .052 | .013 |
| 7. | 4.840 | .034 | .052 | .002 | .012 | .005 | .054 | .013 |
| 8. | 6.020 | .036 | .054 | .003 | .013 | .006 | .057 | .014 |
| 9. | 5.995 | .035 | .053 | .003 | .013 | .006 | .056 | .014 |
| 10. | 5.273 | .030 | .052 | .003 | .012 | .005 | .055 | .013 |
| 11. | 6.404 | .003 | .054 | .003 | .013 | .006 | .057 | .014 |
| 12. | 7.796 | .027 | .056 | .004 | .014 | .008 | .060 | .016 |
| 13. | 9.257 | .046 | .058 | .005 | .014 | .009 | .063 | .017 |
| 14. | 10.734 | .034 | .061 | .005 | .015 | .011 | .066 | .019 |
| 15. | 12.236 | .036 | .063 | .006 | .016 | .012 | .069 | .020 |
| 16. | 14.146 | .046 | .066 | .007 | .017 | .014 | .073 | .022 |
| 17. | 15.817 | .057 | .069 | .008 | .018 | .016 | .077 | .024 |
| 18. | 17.328 | .068 | .071 | .009 | .019 | .017 | .080 | .025 |
| 19. | 18.219 | .059 | .073 | .009 | .019 | .018 | .082 | .027 |
| 20. | 17.650 | .050 | .072 | .009 | .019 | .018 | .081 | .027 |
| 21. | 16.455 | .075 | .070 | .008 | .018 | .016 | .078 | .024 |
| 22. | 15.974 | .104 | .069 | .008 | .018 | .016 | .077 | .024 |
| 23. | 14.646 | .106 | .067 | .007 | .017 | .015 | .073 | .023 |
| 24. | 12.779 | .119 | .064 | .006 | .016 | .013 | .070 | .021 |
| 25. | 11.512 | .102 | .062 | .006 | .016 | .012 | .068 | .020 |
| 26. | 3.690 | −.009 | .050 | .002 | .012 | .004 | .052 | .013 |
| 27. | 6.395 | .021 | .054 | .003 | .013 | .006 | .057 | .014 |
| 28. | 9.557 | .051 | .059 | .005 | .015 | .010 | .064 | .018 |
| 29. | 3.778 | .056 | .050 | .002 | .012 | .004 | .052 | .013 |
| 30. | 6.383 | .037 | .054 | .003 | .013 | .006 | .057 | .014 |
| 31. | 9.718 | .071 | .059 | .005 | .015 | .010 | .064 | .018 |
| 32. | 14.682 | .062 | .067 | .007 | .017 | .015 | .074 | .023 |
| 33. | 18.566 | .056 | .074 | .009 | .019 | .019 | .083 | .027 |
| 34. | 3.760 | .056 | .050 | .002 | .012 | .004 | .052 | .013 |
| 35. | 6.553 | .026 | .054 | .003 | .013 | .007 | .057 | .015 |
| 36. | 9.935 | .049 | .059 | .005 | .015 | .010 | .064 | .018 |
| 37. | 15.085 | .045 | .067 | .008 | .017 | .015 | .075 | .023 |
| 38. | 18.979 | .060 | .074 | .009 | .019 | .019 | .083 | .027 |
| 39. | 6.591 | .086 | .055 | .003 | .013 | .007 | .058 | .015 |
| 40. | 3.874 | .105 | .051 | .002 | .012 | .004 | .053 | .013 |
| 41. | 3.744 | −.012 | .050 | .002 | .012 | .004 | .052 | .013 |
| 42. | 6.516 | −.001 | .054 | .003 | .013 | .007 | .057 | .015 |
| 43. | 6.527 | .037 | .054 | .003 | .013 | .007 | .057 | .015 |
| 44. | 9.899 | .037 | .060 | .005 | .015 | .010 | .065 | .018 |
| 45. | 15.033 | .053 | .068 | .008 | .017 | .015 | .076 | .023 |
| 46. | 19.070 | .060 | .074 | .010 | .019 | .019 | .084 | .027 |
| 47. | 19.107 | .057 | .075 | .010 | .020 | .019 | .085 | .028 |
| 48. | 15.115 | .075 | .068 | .008 | .017 | .015 | .076 | .023 |
| 49. | 9.983 | .079 | .060 | .005 | .015 | .010 | .065 | .018 |
| 50. | 6.542 | .043 | .055 | .003 | .013 | .007 | .058 | .015 |
| 51. | 6.532 | .033 | .055 | .003 | .013 | .007 | .058 | .015 |
| 52. | 3.827 | .061 | .051 | .002 | .012 | .004 | .053 | .013 |

[a]Calculated by means of eq. (5) as described in section 5.

sured differences were fitted by least squares methods to a linear curve in terms of measured mixing ratio.

The result is

$$\Delta r_{meas} = 0.025 + 0.0024\, r \qquad (a)$$

where $\Delta r_{meas}$ is the measured difference in mixing ratio between the generator and this instrument and $r$ is the mixing ratio measured by this instrument. The residual standard deviation of this fit is 0.024.

The estimated systematic difference was similarly fitted to a linear equation and the result is

$$\Delta r_{est} = 0.044 + 0.0021\, r \qquad (b)$$

where $\Delta r_{est}$ is the estimated maximum systematic difference and $r$ is the measured mixing ratio. The root mean square of the estimated random errors is 0.019. The smoothed measured systematic difference is less than the smoothed estimate of the maximum systematic difference expected. The random component of the measured differences exceeds the estimate of the random difference by about 26 percent.

The results were further analyzed by comparing the difference between the measured exit temperature of the psychrometer and that exit temperature necessary to obtain values identical with the generator, all other measurements remaining as measured. The results are shown in table 3 along with the estimated total systematic uncertainty computed in terms of exit temperature and the estimated random uncertainty computed in similar terms.

The measured difference in terms of exit temperature is essentially a constant and the mean value is 0.032 °C with a residual standard deviation of 0.017°C. Except for a slight slope due to the fact that the estimates of the uncertainties in the generator are linearly dependent on the generated value of the mixing ratio, the estimated systematic uncertainty is essentially constant at 0.042 °C and the estimate of random uncertainty is also nearly constant with a root mean square value of 0.012 °C.

In terms of exit temperature, the measured difference and the estimated total uncertainty are both essentially a constant with the estimated value exceeding the measured value. The residual standard deviation of the measured value exceeds the estimated random uncertainty by about 42 percent.

The results indicate that the instrument performs in general within the limits that would be expected on the basis of eq (5).

The time constant of the instrument was measured and found to be approximately 3 min from the dry-to-wet condition and slightly less in the wet-to-dry condition. This can have an effect on the instrument indication.

Calibration points 9 through 25 were performed sequentially, some as closely spaced as 11 min apart. Part of the time between successive points was used in changing and stabilizing the humidity generator. Therefore, the actual time provided for the psychrometer to come to equilibrium was less than the time between points.

Due to the short time allowed for a stable reading, the measured mixing ratio for points 11 through 15 are probably somewhat lower than they would be at complete equilibrium. Likewise, points 21 through 24 are probably somewhat higher than they would have been had complete equilibrium been achieved. Adequate data are not available for a quantitative evaluation of this nonequilibrium effect but the direction is consistent with the change in generated humidity and, due to its dual nature, should have small effect on the overall calibration results.

The inlet temperature had a variation of 1½ degrees throughout the entire calibration. Though this in itself is of no great importance, the rate at which it changed is. The maximum rate of change detected was 0.026 °C per minute. A difference of 0.026 °C in inlet temperature

TABLE 3. *Error analysis*
(All errors assigned as exit temperature errors)

| No. | Measured exit temp. °C | Exit temp[a] difference °C | Estimated[b] systematic difference °C | Estimated[b] random difference °C |
|---|---|---|---|---|
| 1. | 16.799 | 0.036 | 0.040 | 0.010 |
| 2. | 17.026 | .046 | .041 | .010 |
| 3. | 17.298 | .035 | .042 | .009 |
| 4. | 17.540 | −.034 | .043 | .009 |
| 5. | 18.321 | .023 | .042 | .010 |
| 6. | 17.885 | −.051 | .041 | .010 |
| 7. | 18.607 | .026 | .041 | .010 |
| 8. | 19.542 | .027 | .042 | .011 |
| 9. | 19.538 | .026 | .042 | .011 |
| 10. | 18.966 | .023 | .042 | .010 |
| 11. | 19.848 | .002 | .042 | .011 |
| 12. | 20.877 | .019 | .042 | .011 |
| 13. | 21.894 | .031 | .043 | .012 |
| 14. | 22.886 | .022 | .042 | .013 |
| 15. | 23.866 | .022 | .043 | .013 |
| 16. | 25.064 | .027 | .043 | .013 |
| 17. | 26.040 | .032 | .043 | .014 |
| 18. | 26.904 | .036 | .043 | .013 |
| 19. | 27.406 | .032 | .044 | .015 |
| 20. | 27.102 | .027 | .043 | .015 |
| 21. | 26.460 | .041 | .043 | .013 |
| 22. | 26.198 | .058 | .043 | .013 |
| 23. | 25.445 | .061 | .042 | .013 |
| 24. | 24.332 | .072 | .042 | .012 |
| 25. | 23.530 | .063 | .042 | .013 |
| 26. | 17.846 | −.007 | .041 | .010 |
| 27. | 19.922 | .016 | .042 | .010 |
| 28. | 22.118 | .034 | .043 | .013 |
| 29. | 17.896 | .044 | .043 | .010 |
| 30. | 19.969 | .027 | .042 | .010 |
| 31. | 22.283 | .047 | .041 | .011 |
| 32. | 25.392 | .036 | .043 | .013 |
| 33. | 27.584 | .029 | .043 | .015 |
| 34. | 17.759 | .044 | .041 | .010 |
| 35. | 19.958 | .019 | .042 | .010 |
| 36. | 22.302 | .032 | .042 | .011 |
| 37. | 25.549 | .026 | .043 | .013 |
| 38. | 27.807 | .031 | .043 | .015 |
| 39. | 20.258 | .062 | .042 | .010 |
| 40. | 18.152 | .083 | .042 | .010 |
| 41. | 17.856 | −.010 | .041 | .010 |
| 42. | 20.052 | −.001 | .042 | .010 |
| 43. | 20.154 | .027 | .041 | .010 |
| 44. | 22.519 | .024 | .043 | .011 |
| 45. | 25.713 | .030 | .044 | .013 |
| 46. | 27.950 | .031 | .044 | .013 |
| 47. | 27.997 | .029 | .043 | .014 |
| 48. | 25.862 | .043 | .044 | .013 |
| 49. | 22.725 | .052 | .043 | .011 |
| 50. | 20.326 | .031 | .042 | .010 |
| 51. | 20.303 | .024 | .042 | .010 |
| 52. | 18.202 | .048 | .042 | .010 |
| Mean | | 0.030 | 0.042 | 0.011 |
| Standard deviation | | .023 | | |
| Excluding Points 4, 6, and 40 | | | | |
| Mean | | 0.032 | 0.042 | 0.012 |
| Standard deviation | | .017 | | |

[a] Measured exit temperature less the exit temperature that would give the generated mixing ratio values.
[b] Calculated by means of eq. (5) as described in section 5.

is equivalent to approximately 0.014 mg/g mixing ratio indication in the instrument. If the inlet temperature changed continuously at a rate of 0.026 °C per minute monotonically over a long period of time, an error in instrument indication would result amounting about 0.04 mg per gram in mixing ratio. Examination of the calibration data indicates that the usual rate of change was much smaller and did not generally persist in one direction for long periods. This is not believed to have caused large errors. The standard deviation is probably larger due to this effect than would have been the case with constant inlet temperature, especially since all readings could not be taken simultaneously.

Examination of the calibration data further indicates some correlation between the inlet temperature and the temperature difference. This may have been due to conduction along the inlet thermistor giving an inlet temperature reading lower than the true inlet temperature. This would have the effect of causing larger values in measured $r$, and thereby could account for some of the error found in calibration. This effect is such that it would be more pronounced at lower values of $r$.

## 6. Summary and Conclusion

A heated-air adiabatic saturation psychrometer has been built that measures the mixing ratio of water from 0 to 50 g/kg. If three of the 52 calibration points are excluded as being statistically unrepresentative, the mean difference between the measured value and the generated value in the calibration over the range of 2.5 to 19 g/kg was 0.050. In terms of partial pressure of vapor the mean difference was 0.078 mbar and in terms of dewpoint temperature the mean difference was 0.088 °C.

Analysis of the calibration results indicates that the instrument performs as an adiabatic instrument within the estimated uncertainty in the measured parameters of both the instrument and the humidity generator used in the calibration process. We conclude that the adiabatic saturation theory applies to this instrument at nonzero values of humidity, as well as at zero values.

Heating the inlet air broadens the mixing ratio range over which this instrument can be used and increases the ambient temperature range over which it can successfully operate but reduces the accuracy of the instrument at low values of humidity. It is therefore apparent that this type of instrument would find greater value in the measurement of high values of humidity. Increased accuracy is obtainable over the entire humidity range by increased accuracy and precision in the determination of exit temperature first, the entrance temperature next and the pressure last.

Were the entrance temperature to be better controlled, one would expect the random uncertainty to be decreased and the ease of taking measurements improved. Control of the entrance temperature to at least 0.1 deg C would make entrance temperature readings unnecessary for determination where the uncertainty in the humidity can be as large as 0.05 g/kg.

Where the instrument is to be operated at mixing ratios which will never exceed 20 g/kg, one could control the entrance temperature at 25 °C and obtain greater accuracy than with the 41 °C now used in the instrument.

## 7. References


[1] Greenspan, L., and Wexler, A. An Adiabatic Saturation Psychrometer. J. Res. Nat. Bur. Stand. (U.S.), **72C** (Eng. & Instr.) No. 1, 33-47 (Jan.-Mar. 1968).

[2] Wexler, A., Humidity Standards, Tappi **44,** 180A, (June 1961).

[3] Wexler, A. Calibration of Humidity Measuring Instruments at the National Bureau of Standards, Analysis Instrumentation **6,** 161 (Plenum Press, 1969).

[4] Smithsonian Meteorological Tables, Smithsonian Institution, Washington, D. C. (1951).

[5] Goff, J. A., and Gratch, S., Thermal properties of moist air, ASHVE Journal Section, Heating, Piping and Air Conditioning **51,** 334 (June 1945).

[6] Harrison, L. P., Fundamental Concepts and Definitions Relating to Humidity, Humidity and Moisture **3,** 49 (Reinhold Publishing Corp., New York 1965).

[7] Goff, J. A., Saturation Pressure of Water on the New Kelvin Scale, Humidity and Moisture **3,** 289 (Reinhold Publishing Corp., New York 1965).

[8] Ku, H. H., Notes on the Use of Propagation of Error Formulas. J. Res. Nat. Bur. Stand. (U.S.), **70C** (Eng. & Instr.) No. 4, 263-273 (Oct.-Dec. 1966).


(Paper 75C2–314)

JOURNAL OF RESEARCH of the National Bureau of Standards—C. Engineering and Instrumentation
Vol. 75C, No. 2, April-June 1971

# Computation of the Temperature Distribution in Cylindrical High-Pressure Furnaces

**Meyer Waxman and John R. Hastings**

**Institute for Basic Standards, National Bureau of Standards, Washington, D.C. 20234**

**(April 22, 1971)**

The steady-state temperature distribution in typical cylindrical high-pressure furnaces has been computed from analytic solutions for various boundary conditions. Either the temperature variation along the cylindrical heater or the power dissipation per unit length is prescribed. The results are tabulated and discussed as an aid in the design of high-pressure furnaces and in the estimation of temperature gradients. Topics considered include: (1) the reduction of temperature gradients around the center of the furnace, (2) the effect of temperature irregularities along the heater, and (3) the effect of the relative thermal conductivity of neighboring components.

Key words: Analytic solutions; boundary conditions; computation, temperature distribution; furnaces, high-pressure; high-pressure furnaces; high-temperature, high-pressure research; power dissipation; temperature distribution, steady-state; temperature gradients; temperature irregularities; temperature variation; thermal conductivity.

## 1. Introduction

Activity in high-temperature, high-pressure research has greatly increased in recent years. Such work is of both scientific and technological importance and significantly extends our knowledge of the phase diagrams and equations of state of the solids and liquids studied. In the design of experiments and in the detailed interpretation of results, the accuracy and uniformity of the temperature and pressure require careful attention. This paper deals with the computation of the temperature distribution in cylindrical furnaces of the type characteristic of static high-pressure apparatus. Since the pressure does not appear explicitly in the computation, the results are equally applicable to furnaces at any pressure if the geometry and the boundary conditions assumed in this paper are a suitable approximation to the actual physical conditions.

Several problems arise in the maintenance and measurement of high temperatures in high-pressure media. The small size of the pressurized region within a massive metal apparatus restricts the size of the furnace components and thus limits the amount of thermal insulation that separates the sample from the heater and from the surroundings. As a result there may be a large flux of heat across the sample with correspondingly large temperature gradients. Temperature irregularities along the heater may cause additional gradients across the sample. Temperatures in high-pressure furnaces are usually measured with thermocouples. Pressure modifies the temperature-emf relationship of a thermocouple by as much as an estimated 5 to 10 percent under experimental conditions [1,2].[1] Because of the temperature and pressure gradients, the details of positioning the thermocouples influence the readings obtained with them [3].

This paper grew out of our interest in designing a high-pressure furnace in which temperature gradients across the sample would be both small and well-known—for

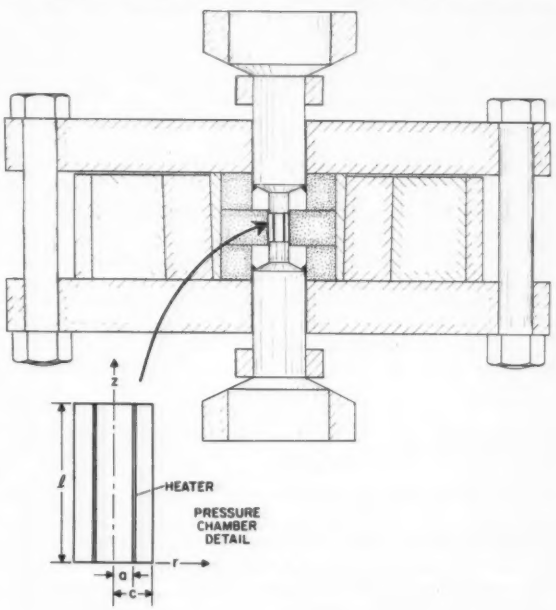


FIGURE 1. *Schematic diagram of typical high-pressure furnace with coaxial cylindrical heater.*

[1] Figures in brackets indicate the literature references at the end of this paper.

example, known to within 0.1 percent of the difference between the highest temperature in the furnace and the temperature of the surrounding metal apparatus. A survey of the literature indicated that the kind of detailed temperature distribution data needed in the design of such a furnace was not available. Because of the various difficulties in the determination of this sort of data by experimental trial and error for different furnace designs, we chose, instead, to compute the temperature distribution for several alternative conditions. Most high-pressure furnace designs can be described by one or a combination of these conditions.

In the present work the steady-state temperature distribution in typical cylindrical high-pressure furnaces has been computed from analytic solutions for various boundary conditions. A schematic diagram of such a typical furnace is shown in figure 1, in which a cylindrical heater of negligible thickness, radius $a$, and length $l$ is located between opposed pistons in a massive metal apparatus. Either the temperature variation along the cylindrical heater or the power dissipation per unit length is prescribed. Perfect thermal contact is assumed at all boundaries because of the intimate contact created by the high pressure. Angular symmetry and homogeneous, isotropic materials are also assumed throughout this paper.

## 2. General Solution for a Prescribed Surface Temperature Variation

Consider a simple cylinder, $0 \leq r < a$, $0 < z < l$, with a prescribed temperature $f(z)$ along the cylindrical surface at $r = a$ and a constant temperature, taken as zero for convenience, over the end surfaces. The temperature potential $v(r,z)$ within the cylinder, measured from the temperature at either end, is given by Carslaw and Jaeger [4] as

$$v(r,z) = \frac{2}{l}\sum_{n=1}^{\infty}\frac{I_0(n\pi r/l)}{I_0(n\pi a/l)}\sin\frac{n\pi z}{l}\int_0^l f(z')\sin\frac{n\pi z'}{l}dz', \quad (1)$$

where $I_0(x)$ is the modified Bessel function of the first kind of zero order. We now consider the application of eq (1) for several explicit surface temperature variations.

### 2.1. Parabolic Surface Temperature

For typical furnaces with a smooth temperature variation along the heater from a hot middle to cooler ends, the surface temperature may be approximated by a parabolic function

$$f(z) = A - (Bz - C)^2. \quad (2)$$

By requiring $f(z)$ to be zero at $z = 0$ and $z = l$, we obtain $A = C^2$, $B = 2C/l$, and

$$f(z) = 2BCz - B^2z^2 = (4C^2z/l)(1 - z/l). \quad (3)$$

After performing the integration in eq (1), we have

$$v(r,z) = \frac{16C^2}{\pi^3}\sum_{n=1}^{\infty}\frac{1}{n^3}\frac{I_0(n\pi r/l)}{I_0(n\pi a/l)}\sin\frac{n\pi z}{l}(1-\cos n\pi), \quad (4)$$

where $C$ is an arbitrary scaling factor. The temperature potential within cylindrical furnaces for the particular geometrical conditions $l = 8a$ and $l = 16a$ is shown in table 1 and table 2, respectively. Since the furnaces are symmetric about the midplane, $z/l = 0.50$, the tables show the potential explicitly for only half the furnace. The computed potential is scaled so that its value in the midplane at $r/a = 1.0$, the middle of the heater, is unity.

TABLE 1. *Temperature potential within a cylindrical furnace: parabolic surface temperature, $l = 8a$*

| $z/l$ \ $r/a$ | 0.0 | 0.3 | 0.6 | 0.8 | 1.0 |
|---|---|---|---|---|---|
| 0.50 | 0.9688 | 0.9716 | 0.9800 | 0.9888 | 1.0000 |
| .45 | .9588 | .9616 | .9700 | .9788 | .9900 |
| .40 | .9288 | .9316 | .9400 | .9488 | .9600 |
| .35 | .8788 | .8816 | .8900 | .8988 | .9100 |
| .30 | .8089 | .8117 | .8201 | .8288 | .8400 |
| .25 | .7190 | .7218 | .7302 | .7388 | .7500 |
| .20 | .6095 | .6122 | .6204 | .6289 | .6400 |
| .15 | .4807 | .4832 | .4911 | .4993 | .5100 |
| .10 | .3338 | .3360 | .3428 | .3501 | .3600 |
| .05 | .1715 | .1729 | .1774 | .1825 | .1900 |
| .00 | .0000 | .0000 | .0000 | .0000 | .0000 |

TABLE 2. *Temperature potential within a cylindrical furnace: parabolic surface temperature, $l = 16a$*

| $z/l$ \ $r/a$ | 0.0 | 0.3 | 0.6 | 0.8 | 1.0 |
|---|---|---|---|---|---|
| 0.50 | 0.9922 | 0.9929 | 0.9950 | 0.9972 | 1.0000 |
| .45 | .9822 | .9829 | .9850 | .9872 | .9900 |
| .40 | .9522 | .9529 | .9550 | .9572 | .9600 |
| .35 | .9022 | .9029 | .9050 | .9072 | .9100 |
| .30 | .8322 | .8329 | .8350 | .8372 | .8400 |
| .25 | .7422 | .7429 | .7450 | .7472 | .7500 |
| .20 | .6322 | .6329 | .6350 | .6372 | .6400 |
| .15 | .5022 | .5029 | .5050 | .5072 | .5100 |
| .10 | .3524 | .3531 | .3551 | .3572 | .3600 |
| .05 | .1834 | .1840 | .1857 | .1875 | .1900 |
| .00 | .0000 | .0000 | .0000 | .0000 | .0000 |

The temperature potential $v(r,z)$ at any point within the cylindrical furnace is very simply related to the actual temperature $T(r,z)$ at that point by the equation

$$v(r,z) = \frac{T(r,z) - T(r,0)}{T(a,l/2) - T(r,0)},$$

where $T(r,0)$ is the reference temperature over the ends of the furnace and $T(a,l/2)$ is the temperature at the middle of the heater. If, for example, the middle of the heater is 1000 °C hotter than the ends of the furnace, table 1 shows that the cylindrical midpoint, $r/a = 0.0$ and $z/l = 0.50$, is 968.8 °C hotter than the ends of the furnace. If the temperature over the ends of the furnace is 100 °C, the temperature at these other locations becomes 1100 °C and 1068.8 °C, respectively.

Table 1 shows that the temperature potential in the midplane at $r/a = 0.0$, the cylindrical midpoint, is approximately 3 percent less than that at $r/a = 1.0$, the middle of the heater, and 2 percent less than that at $r/a = 0.8$. In terms of the preceding example, these potential differences represent temperature differences of approximately

30 and 20 °C. The longitudinal variation from $z/l = 0.50$ to 0.45 at any radius is 1 percent. The cylindrical midpoint is a saddle point at which the radial temperature gradient is positive and the longitudinal gradient is negative. For the more elongated furnace of table 2 the potential at the cylindrical midpoint is only 0.8 percent less than that at the middle of the heater and 0.5 percent less than that at $r/a = 0.8, z/l = 0.50$. The longitudinal variation from $z/l = 0.50$ to 0.45 is still 1 percent, of course, although relative to the radius, the corresponding longitudinal displacement is twice as long as in table 1.

### 2.2. Generalized Parabolic Surface Temperature With a Constant Central Section

In practice the small size of the pressurized region restricts the opportunity for elongation of the furnace in order to reduce the temperature gradients around its center. Another way to reduce these gradients is to supply extra heat near the ends of the furnace to compensate for the large losses to the surroundings and thus maintain a substantially constant temperature about the middle of the heater. To represent this section of constant temperature, we generalize the preceding problem by splitting the parabola at its midpoint and inserting a horizontal line segment there. Since the maximum value of $f(z)$ is $C^2$, which occurs at $z = C/B$, we obtain

$$\begin{aligned} f(z) &= 2BCz - B^2z^2, 0 < z \leqslant C/B, \\ &= C^2, \; C/B \leqslant z \leqslant l - C/B, \\ &= 2BC(l-z) - B^2(l-z)^2, \; l - C/B \leqslant z < l. \end{aligned} \tag{5}$$

After substituting in eq (1) and performing the integration, we have

$$v(r,z) = \frac{4B^2l^2}{\pi^3} \sum_{n=1}^{\infty} \frac{1}{n^3} \frac{I_0(n\pi r/l)}{I_0(n\pi a/l)} \sin\frac{n\pi z}{l} (1 - \cos n\pi) \cdot \left(1 - \cos\frac{n\pi C}{Bl}\right). \tag{6}$$

When $C/B = l/2$, eq (5) reduces to eq (3) and eq (6) reduces to eq (4), since $\cos n\pi/2$ vanishes for odd $n$ and $1 - \cos n\pi$ vanishes for even $n$. The temperature potential within cylindrical furnaces for which $l = 8a$ is shown in table 3 for $C/B = l/2.5$ and in table 4 for $C/B = l/4$.

TABLE 3. *Temperature potential within a cylindrical furnace: generalized parabolic surface temperature with central fifth at constant temperature,* $l = 8a$

| z/l \ r/a | 0.0 | 0.3 | 0.6 | 0.8 | 1.0 |
|---|---|---|---|---|---|
| 0.50 | 0.9922 | 0.9931 | 0.9957 | 0.9979 | 1.0000 |
| .45 | .9885 | .9898 | .9934 | .9967 | 1.0000 |
| .40 | .9750 | .9773 | .9841 | .9911 | 1.0000 |
| .35 | .9454 | .9487 | .9588 | .9697 | .9844 |
| .30 | .8927 | .8966 | .9085 | .9210 | .9375 |
| .25 | .8125 | .8166 | .8292 | .8423 | .8594 |
| .20 | .7029 | .7071 | .7197 | .7329 | .7500 |
| .15 | .5638 | .5678 | .5799 | .5927 | .6094 |
| .10 | .3966 | .4000 | .4106 | .4221 | .4375 |
| .05 | .2056 | .2077 | .2146 | .2226 | .2344 |
| .00 | .0000 | .0000 | .0000 | .0000 | .0000 |

The temperature variations around the cylindrical midpoint are indeed much smaller in these tables than in table 1. For example, the total radial variation in the midplane is 3.1 percent in table 1, 0.8 percent in table 3, and 0.1 percent in table 4.

TABLE 4. *Temperature potential within a cylindrical furnace: generalized parabolic surface temperature with central half at constant temperature,* $l = 8a$

| z/l \ r/a | 0.0 | 0.3 | 0.6 | 0.8 | 1.0 |
|---|---|---|---|---|---|
| 0.50 | 0.9989 | 0.9990 | 0.9994 | 0.9997 | 1.0000 |
| .45 | .9983 | .9985 | .9991 | .9996 | 1.0000 |
| .40 | .9961 | .9966 | .9979 | .9990 | 1.0000 |
| .35 | .9901 | .9913 | .9945 | .9973 | 1.0000 |
| .30 | .9748 | .9776 | .9855 | .9927 | 1.0000 |
| .25 | .9386 | .9441 | .9606 | .9778 | 1.0000 |
| .20 | .8635 | .8715 | .8963 | .9232 | .9600 |
| .15 | .7327 | .7418 | .7697 | .7998 | .8400 |
| .10 | .5388 | .5471 | .5731 | .6015 | .6400 |
| .05 | .2874 | .2928 | .3101 | .3302 | .3600 |
| .00 | .0000 | .0000 | .0000 | .0000 | .0000 |

### 2.3. Surface Temperature, a Rectangular Function of Finite Width

Temperature irregularities exist along real heaters. A detailed model of the irregularities in an actual furnace would greatly increase the complexity of the mathematical analysis; for example, the angular symmetry assumed in the derivation of eq (1) would not generally exist. Rather than neglect such irregularities altogether, we may explore their effect by considering a rectangular function of finite width for the surface temperature

$$\begin{aligned} f(z) &= 0, \qquad 0 < z < g, \\ &= D, \qquad g < z < h, \\ &= 0, \qquad h < z < l, \end{aligned} \tag{7}$$

where, in general, $g \neq l - h$; that is, the step is not centered at the midplane. After performing the integration in eq (1), we have

$$v(r,z) = \frac{2D}{\pi} \sum_{n=1}^{\infty} \frac{1}{n} \frac{I_0(n\pi r/l)}{I_0(n\pi a/l)} \sin\frac{n\pi z}{l} \left(\cos\frac{n\pi g}{l} - \cos\frac{n\pi h}{l}\right). \tag{8}$$

The temperature potential within a furnace for which $l = 8a$ is shown in tables 5 and 6 for steps of width 0.01 $l$ and 0.05 $l$ centered at $z/l = 0.30$.

The tables show certain features which can be expected as general results of local irregularities in the temperature along the heater. The gradients due to an irregularity modify the gradients otherwise present to an extent that depends upon the width and the height or depth of the irregularity. The radial gradient along a radius leading to a hot spot is increased. The radial gradient elsewhere includes a component due to the hot spot that may be

negative along the entire radius or positive near the axis and negative near the heater; the latter characteristic is illustrated by the data in the tables for $z/l = 0.25$ and 0.35. Longitudinal gradients are also modified. The tables show a slight asymmetry in the gradients above and below the plane of the irregularity as a result of the temperature asymmetry along the heater.

TABLE 5. *Temperature potential within a cylindrical furnace: surface temperature, a rectangular function of finite width* ($f(z) = 0$ *for* $0 < z < g$ *and* $h < z < l$, $f(z) = D$ *for* $g < z < h$, $g = 0.295l$, $h = 0.305l$), $l = 8a$

| z/l \ r/a | 0.0 | 0.3 | 0.6 | 0.8 | 1.0 |
|---|---|---|---|---|---|
| 1.00 | 0.0000 | 0.0000 | 0.0000 | 0.0000 | 0.0000 |
| .95 | .0000 | .0000 | .0000 | .0000 | .0000 |
| .90 | .0000 | .0000 | .0000 | .0000 | .0000 |
| .85 | .0000 | .0000 | .0000 | .0000 | .0000 |
| .80 | .0000 | .0000 | .0000 | .0000 | .0000 |
| .75 | .0000 | .0000 | .0000 | .0000 | .0000 |
| .70 | .0001 | .0001 | .0000 | .0000 | .0000 |
| .65 | .0002 | .0002 | .0001 | .0000 | .0000 |
| .60 | .0005 | .0004 | .0003 | .0001 | .0000 |
| .55 | .0013 | .0011 | .0007 | .0003 | .0000 |
| .50 | .0033 | .0029 | .0018 | .0009 | .0000 |
| .45 | .0083 | .0074 | .0048 | .0024 | .0000 |
| .40 | .0199 | .0185 | .0132 | .0071 | .0000 |
| .35 | .0400 | .0405 | .0391 | .0280 | .0000 |
| .30 | .0530 | .0579 | .0810 | .1408 | 1.0000 |
| .25 | .0400 | .0405 | .0391 | .0280 | 0.0000 |
| .20 | .0199 | .0185 | .0132 | .0071 | .0000 |
| .15 | .0083 | .0074 | .0048 | .0024 | .0000 |
| .10 | .0032 | .0028 | .0018 | .0009 | .0000 |
| .05 | .0011 | .0009 | .0006 | .0003 | .0000 |
| .00 | .0000 | .0000 | .0000 | .0000 | .0000 |

TABLE 6. *Temperature potential within a cylindrical furnace: surface temperature, a rectangular function of finite width* ($f(z) = 0$ *for* $0 < z < g$ *and* $h < z < l$, $f(z) = D$ *for* $g < z < h$, $g = 0.275l$, $h = 0.325l$), $l = 8a$

| z/l \ r/a | 0.0 | 0.3 | 0.6 | 0.8 | 1.0 |
|---|---|---|---|---|---|
| 1.00 | 0.0000 | 0.0000 | 0.0000 | 0.0000 | 0.0000 |
| .95 | .0000 | .0000 | .0000 | .0000 | .0000 |
| .90 | .0000 | .0000 | .0000 | .0000 | .0000 |
| .85 | .0000 | .0000 | .0000 | .0000 | .0000 |
| .80 | .0001 | .0000 | .0000 | .0000 | .0000 |
| .75 | .0001 | .0001 | .0001 | .0000 | .0000 |
| .70 | .0004 | .0003 | .0002 | .0001 | .0000 |
| .65 | .0010 | .0008 | .0005 | .0003 | .0000 |
| .60 | .0025 | .0022 | .0014 | .0007 | .0000 |
| .55 | .0065 | .0057 | .0036 | .0018 | .0000 |
| .50 | .0169 | .0148 | .0094 | .0046 | .0000 |
| .45 | .0428 | .0382 | .0249 | .0126 | .0000 |
| .40 | .1017 | .0948 | .0692 | .0379 | .0000 |
| .35 | .1987 | .2026 | .2029 | .1620 | .0000 |
| .30 | .2588 | .2807 | .3757 | .5599 | 1.0000 |
| .25 | .1987 | .2026 | .2029 | .1620 | 0.0000 |
| .20 | .1016 | .0947 | .0691 | .0379 | .0000 |
| .15 | .0427 | .0381 | .0249 | .0126 | .0000 |
| .10 | .0165 | .0145 | .0092 | .0045 | .0000 |
| .05 | .0055 | .0049 | .0030 | .0015 | .0000 |
| .00 | .0000 | .0000 | .0000 | .0000 | .0000 |

## 3. Solution for Uniform Heating Along the Full Length of the Heater

In the problems considered thus far, we have prescribed the surface temperature variation along the cylindrical heater. We now prescribe a particular power dissipation along it. Consider a special form of a general problem treated by Laubitz [5]. A composite cylinder of length $l$ and radius $c$, shown in figure 1, contains a coaxial cylindrical heater of the same length, negligible thickness, and radius $a$, whose power dissipation per unit length $Q$ is independent of time and position; the thermal conductivity is $k_1$ for $0 \leq r < a$ and $k_2$ for $a < r < c$, and the boundary conditions are $v(c,z) = v(r,l) = v(r,0) = 0$. The distinction between the conductivities, which are assumed to be independent of temperature and pressure, arises because the temperature along the heater is not prescribed. The boundary conditions express the physical fact that the apparatus surrounding the furnace acts as a heat sink.

For the region inside the heater, $0 \leq r < a$, $0 < z < l$, the temperature potential is

$$v(r,z) = \frac{2Ql}{\pi^3 k_2 a} \sum_{n=1}^{\infty} \frac{1}{n^2} \cdot \left[ \frac{(l/n\pi a) I_0(n\pi c/l)}{I_0(n\pi c/l) K_0(n\pi a/l) - K_0(n\pi c/l) I_0(n\pi a/l)} + \left(\frac{k_1}{k_2} - 1\right) I_1\left(n\pi a/l\right) \right]^{-1} I_0\left(\frac{n\pi r}{l}\right) \sin^2\left(\frac{n\pi}{2}\right) \cdot \sin\left(\frac{n\pi z}{l}\right), \quad (9)$$

where $I_0(x)$ and $I_1(x)$ are the modified Bessel functions of the first kind and of zero and first order and $K_0(x)$ is the modified Bessel function of the second kind of zero order. If $k_1 = k_2$, eq (9) reduces to

$$v(r,z) = \frac{2Q}{\pi^2 k_2} \sum_{n=1}^{\infty} \frac{1}{n} \left[ K_0\left(\frac{n\pi a}{l}\right) - K_0\left(\frac{n\pi c}{l}\right) \right] \frac{I_0(n\pi a/l)}{I_0(n\pi c/l)} \cdot I_0\left(n\pi r/l\right) \sin^2(n\pi/2) \sin\left(n\pi z/l\right). \quad (10)$$

The temperature potential inside the heater of a furnace for which $l = 4c = 8a$ is shown in tables 7 through 9 for $k_1/k_2 = 0.1$, 1, and 10. As in the earlier tables, the potential is scaled to a maximum value of unity.

Three observations may be made regarding the tables. Near the midplane the temperature along the heater is quite uniform for $k_1/k_2 < 1$ and becomes more nearly parabolic as $k_1/k_2$ increases. To be more specific, for $r/a = 1.0$ the potential at $z/l = 0.40$ is 0.2 percent less than that at $z/l = 0.50$ for $k_1/k_2 = 0.1$, 2.8 percent less for $k_1/k_2 = 10$, and 4 percent less for the parabolic surface temperature of table 1. In practice an experimental sample is commonly located in the vicinity of the axis and the midplane — for example, within the cylindrical volume bounded by $z/l = 0.40$ and 0.60 and $r/a = 0.6$. Within this volume the maximum potential difference is 0.5 percent of the reference value of unity for $k_1/k_2 = 0.1$, 3.8 percent for $k_1/k_2 = 10$, and 5.1 percent for the parabolic surface temperature of table 1. For constant $Q$ and $k_2$ an increase

in $k_1$ causes a decrease in the temperature for $r < a$. This result follows directly from eq (9) and is related physically to the greater flux of heat to the anvils. It is not apparent in the tables because of the scaling.

TABLE 7. *Temperature potential within a cylindrical furnace: uniform heating along the full length of the heater of radius* a, $l = 4c = 8a$, *(thermal conductivity for* $0 \leq r < a) = 0.1$ *(thermal conductivity for* $a < r < c)$

| z/l \ r/a | 0.0 | 0.3 | 0.6 | 0.8 | 1.0 |
|---|---|---|---|---|---|
| 0.50 | 0.9975 | 0.9978 | 0.9985 | 0.9992 | 1.0000 |
| .45 | .9965 | .9968 | .9978 | .9986 | .9996 |
| .40 | .9931 | .9937 | .9951 | .9965 | .9981 |
| .35 | .9858 | .9868 | .9895 | .9920 | .9950 |
| .30 | .9714 | .9732 | .9783 | .9830 | .9886 |
| .25 | .9439 | .9472 | .9565 | .9655 | .9760 |
| .20 | .8920 | .8979 | .9150 | .9316 | .9512 |
| .15 | .7967 | .8068 | .8365 | .8662 | .9022 |
| .10 | .6290 | .6439 | .6902 | .7400 | .8042 |
| .05 | .3596 | .3740 | .4249 | .4919 | .5985 |
| .00 | .0000 | .0000 | .0000 | .0000 | .0000 |

TABLE 8. *Temperature potential within a cylindrical furnace: uniform heating along the full length of the heater of radius* a, $l = 4c = 8a$, *(thermal conductivity for* $0 \leq r < a) =$ *(thermal conductivity for* $a < r < c)$

| z/l \ r/a | 0.0 | 0.3 | 0.6 | 0.8 | 1.0 |
|---|---|---|---|---|---|
| 0.50 | 0.9932 | 0.9939 | 0.9958 | 0.9977 | 1.0000 |
| .45 | .9908 | .9916 | .9937 | .9958 | .9984 |
| .40 | .9830 | .9840 | .9869 | .9897 | .9931 |
| .35 | .9680 | .9695 | .9737 | .9779 | .9830 |
| .30 | .9423 | .9445 | .9512 | .9577 | .9657 |
| .25 | .8999 | .9035 | .9140 | .9243 | .9370 |
| .20 | .8314 | .8370 | .8535 | .8699 | .8900 |
| .15 | .7225 | .7309 | .7559 | .7815 | .8133 |
| .10 | .5538 | .5649 | .5998 | .6375 | .6869 |
| .05 | .3087 | .3188 | .3539 | .3994 | .4713 |
| .00 | .0000 | .0000 | .0000 | .0000 | .0000 |

TABLE 9. *Temperature potential within a cylindrical furnace: uniform heating along the full length of the heater of radius* a, $l = 4c = 8a$, *(thermal conductivity for* $0 \leq r < a) = 10$ *(thermal conductivity for* $a < r < c)$

| z/l \ r/a | 0.0 | 0.3 | 0.6 | 0.8 | 1.0 |
|---|---|---|---|---|---|
| 0.50 | 0.9776 | 0.9796 | 0.9857 | 0.9920 | 1.0000 |
| .45 | .9702 | .9723 | .9786 | .9850 | .9931 |
| .40 | .9480 | .9502 | .9568 | .9636 | .9723 |
| .35 | .9098 | .9122 | .9195 | .9270 | .9366 |
| .30 | .8541 | .8569 | .8652 | .8737 | .8845 |
| .25 | .7786 | .7819 | .7914 | .8013 | .8138 |
| .20 | .6803 | .6840 | .6952 | .7068 | .7216 |
| .15 | .5551 | .5595 | .5726 | .5863 | .6039 |
| .10 | .3993 | .4040 | .4185 | .4342 | .4551 |
| .05 | .2114 | .2150 | .2273 | .2426 | .2662 |
| .00 | .0000 | .0000 | .0000 | .0000 | .0000 |

Further calculations have been performed to study the effects of varying the furnace parameters. The results, which are not shown in the tables, display considerable complexity. For example, for $l = 4c$ the changes in the radial and longitudinal temperature gradients in the vicinity of the axis and the midplane that are caused by a decrease in $a/c$ from 0.50 to 0.25 depend in sign as well as in magnitude on the value of $k_1/k_2$. Consider the cylindrical volume bounded by $z/l = 0.45$ and 0.55 and $r/c = 0.25$. Within this volume the maximum potential difference increases slightly from 0.14 percent to 0.18 percent of the reference value of unity as $a/c$ decreases from 0.50 to 0.25 for $k_1/k_2 = 0.01$. For $k_1/k_2 = 0.1$ the increase is from 0.17 percent to 0.19 percent. For $k_1/k_2 = 1$ the maximum potential difference decreases from 0.43 percent to 0.29 percent as $a/c$ decreases from 0.50 to 0.25. For $k_1/k_2 = 10$ the decrease is from 1.30 percent to 0.99 percent, and for $k_1/k_2 = 100$ it is from 1.69 percent to 1.65 percent. For $k_1/k_2 = 1000$ the maximum potential difference is barely influenced by the decrease in $a/c$, changing from 1.75 percent to 1.76 percent.

## 4. Comments

Although the results shown in the tables are based upon several simplifying assumptions, we believe that they are sufficiently general to be helpful in the design of high-pressure furnaces and in the estimation of temperature gradients. By superposition of these results the results of more complicated problems may be obtained. This is the reason for the inclusion of the problem in which temperature irregularities along the heater are approximated by the assumption that the surface temperature is a rectangular function of finite width.

Reported furnace designs have not always illustrated an optimum choice of environmental materials so far as the thermal conductivities are concerned. The tables show that the temperature gradients in the sample region are significantly affected by the relative thermal conductivity of neighboring components as well as by the temperature variation along the heater. In many cases temperature irregularities along the heater may impose a lower limit to the magnitude of the temperature gradients in the sample region.

It is a pleasure to thank Bradley A. Peavy, Jr. for several helpful discussions.

## 5. References

[1] Bundy, F. P., Effect of pressure on emf of thermocouples, J. Appl. Phys. **32**, 483–488 (1961).

[2] Hanneman, R. E., and Strong, H. M., Pressure dependence of the emf of thermocouples to 1300°C and 50 kbar, J. Appl. Phys. **36**, 523–528 (1965).

[3] Hanneman, R. E., and Strong, H. M., Pressure dependence of the emf of thermocouples, J. Appl. Phys. **37**, 612–614 (1966).

[4] Carslaw, H. S., and Jaeger, J. C., Conduction of Heat in Solids, 2nd ed. (Clarendon Press, Oxford, 1959), p. 220.

[5] Laubitz, M. J., Mathematical treatment of a four-component furnace, Can. J. Phys. **39**, 951–955 (1961).

JOURNAL OF RESEARCH of the National Bureau of Standards—C. Engineering and Instrumentation
Vol. 75C, No. 2, April-June 1971

# Rotating Adjustable Transmission Optical Step Attenuator

**Ared Cezairliyan**

**Institute for Materials Research, National Bureau of Standards, Washington, D.C. 20234**

(March 12, 1971)

A rotating wavelength-independent optical attenuator is described that generates four radiance steps. Radiance ratios between the steps can be continuously varied. Experiments are performed to assess the operational characteristics of the attenuator. Radiance is determined from measurements with a high-speed photoelectric pyrometer. Recording of signals is made with a high-speed digital data acquisition system. The combined measuring and recording systems have a full-scale signal resolution of approximately one part in 8000 and a time resolution of 0.4 ms. The results of several experiments on radiance ratio measurements are found to be in agreement within one part in 1000.

Key words: High-speed measurements; optical attenuator; photometry; radiance.

## 1. Introduction

Rotating step attenuators are used to evaluate the linearity of transmission of optical systems and to calibrate radiation detectors. However, in general they are made of radiation absorbing materials, such as neutral density filters. They have limitations due to the fact that filter transmission is, to some extent, dependent on the wavelength of radiation. In addition, such attenuators are not capable of producing variable radiance ratios between the steps, and they are used for steady-state type calibrations.

In this paper a rotating, wavelength-independent, optical attenuator is described that generates four radiance steps. Radiance ratios between the steps can be continuously varied, and the attenuator can be used for calibrations under dynamic conditions.

## 2. Method and Apparatus

The method of step attenuation is based on varying the aperture stop of an optical system shown in figure 1. The optical system consists of a radiance source (tungsten filament lamp), a rotating disk, special diaphragms, a high-speed pyrometer, and other pertinent components.

The rotating disk has four circular slits of different widths (fig. 2). Because the simple milling of a slit may not produce an optically smooth edge, a fabrication technique was used in which four grooves of different width and depth were cut on a lathe on one side of a disk. The other side of the disk was then milled to a different depth in each quadrant and to a greater width than the groove. Cross section of the disk at the midplane of each slit is shown in figure 3. The disk was dynamically balanced.

The diaphragm (D in fig. 1) with a fixed rectangular opening defines the maximum aperture stop of the optical system. There are four individually adjustable diaphragms (fig. 4), which are used to vary the attenuation

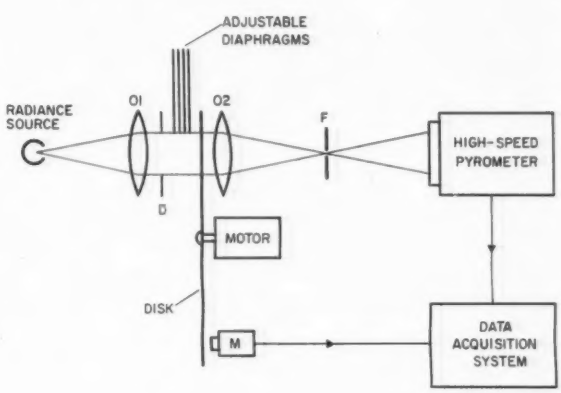


FIGURE 1. *Schematic diagram of optical system for generation of adjustable-amplitude radiance steps.*

ratio between the steps. The aperture stop at a given time is defined by the position of the adjustable diaphragms and the particular slit in the optical path. The lenses (01 and 02 in fig. 1) are 25 mm in diameter with $f/2.5$.

Rotation of the disk was synchronized with other measuring equipment by a signal obtained from a magnetic pickup. The magnetic pickup M (fig. 1) generated a signal each time a magnetic material embedded in the disk was in line with the pickup.

Relative radiance of the source after attenuation was measured with a high-speed photoelectric pyrometer.[1] The electrical signals from the pyrometer were recorded with a high-speed digital data acquisition system.[2] The combined measuring and recording system has a full-scale signal resolution of approximately one part in 8000 and a

[1] Foley, G. M., Rev. Sci. Instr. 41, 827 (1970).

[2] Cezairliyan, A., M. S. Morse, H. A. Berman, and C. W. Beckett, J. Res. Nat. Bur. Stand. (U.S.) 74A (Phys. and Chem.), 65 (1970).

time resolution of 0.4 ms. The photomultiplier in the pyrometer was alternately exposed to the radiance from the tungsten filament lamp and to the radiance from a reference lamp. This scheme eliminated errors that result from photomultiplier fatigue, etc.

A typical oscilloscope trace photograph of the pyrometer output for the case where the adjustable diaphragms are not in the optical path is shown in figure 5. Dots forming the short horizontal lines correspond to radiances from different slits. Dots forming the long horizontal lines correspond to radiances from the reference source.

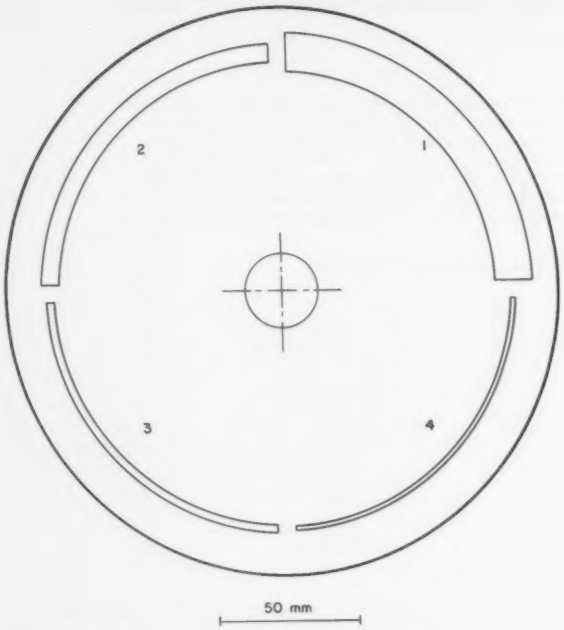


FIGURE 2. *Attenuator disk, showing effective opening of each slit.*

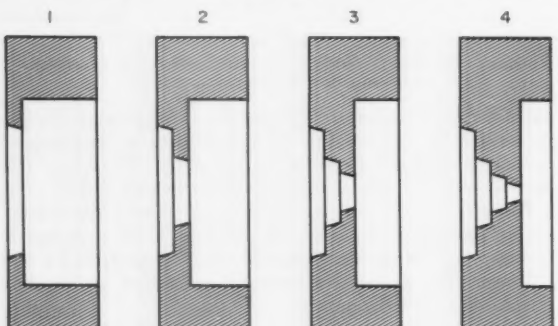


FIGURE 3. *Cross section of attenuator disk at midplane of each slit.*

Amplitude of the radiance pulses is proportional to the effective aperture stop. For the case in which the adjustable diaphragms are not in the optical path, the ratio of radiances corresponding to different slits is almost equal to the ratio of the slit widths. By inserting different diaphragms in the optical path by different amounts, the radiance ratios can be varied continuously.

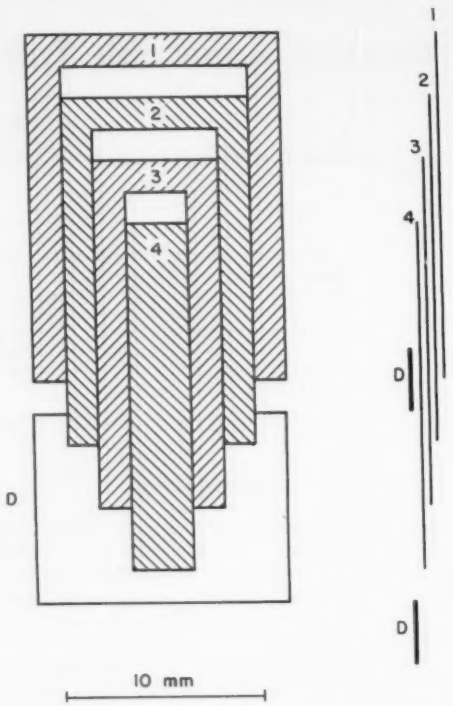


FIGURE 4. *The adjustable diaphragms.*

## 3. Experimental Results

In order to assess the operational characteristics of the optical attenuator system several experiments were conducted which are summarized in the following paragraphs.

Four experiments were performed at different disk speeds ranging from 500 to 1800 rpm. In all the experiments, the adjustable diaphragms were removed from the optical path. The experiments were similar to the one shown in figure 5. The experimental quantities obtained using the high-speed digital data acquisition system were processed with a computer.

Radiances obtained from four different slits enable the computation of six radiance ratios, $\tau_{ij}$, which are defined by

$$\tau_{ij} = \frac{L_j}{L_i} \tag{1}$$

where $L_i$ and $L_j$ are radiances corresponding to slits i and j respectively.

The ratio of radiances corresponding to various slits are given in table 1. It may be seen that, on the average, the results of four experiments are in agreement with each other within one part in 1000.

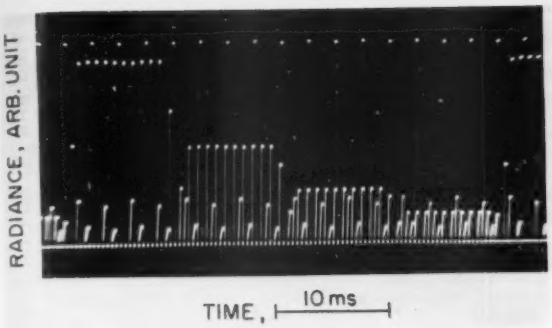


FIGURE 5. *Typical oscilloscope trace photograph of pyrometer output showing the four radiance steps.*

TABLE 1. *Radiance ratios corresponding to various slit combinations*

| $\tau_{ij}$* | Exp. 1 (1800 rpm) | Exp. 2 (1100 rpm) | Exp. 3 (750 rpm) | Exp. 4 (500 rpm) | Avg. of Four Expts. | Avg. Absolute Diff. (%) |
|---|---|---|---|---|---|---|
| $\tau_{12}$ | 0.5118 | 0.5118 | 0.5114 | 0.5108 | 0.5115 | 0.07 |
| $\tau_{13}$ | .2638 | .2634 | .2637 | .2633 | .2636 | .08 |
| $\tau_{14}$ | .1281 | .1279 | .1276 | .1278 | .1279 | .08 |
| $\tau_{23}$ | .5154 | .5147 | .5156 | .5154 | .5153 | .05 |
| $\tau_{24}$ | .2503 | .2498 | .2497 | .2503 | .2500 | .11 |
| $\tau_{34}$ | .4855 | .4854 | .4840 | .4856 | .4851 | .12 |

*$\tau_{ij}$ is defined by eq. (1); subscripts refer to slits as marked on figure 2.

Internal consistency of the results was checked by computing new ratios from a group of directly measured ratios according to the following relations:

$$\tau_{ij} = \frac{\tau_{ik}}{\tau_{jk}} \tag{2}$$

$$\tau_{ij} = (\tau_{ik})\ (\tau_{kj}) \tag{3}$$

$$\tau_{ij} = (\tau_{ik})\ (\tau_{kl})\ (\tau_{lj}) \tag{4}$$

For numerical calculations, ratios corresponding to the average of four experiments were used. A comparison of directly measured and computed radiance ratios is given in table 2. It may be seen that the agreement is better than 5 parts in 10,000.

The uniformity of the slits in the disk was checked under steady-state conditions using the same optical arrangement with the exception that an automatic photoelectric pyrometer was used. A total of 40 measurements were made at different slit positions. The results indicate that average radiance nonuniformity created by nonuniformities of the slits is less than 0.1 percent. The contribution of random noise of the high-speed pyrometer to an individual radiance measurement is approximately 0.2 percent. However, when a large number of points is averaged the reliability of the final result is better than 0.2 percent.

Several experiments were conducted in which the adjustable diaphragms were used to obtain different radiance ratios. Oscilloscope trace photographs of the high-speed pyrometer output are shown in figures 6, 7, and 8 for various diaphragm positions and combinations. In all cases, the individual diaphragms were either completely in or completely out of the optical path. By placing the diaphragms in intermediate positions continuous variation in the radiance ratios can be obtained.

## 4. Conclusions

The results of the experiments described show the feasibility of generating adjustable-amplitude radiance steps. Attenuation of the disk and adjustable diaphragms is independent of wavelength. The radiance ratio between steps can be adjusted continuously. Results of radiance ratio measurements at four disk speeds agree to 1 part in 1000.

The optical step attenuating system described in this paper allows determination of the linearity of a radiation detector under dynamic conditions. Because of its versatility in generating radiance pulses, this system may find application in experiments involving high-speed heating or cooling of specimens.

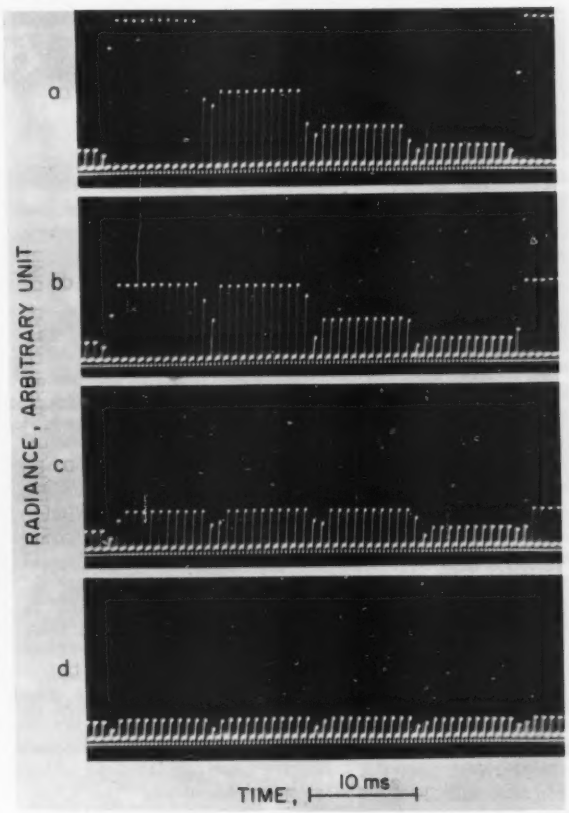


FIGURE 6. *Oscilloscope trace photographs of pyrometer output showing radiance steps corresponding to various adjustable diaphragm settings: (a) no diaphragm in optical path; (b) only diaphragm 1 in; (c) diaphragms 1 and 2 in; (d) diaphragms 1, 2, and 3 in.*

TABLE 2. *Comparison of radiance ratios determined from direct measurements and from combination of related ratios*

| $\tau_{ij}$* | Determined from direct measurements** | Determined from the Ratios | | | | Determined from the Products | | |
|---|---|---|---|---|---|---|---|---|
| | | $\frac{\tau_{13}}{\tau_{23}}$ | $\frac{\tau_{14}}{\tau_{24}}$ | $\frac{\tau_{14}}{\tau_{34}}$ | $\frac{\tau_{24}}{\tau_{34}}$ | $\tau_{13}\,\tau_{23}$ | $\tau_{23}\,\tau_{34}$ | $\tau_{12}\,\tau_{23}\,\tau_{34}$ |
| $\tau_{12}$ | 0.5115 | 0.5115 | 0.5116 | | | | | |
| $\tau_{13}$ | 0.2636 | | | 0.2637 | | 0.2636 | | |
| $\tau_{14}$ | 0.1279 | | | | | | | 0.1279 |
| $\tau_{23}$ | 0.5153 | | | | 0.5153 | | | |
| $\tau_{24}$ | 0.2500 | | | | | | 0.2500 | |
| $\tau_{34}$ | 0.4851 | | | | | | | |

*$\tau_{ij}$ is defined by eq. (1); subscripts refer to slits as marked on figure 2.
**Averages of four experiments are used.

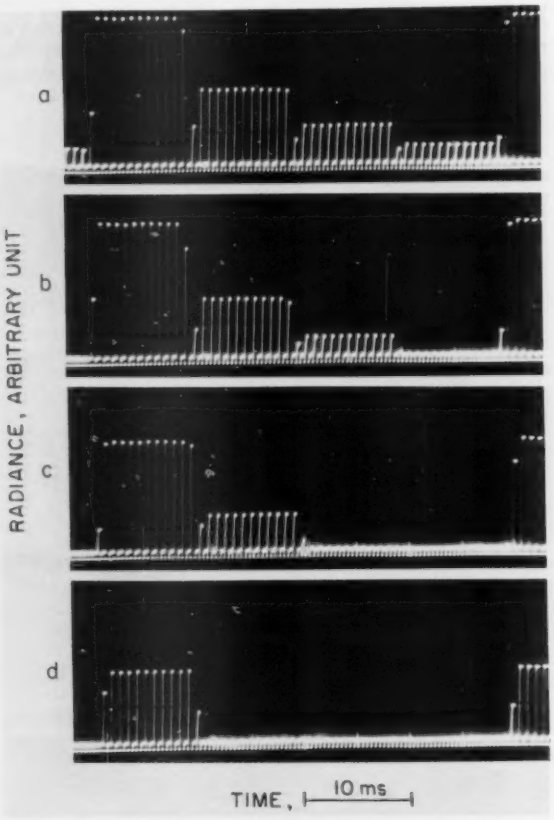


FIGURE 7. *Oscilloscope trace photographs of pyrometer output showing radiance steps corresponding to various adjustable diaphragm settings: (a) no diaphragm in optical path; (b) only diaphragm 4 in; (c) diaphragms 3 and 4 in; (d) diaphragms 2, 3and 4 in.*

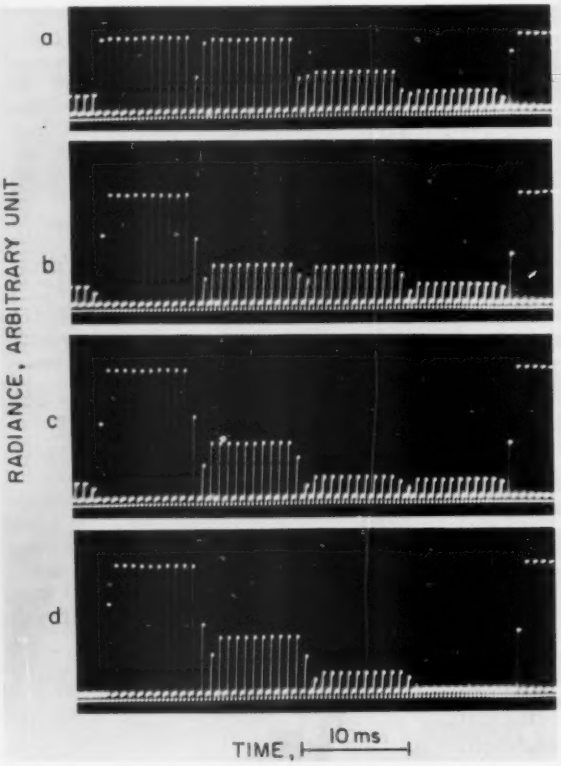


FIGURE 8. *Oscilloscope trace photographs of pyrometer output showing radiance steps corresponding to various adjustable diaphragm settings: (a) only diaphragm 1 in optical path; (b) only diaphragm 2 in; (c) only diaphragm 3 in; (d) only diaphragm 4 in.*

(Paper 75C2–316)

JOURNAL OF RESEARCH of the National Bureau of Standards—C. Engineering and Instrumentation
Vol. 75C, No. 2, April-June 1971

# An Improved Method for Microwave Power Calibration, With Application to the Evaluation of Connectors*

**Glenn F. Engen****

**Institute for Basic Standards, National Bureau of Standards, Boulder, Colorado 80302**

**(April 23, 1971)**

In the procedures for microwave power calibration, which are well documented, the subject of mismatch errors (or corrections) plays a major role. In particular, the evaluation of mismatch corrections requires the measurement of complex reflection coefficients; and the accuracy of this measurement is limited, in part, by connector imperfections.

The application of recently developed "power equation" methods to this problem provides both a simplified determination of the mismatch correction ($M_{gm}$) and improved accuracy. In particular, the intermediate step of measuring the reflection coefficients is eliminated, and the precision connector requirement is greatly relaxed. If this new method were adopted at each level of the usual calibration hierarchy, the accuracy of disseminating measurements referenced to the primary standards at NBS would be greatly improved.

The accuracy potential was demonstrated in a series of experiments involving the Type N, GPC-7, and waveguide flange connectors. The outcome of this experimental evaluation, in which the "ordinary" Type N performed on a par with GPC-7, raises some rather serious questions relative to current trends in connector development.

Key words: Calibration; connectors; mismatch; power equation; power measurement.

## 1. Introduction

The use of a calibration heirarchy, as means of disseminating measurements referenced to the primary standards at NBS, is a long established practice. Unfortunately, it is a general and apparently unavoidable feature of calibration heirarchies that the measurement accuracy is degraded at every step between the primary reference laboratory (NBS) and the field working level.

In the case of microwave power, the calibrated items are usually bolometer mounts or directional coupler-bolometer mount combinations. Here the practical problems, in comparing one mount against another for example, are substantial, and the relative loss in accuracy at each step is much larger than occurs in other parameters such as mass or d-c voltage. Indeed, although reliable data are not available, the probable loss in accuracy appears to be such that serious questions have been raised about the usefulness of the calibration heirarchy (for this parameter) other than that of satisfying the contractual requirement for measurement "traceability."

Much of this difficulty centers around the problem of "mismatch" corrections. Until recently, there has been no simple and direct method of measuring and applying this correction. The approach has sometimes been a hybrid one of adjusting for a generator match, then measuring the other parameters. More often, particularly at the lower levels, this correction is ignored and thus becomes an error whose magnitude depends upon the attendant impedance parameters, and whose total value may be substantial if permitted to accumulate throughout the hierarchy.

It is the purpose of this paper to review this problem from the viewpoint of the recently developed "power equation" technology [1][1] and present a simplified, yet more accurate, method of measuring the mismatch factor.

## 2. General Description

The measurement problem is conveniently visualized with the help of figure 1. The measurement cycle usually begins with a "standard" power meter which may be either in the form of a calorimeter [2], or of the bolometric type, where the bolometer mount properties have been evaluated by microcalorimetric [3] or impedance [4] methods. The standard power meter is used to calibrate a signal generator, this, in turn, is used to calibrate another power meter. This item is then sent to another calibration laboratory where it becomes the reference standard and the process is repeated.

With regard to the signal generator calibration, it may be noted that microwave generators do not ordinarily possess sufficient stability to warrant their calibration as such. The signal generator calibration, which is obtained in the calibration transfer from one power meter to another, may thus be of interest only during the measurement procedure and not even explicitly extracted from the

*Presented at the 1970 Fall Meeting of URSI, September 15-17, Ohio State University, Columbus, Ohio, 43210.

**Electromagnetics Division, Senior Research Scientist, National Bureau of Standards, Boulder, Colo. 80302.

[1] Figures in brackets indicate the literature references at the end of this paper.

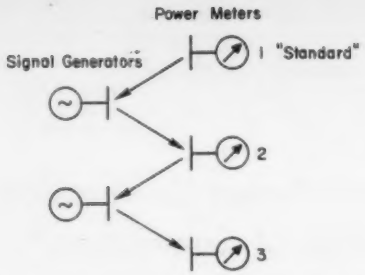


FIGURE 1. *Illustrating the power calibration hierarchy.*

measurement data. There is no loss in generality, however, in describing the procedure in this framework.

Alternatively, the signal source may be provided with an output monitor—in the form of a directional coupler and side-arm power meter, for example. Here the "generator calibration" is in reality a calibration of this output monitor, and is usually of future interest. This, in fact, is the recommended mode of operation and will be explained in greater detail in what follows.

Returning to figure 1, it is tempting, and in many cases correct, to interpret the column of power meters as the "working" or "interlaboratory" standards for the several echelons in the calibration hierarchy. It is also noted, however, that the number of calibration steps is reduced by approximately one-half when the calibrated signal generator is adopted as the working standard at the alternate levels. This should also reduce the error accumulation, but at present, there is no universally accepted practice in this matter.

Each step of the "power equation" calibration procedure is described by the equation,

$$P_{gm} = P_g M_{gm}, \tag{1}$$

where $P_{gm}$ is the (net) power absorbed by the meter, $P_g$ is the *available* power from the signal generator, and $M_{gm}$ is a "mismatch" factor which expresses to what extent the conditions for maximum power transfer between generator and termination (power meter) are satisfied. It should be noted that $P_g$ is a property of the generator only, while $M_{gm}$ (and thus $P_{gm}$) is a property of the signal generator and power meter combination.

In the first step, the "first" generator and standard power meter are mated. Subject to certain efficiency corrections, the standard power meter indicates $P_{gm}$, and if $M_{gm}$ is also known, $P_g$ may be obtained from (1).

In the second step, the first generator is connected to the second power meter. Assuming the $M_{gm}$ for this combination of components is measured, $P_{gm}$ may be determined from (1) since $P_g$ is a property of the generator only. The calibration of this second meter is now obtained by comparing its reading with the value of $P_{gm}$ thus obtained. This process is repeated at each calibration laboratory. It will be immediately recognized that the determination of $M_{gm}$ plays a major role in this procedure.

## 3. Measurement of $M_{gm}$

As already noted, the recommended "signal generator" includes an output monitor which is usually a directional coupler with a bolometric detector or power meter on the sidearm as shown in figure 2. It is convenient (but not essential) to postulate feedback such that this sidearm power is constant. It has been shown [5] that the impedance of the "equivalent generator" which obtains at the output port (2) depends only on the coupler parameters and is independent of the actual signal source. The available power, at the output port, also depends only on the coupler parameters and is linearly related to the sidearm power level. For these reasons, it is convenient to interpret the measurement of the pertinent coupler parameters as a signal generator calibration.

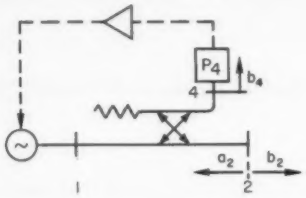


FIGURE 2. *Signal generator with output "Monitor"*

The sidearm detector and power meter to be calibrated are often of the bolometric type. Although the attendant problems are by no means trivial, they are well understood and the associated instrumentation is highly developed [6]. The major existing problems are associated with the measurement of $M_{gm}$. Here the power meter mismatch, imperfect coupler directivity, connector imperfectons, etc. enter the picture.

A measurement of $M_{gm}$ may be effected by the addition of a second coupler, power detector ($P_3$), and tuning transformer as shown in figure 3. With the power meter, for which $M_{gm}$ is required, connected to port 2, tuner $T_y$ is adjusted such that $P_3$ vanishes.[2] This power meter is next replaced by a moving short. In response to motion of the short, $P_3$ will undergo cyclic variations of which the maximum, $P_{3M}$, and minimum, $P_{3m}$, values are observed.

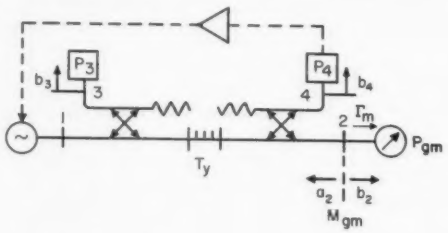


FIGURE 3. *Addition of a second coupler and tuning transformer ($T_y$) to permit the measurement of $M_{gm}$.*

In the following section, it will be shown that $M_{gm}$ is given by:[3]

$$M_{gm} = 1 - \left[\frac{\sqrt{P_{3M}} - \sqrt{P_{3m}}}{\sqrt{P_{3M}} + \sqrt{P_{3m}}}\right]^2. \tag{2}$$

[2] Ordinarily, the ratio of the power meter reading to $P_4$ will also be obtained at this time as part of the overall calibration procedure.

[3] In the event that $P_4$ is not constant $P_{3M}$ and $P_{3m}$ should be replaced by $\left(\frac{P_3}{P_4}\right)_M$ and $\left(\frac{P_3}{P_4}\right)_m$.

It is to be emphasized that this procedure *completely* accounts for arbitrary power meter impedance, imperfect coupler directivity and impedance, and for connector imperfections, provided only that the connector dissipation is repeatable.[4]

It is of interest to note that the expression in the parenthesis is also that used to convert VSWR to reflection coefficient. It is thus possible to visualize the procedure in the context of a matched (reflectionless) generator, slotted line, and mismatched load. The slotted line is used to measure the load VSWR, from which the reflection coefficient, $\Gamma$, is obtained. The mismatch factor, M, is then computed from the equation:

$$M=1-|\Gamma|^2. \tag{3}$$

## 4. Analysis

It is the purpose of this section to provide the theoretical basis for the described procedure.

Beginning with the directional coupler of figure 2, a solution of the scattering equations yields:

$$b_2=\frac{b_4}{D}-\frac{C}{D}\,a_2 \tag{4}$$

where $C$, $D$ are functions of the coupler scattering parameters, and the reflection coefficient of the power detector terminating arm 4, *but not of the generator which feeds arm 1.*

In general the equation for a source is written

$$b_2=b_g+a_2\Gamma_g \tag{5}$$

where $b_g$ is the "generator wave," and $\Gamma_g$ the source reflection coefficient [8]. Comparison of (4) and (5) indicates that:[5]

$$\frac{b_4}{D}=b_g \tag{6}$$

$$-\frac{C}{D}=\Gamma_g \quad . \tag{7}$$

Equation (4) may be solved for $b_4$ to obtain

$$b_4=Ca_2+Db_2 \tag{8}$$

Referring next to figure 3, $b_3$ is also expressible as a linear combination of $a_2$, $b_2$

$$b_3=Aa_2+Bb_2 \tag{9}$$

and taking the ratio of (9) and (8) leads to

$$\frac{b_3}{b_4}=\frac{A\Gamma_l+B}{C\Gamma_l+D} \tag{10}$$

where $\Gamma_l$ is the reflection coefficient of the termination on port 2, i.e.,

$$\Gamma_l=\frac{a_2}{b_2}. \tag{11}$$

Equation (10) is the usual starting point in reflectometer theory [9].

By hypothesis, $Ty$ is adjusted[6] such that $b_3$ ($P_3$) vanishes when $\Gamma_l$ equals the power meter reflection coefficient, $\Gamma_m$. Therefore,

$$B=-A\Gamma_m. \tag{12}$$

With the sliding short connected to the output port (2), $\Gamma_l=e^{i\theta}$, where $\theta$ is determined by the short position.[7] Substitution in (10) yields:

$$\frac{b_3}{b_4}=\frac{Ae^{i\theta}+B}{Ce^{i\theta}+D}\equiv\frac{BD^*-AC^*}{|D|^2-|C|^2}+\\ +\frac{(AD-BC)e^{i\theta}(D^*+C^*e^{-i\theta})}{(|D|^2-|C|^2)(D+Ce^{i\theta})}. \tag{13}$$

By inspection

$$\left|\frac{b_3}{b_4}\right|_{max}=\left|\frac{BD^*-AC^*}{|D|^2-|C|^2}\right|+\left|\frac{AD-BC}{|D|^2-|C|^2}\right| \tag{14}$$

and combining this with (7) and (12) leads to:

$$\left|\frac{b_3}{b_4}\right|_{max}=\left|\frac{A}{D}\right|\frac{(|1-\Gamma_m\Gamma_g|+|\Gamma_m-\Gamma_g^*|)}{(1-|\Gamma_g|^2)} \tag{15}$$

It is easy to show that the first term in the numerator exceeds the second if $|\Gamma_g|<1$, $|\Gamma_m|<1$; therefore:

$$\left|\frac{b_3}{b_4}\right|_{min}=\left|\frac{A}{D}\right|\frac{(|1-\Gamma_m\Gamma_g|-|\Gamma_m-\Gamma_g^*|)}{(1-|\Gamma_g|^2)} \tag{16}$$

Finally:

$$1-\left[\frac{\left|\frac{b_3}{b_4}\right|_{max}-\left|\frac{b_3}{b_4}\right|_{min}}{\left|\frac{b_3}{b_4}\right|_{max}+\left|\frac{b_3}{b_4}\right|_{min}}\right]^2=1-\left|\frac{\Gamma_m-\Gamma_g^*}{1-\Gamma_m\Gamma_g}\right|^2 \tag{17}$$

and

$$1-\left|\frac{\Gamma_m-\Gamma_g^*}{1-\Gamma_m\Gamma_g}\right|^2\equiv\frac{(1-|\Gamma_g|^2)\,(1-|\Gamma_m|^2)}{|1-\Gamma_m\Gamma_g|^2} \tag{18}$$

This last expression will be recognized as the conversion factor between the *available* power and the *net* power delivered to the load $\Gamma_m$ [10]. It is thus equal to $M_{gm}$.

## 5. An Alternative Procedure for Measuring $M_{gm}$

For the sake of completeness, the existence of an alternative procedure for measuring $M_{gm}$ should be noted.

Returning to figure 3, $Ty$ is adjusted such that the ratio $P_3/P_4$ is constant with respect to the motion of a short at arm 2. Then it has been shown [1, 11] that $M_{gm}$ is given by:

$$M_{gm}=1-\frac{\left[\frac{P_3}{P_4}\right]_m}{\left[\frac{P_3}{P_4}\right]_s} \tag{19}$$

where the subscripts $m$, $s$ represent the values of $P_3/P_4$ with the meter and short connected respectively.

---

4 Impedance properties of the connector are not a consideration. For a more complete discussion see [1] and [7].

5 The (implicit) definitions for C, D have been chosen in such a way as to permit a ready comparison with a number of earlier results.

6 It is important to note that this adjustment of the ratio $B/A$ does not affect the values of $C$, $D$ since these are parameters only of the coupler on the right.

7 The short is assumed to be lossless. A theory which accounts for this loss has been developed; however the error due to this source, in this application, is negligible.

As compared with the previous method, the prescribed adjustment of $Ty$ is more difficult to realize, but once obtained is the same for all terminations (power meters). A more complete description is found in the references (e.g., [1, 7, 9, 11]); the discussion which follows pertains entirely to the first procedure. Finally, it is possible to eliminate the tuning operation entirely if the phase difference between $b_3$ and $b_4$ is measured. This, however, is the subject of a paper to follow.

## 6. Experimental Evaluation

A series of tests have been made of this technique which will now be described. The initial objective was to demonstrate the performance potential in a simulated calibration hierarchy using "ordinary" waveguide hardware. To this end a frequency of 9 GHz and the type "N" connector were chosen.

Referring to figure 1, six power meters and six "signal generators" were prepared. The calibration was propagated through the simulated hierarchy as described, and the last (sixth) item then compared directly against the first. This provided an indication of the error accumulation in the process. (It should be noted that an "absolute" calibration of the first item (standard) was not required.)

The components comprising the "signal generators" (figure 3) were in waveguide with a transition to type "N" at the output port. Although a recently improved version of the type "N" was incorporated in several of the components, a substantial number of the items had been in use for many years. The "equivalent generator" VSWR included values as large as 2.5. Finally, the powers $P_3$, $P_4$ were measured with Type II NBS bridges [6].

The "six level" experiment outlined above was repeated four times and gave error accumulations of 0.33 percent, —0.23 percent, 0.66 percent, and 0.43 percent. The mean of these values is 0.30 percent, while the standard deviation is 0.48 percent.

The design was also such as to permit a comparison of the relative error contributions of the individual components. Within the sensitivity of experiment, there was no deterioration in accuracy with the "older" connectors as compared with the more recent versions, or with the poorly matched generators as compared with those of small VSWR.

Although the above analysis has some intuitive appeal, considerably more information can be obtained through a more sophisticated analysis based on the method of least squares. Here an estimate of the standard deviation of a single calibration transfer from one meter, through a generator, to the next meter is obtained. For the first experiment this standard deviation, of a single calibration transfer, is 0.12 percent.

It was next decided to repeat the experiment with a group of "improved" Type N connectors (all of which were of the same model). The repeated experiment gave a standard deviation, for a single transfer, of 0.46 percent: four times the previous result. Examination of the results showed, however, that one of the connectors was contributing a major share of the total error. Fortunately, the experiment was designed in such a way that the effect of individual connectors could be both recognized and deleted. When this was done, the standard deviation became 0.22 percent.

The experiment was then repeated a third time with a different set of "improved" Type N connectors. The results were essentially identical to those obtained in the second run: one connector was defective, and when this was eliminated the standard deviation was 0.24 percent.

In the fourth experiment, the GPC–7 connector was substituted for the Type N; this gave a standard deviation of 0.13 percent. Finally, the experiment was repeated a fifth time in waveguide using conventional flange connectors. This gave a standard deviation of 0.054 percent. In the fourth and fifth experiments, three "outlying observations" were discarded, but these were single measurements rather than all measurements associated with one connector as had been eliminated in experiments two and three.

Thus far the discussion has been primarily concerned with the random error; however, the quoted results of the first experiment raise the question of a possible systematic component as well.

Because the same measurement procedures are employed with both "standard" and "unknown," there is no apparent source of systematic error other than possible instabilities of the several components (bolometer elements, etc.) with respect to time. A further analysis of the results shows that the postulated absence of systematic error is not rejected with 95 percent confidence. Stated in other words, the "apparent" systematic errors observed in the experiments are easily explained by the random errors observed.

The results of the five experiments are summarized in table 1. Again it is emphasized that this method is, in theory, independent of impedance discontinuities in the connector. Thus these figures reflect only the nonrepeatability of the power *dissipation* at the connector interface.

Although the primary emphasis in the experiment was on dissipation repeatability, it is possible to infer something about the impedance repeatability from the repeatability of the mismatch factor ($M_{gm}$).

Unfortunately, the design of the experiment was such as to provide only a minimal amount of information on

TABLE 1. *Measurement results*
(Ability to effect a single calibration transfer)

| Connector | Estimate of standard deviation | 95% Confidence interval for standard deviation |
|---|---|---|
| Type N (Mixed) | 0.12% | (0.091%, 0.18%) |
| Improved Type N (Model 1) | .22% | ( .16%, .34%) |
| Improved Type N (Model 2) | .24% | ( .18%, .37%) |
| GPC-7 | .13% | ( .10%, .18%) |
| Waveguide | .054% | ( .042%, .076%) |

this point, but the results were consistent with expectation. In particular, the waveguide joint showed a marked improvement over the GPC–7, and the GPC–7, some improvement over the Type N. Perhaps of greater interest is the result that three of the Type N connectors showed a substantially poorer mismatch factor repeatability than was typical of the group; in only one case, however, was this accompanied by poorer dissipation repeatability.

Although it is not within the scope of this paper to describe these experiments in greater detail, it is anticipated that this will be included in a later paper. In brief, the pertinent conclusions are:

(1) For a single calibration transfer at NBS, standard deviations of 0.12 percent to 0.25 percent were observed in coax, and 0.054 percent in waveguide. Errors much larger than $\pm 3\sigma$ were occasionally recorded. It appears that the type of connector is a significant factor, but this awaits confirmation. In retrospect it would have been desirable to have used a random ordering instead of segregating the several connector types into separate sequences. The initial objective, however, was to demonstrate the performance potential of the method, rather than make a comparative evaluation among different connector types.

(2) There is no evidence that the taking of several power readings and averaging the results contributed anything to the precision (other than as a guard against errors in data taking). Presumably, however, the precision would be improved by repeating the experiment "from scratch."

(3) No evidence of systematic error was observed during this experiment, which was of such size and precision that a systematic error of the order of 0.1 percent should have been detected. (Note, however, this paper deals only with the calibration transfer process, and says nothing about systematic errors in the reference standard.)

(4) Several of the connectors suffered from apparent problems in the area of dissipation repeatability. The source of this difficulty could not be recognized by a simple visual inspection.

## 7. Summary

A simplified method of disseminating power calibration has been described. This procedure may be regarded as a detailed example of the *power equation* concept. The key feature of this technique is the "direct" measurement of the mismatch factor ($Mgm$) which eliminates the intermediate step of measuring the complex reflection coefficients. The performance potential was demonstrated in a series of experiments at 9 GHz.

Although the hardware requirements present no fundamental difficulty, the technique does call for certain equipment which is not the most common. In particular it is necessary to postulate either a stabilized (leveled) source (with respect to arm 4) or alternatively a direct method of obtaining $P_3/P_4$ is desirable. In addition, coaxial sliding shorts have found but limited application in the existing art. Whereas the method provides a substantial improvement in the accuracy potential with "conventional" hardware components, the associated bolometer bridges, etc. must be of high quality if this potential is to be achieved.

The measurement procedure is simple enough to envision its use at the field level; here the component tolerances are usually the poorest, and the greatest projected benefits may be obtained. A series of measurements at NBS has demonstrated that it is now "possible" to propagate a power calibration through a typical calibration hierarchy with an error accumulation of 0.5 percent or less. (Obviously, however, unless this or a comparable technique is used, and appropriate quality control is maintained at each level, this potential will not be realized.)

Finally, the results of the experimental evaluation raises some rather serious questions relative to current trends in connector development. In particular, in terms of the requirements of this method and these experiments, several "improved" Type N connectors did rather poorly as compared with the "ordinary" Type N, while the GPC–7 was only on a par with it.

The reasons for the "poor" performance of the "improved" Type N is uncertain at this time. It may be associated with the use of stainless steel in its construction. In any case a further study of this subject is desirable.

---

The author expresses his appreciation to M. P. Weidman for the experimental results described above, to B. L. Joiner and P. V. Tryon of the Statistical Engineering Laboratory for their contribution to the design of the experiments and interpretation of results, and to L. E. Huntley for his contribution in the preparation of this manuscript.

## 8. References

[1] Engen, G. F., Power equations: A new concept in the description and evaluation of microwave systems, IEEE Trans. on Instrumentation and Measurement **IM-20,** No. 1, (Feb. 1971).

[2] Crawford, M. L., A new RF-DC substitution calorimeter with automatically controlled reference power, IEEE Trans. on Instrumentation and Measurement **IM-17,** No. 4, 378–384 (Dec. 1968).

[3] Engen, G. F., A refined X-band microwave microcalorimeter, J. Res. Nat. Bur. Stand. (U.S.), **63C** (Eng. and Instr.), No. 1, 77–82 (July-Sept. 1959).

[4] Engen, G. F., A bolometer mount efficiency measurement technique, J. Res. Nat. Bur. Stand. (U.S.), **65C** (Eng. and Instr.), No. 2, 113–124 (April-June 1961).

[5] Engen, G. F., Amplitude stabilization of a microwave signal source, IRE Trans. Microwave Theory and Techniques, **MTT-6,** No. 2, 202–206, (April 1958).

[6] Larsen, N. T., and Clague, F. R., The NBS type II power measurement system, Proceedings 25th Annual ISA Conference.

[7] Engen, G. F., An introduction to the description and evaluation of microwave systems using terminal invariant parameters, Nat. Bur. Stand. (U.S.), Monogr. 112, 25 pages (Oct. 1969).

[8] Kerns, D. M., and Beatty, R. W., Basic Theory of Waveguide Junctions and Introductory Microwave Network Analysis, (Pergamon Press, New York, 1967) p. 51.

[9] Engen, G. F., and Beatty, R. W., Microwave reflectometer techniques, IDS Trans. Microwave Theory and Techniques **MTT-7,** 351–355 (July 1959).

[10] Kerns, D. M., and Beatty, R. W., loc. cit., p. 56.

[11] Engen, G. F., A transfer instrument for the intercomparison of microwave power meters, IRE Trans. Instrumentation **I-9,** No. 2, 202–208 (Sept. 1960).

(Paper 75C2–317)

JOURNAL OF RESEARCH of the National Bureau of Standards—C. Engineering and Instrumentation
Vol. 75C, No. 2, April-June 1971

# Apparatus for Impact-Fatigue Testing*

**R. E. Schramm,** R. L. Durcholz,** and R. P. Reed****
**Institute for Basic Standards, National Bureau of Standards, Boulder, Colorado 80302**

(December 29, 1970)

A standard impact machine was extensively modified to allow the measurement of the response of specimens to repeated, controlled impact pulses. This equipment enables one to vary the temperature (76-297 K), specimen geometry (uniaxial, biaxial, triaxial stress systems), and load levels. At stress levels in the neighborhood of the yield stress, on the order of 10,000 impact cycles are needed to fatigue specimens to fracture. Strain rates achieved are moderately high, of the order of 1000 $min^{-1}$, which conveniently form intermediate data between tensile (max. of about 100 $min^{-1}$) and explosive straining data (about 6000 $min^{-1}$). Contrasted to standard fatigue tests, no constraint is placed on specimen elongation and only unidirectional stresses are imposed. Typical impact-fatigue results for AISI 310 stainless steel are presented.

Key words: Cryostat; fatigue; impact; low temperature; mechanical property equipment; stainless steel.

## 1. Introduction

In many low temperature applications such as in the transportation of dewars or in the transfer of cryogenic liquids through pipe, system components experience periodic sudden jolts or loads. Prediction of expected life of these components can best be accomplished by testing controlled specimens under repeated impact loads which approach values up to the yield load. Such a test, then, can be described as impact-fatigue, as the specimen eventually fractures in a manner similar to conventional fatigue fractures.

To perform such tests, a standard commercial impact machine was extensively modified. These modifications resulted in an apparatus that could repeatedly apply sudden loads in the range 0 to 1800 kg for the long periods sometimes required for specimen fracture. Additionally, the specimen chamber was insulated to allow temperature environments from 76 to 297 K. Our paper describes this new equipment.

A standard Riehle model PI-2[1] impact testing machine was available. This machine has three hammer sizes, 15, 30, and 60 lb (6.8, 13.6, and 27.3 kg) and the hammer drop is continuously adjustable from 0 to 48 in (0 to 1.3 m). Our impact-fatigue life determinations, however, would require a frequency greater than 20,000 in some cases so it became obvious that the single cycle operation for which this machine was designed was not feasible. We designed major modifications to automate the repetition, to allow tests to be conducted at cryogenic temperatures, and to permit the use of specimens in a great variety of configurations. Stress pulses are applied to the specimen in one direction, while the conventional fatigue tests are typically either "push-pull" with alternating tensile and compressive forces or flexure with alternating applied bending forces. Another feature of the impact-fatigue test is that the specimen is not constrained with respect to specimen strain.

## 2. Modifications

Figure 1a is a schematic view of the impact-fatigue tester. A 1/6 hp, 1725 rpm electric motor is geared to

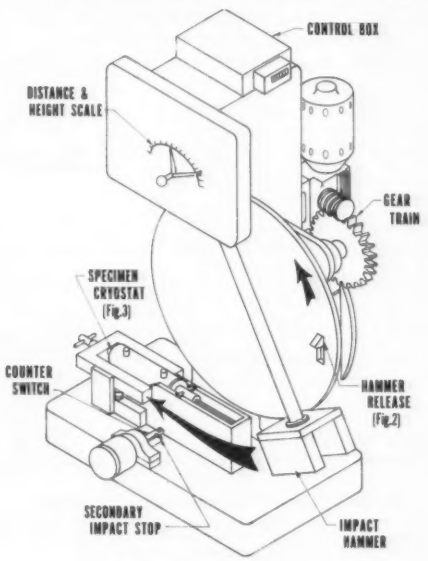


FIGURE 1a. *Schematic view of impact-fatigue tester.*

* This work was carried out at the National Bureau of Standards under contract to the Naval Air Engineering Center, Philadelphia, Pennsylvania 19100.

** Cryogenics Division, National Bureau of Standards, Boulder, Colo. 80302.

[1] The use of trade names in this paper in no way implies endorsement or approval by NBS and is included only to define the experimental procedure.

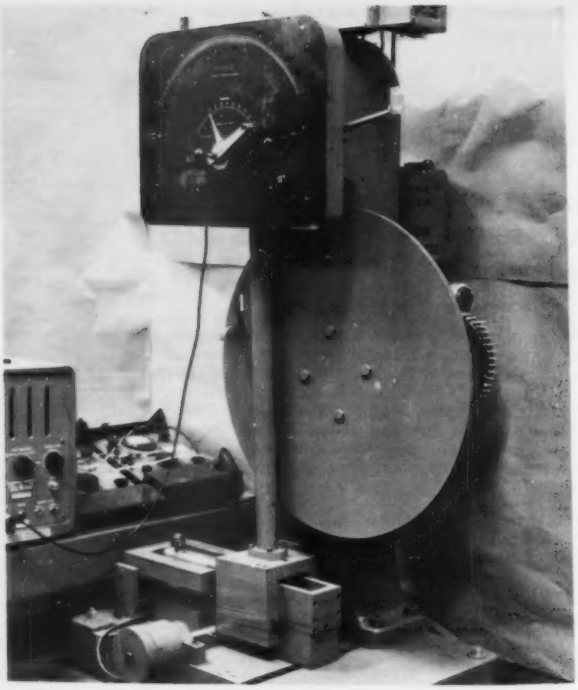

FIGURE 1b. *Photograph of impact-fatigue tester.*

rotate a 24-in diam wheel at 7.3 rpm. The shaft and bearings which support this wheel are clamped to the upright part of the impact machine frame by U-bolts. A brass hammer release arm protruding through the outer edge of this moving wheel serves to pick up the hammer and raise it to a predetermined height. At this point, the trip arm

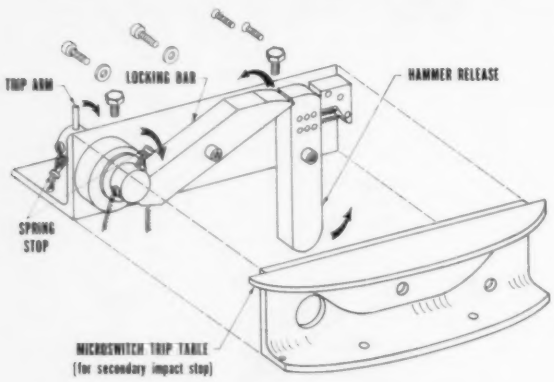


FIGURE 2. *Impact hammer release mechanism.*
The trip arm is rotated by a stationary block fixed at the desired position behind the 24-in wheel. This allows the hammer release to fall back under the hammer weight. Springs then return the mechanism to a locked position.

(figure 2) encounters a block which is supported behind the rotating wheel. The trip arm rotation causes a cam motion which swings a locking bar out of position, allowing the hammer release to simply fall back under the weight of the hammer. A second trip block is at the top of the wheel's revolution to insure that the system does not bind there as it passes the pendulum shaft. After each trip, springs pull the release bar back into a locked position to repeat the cycle.

The standard anvil on the base of the impact machine has been closed off on the right end to serve as the fixed point to which the right specimen pull rod is anchored, either directly or through a load cell (figure 3). The left pull rod passes through a three piece impact yoke assembly held together by eight ¼-in stainless steel bolts. The hammer impact is absorbed by this yoke which transmits it to the specimen, since it is free to move in a right-left direction on four rollers. When the sample breaks, the yoke moves to the left and allows the hammer to strike a switch on the base which removes electrical power from the whole system.

A solenoid system prevents secondary impact by the recoiling hammer (figure 1a). This stop is a ¾-in round bar which rides in a brass bushing inserted into a drilled hole in the impact machine. When this bar is in the fully inserted position, the impact hammer cannot swing past it to strike the yoke. A portion of the bar has a flat depression ground into it so that when the solenoid is activated and the bar partially withdrawn from the anvil the hammer may pass by freely. A switch on the stationary wheel near the block that trips the hammer release mechanism controls the power to the solenoid. As the trip table (figure 2) passes by this switch, the secondary stop is removed from the impact hammer path. By the time the hammer has recoiled, power has been removed from the solenoid and springs have pushed the stop back into position. A pin through this bar operates another switch to advance a cycle counter.

Wherever possible, the springs in the hammer-release mechanism were doubled, so if one fails during a test the second will continue to function until repairs can be made. It is important to use high quality steel springs to minimize difficulty due to breaks; soft, tempered springs were found more reliable than high strength units. Since this modification results in a much higher repetition rate than was originally intended, the welds between the pendulum shaft and fittings on both ends were reinforced.

## 3. Cryostat

The cryostat used for 76 K tests consisted simply of a 2-in diam PTFE rod, 7 inches long, with a 1-in bore through the center. The specimen pull rods are supported and

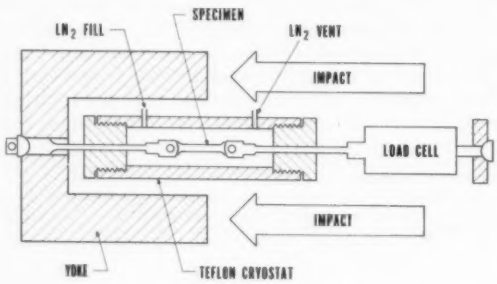


FIGURE 3. *Specimen impact system.*

centered by PTFE end caps screwed into the main chamber (figure 3). Rubber O-rings in both of these caps served as an initial seal around the pull rods to minimize the loss of liquid nitrogen. However, in cooling to 76 K, the PTFE contracts considerably and then serves as the main seal. Because of this great contraction, it is necessary to check for free movement of the pull rods when they are at test temperatures. Two small holes in the side wall serve for filling with liquid nitrogen and venting. A liquid flow of about 6l/hr was generally used to maintain temperature. At room temperature this cryostat was still used to assure the proper positioning of the sample.

For 195 K tests, a slight modification of this system was employed. Instead of the small holes in the side wall for filling and venting nitrogen, a $1 \times 4$ in panel was removed. A polystyrene foam box was attached to act as a reservoir for the powdered dry ice used to fill the cryostat. Consumption in this case was about 0.2 kg/hr.

## 4. Discussion

We used a load cell specially constructed to withstand sudden impacts and a high speed recorder to measure impact loading. When using the 30 lb (13.6 kg) hammer, the impulse time is about 2ms. Load cell response (figure 4) indicates a damped ringing, but this is a characteristic of the load cell. While the specimen probably does vibrate in the uniaxial direction, our system is incapable of measuring the compressive forces it may experience, but they are believed to be very small.

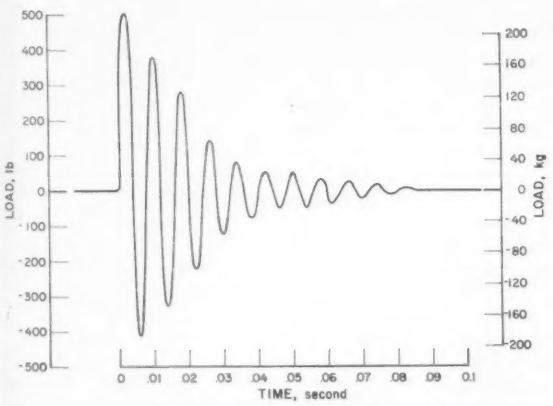


FIGURE 4. *Time response curve recorded by load cell and high speed recorder.*

During the progress of a test the specimen undergoes plastic strain. This allows the yoke to move in the direction of motion of the impact hammer. Thus, by measuring the position of the yoke frequently during a test, it is possible to determine specimen strain as a function of the number of cycles. Naturally, this function depends on variables such as material, temperature, and applied pulse. Figure 5 illustrates a typical curve of strain versus number of cycles for an AISI 310 stainless steel specimen. Initially, the specimen undergoes considerable strain but, after sufficient work hardening (several hundred cycles), its length becomes nearly constant.

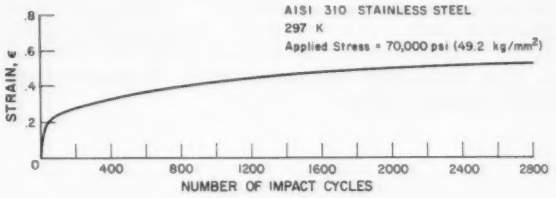


FIGURE 5. *Specimen strain during impact-fatigue life.*

Since each cycle corresponds to a 2 ms impulse time, the coordinate giving the number of cycles is also a time coordinate and its slope gives the strain rate. With our experimental conditions, the maximum initial strain rate was 2100 $min^{-1}$. This is conveniently intermediate between the maximum strain rate in tensile tests of about 100 $min^{-1}$ and the approximate lower limit [2] in explosive straining of 6000 $min^{-1}$.

From the strain readings and load calibration, a typical stress-strain curve may be constructed. Figure 6 shows this curve for AISI 310 at 297 K. The stress used to construct this curve is the engineering stress, i.e., load divided by original area. This stress level is constant throughout the test.

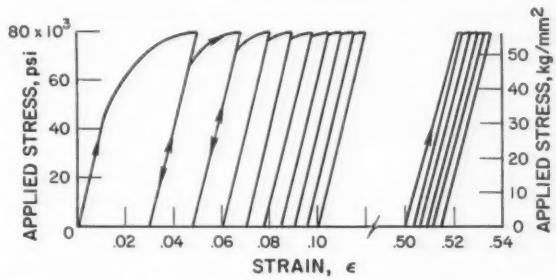


FIGURE 6. *Typical stress-strain curve for AISI 310 stainless steel showing repeated impact cycles at 297K (1 kg/mm² = 9.8 × 10⁶ N/m²).*

Compressive stresses due to recoil of specimen upon itself are very small and not shown.

[2] E. K. Henriksen, I. Lieberman, J. F. Wilkin, and W. B. McPherson, Metallurgical Effects of Explosive Straining, in Symposium on Dynamic Behavior of Materials (ASTM Spec. Tech. Pub. No. 336, 1963), p. 104.

By varying the height of the hammer (stress amplitude), a typical fatigue (S–N) curve of stress level versus number of cycles to failure may be obtained. The shape of such curves for AISI 310 at 297, 195 and 76 K, as shown in figure 7, is very similar to those obtained by conventional fatigue tests in which the high strain rates are not achieved and either the load or specimen deflection amplitude is held constant.

Any specimen configuration, limited only by length (about 5 in), may be measured. In practice, we have measured both uniaxial (tensile), biaxial, and triaxial (notch tensile) specimens of both AISI 304 and 310 stainless steels at 76, 195, and 297 K. These test results will be published later.

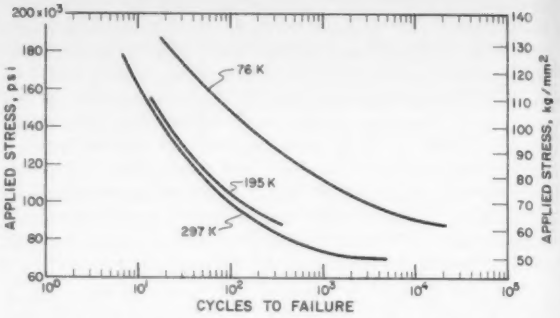


FIGURE 7. *Fatigue life curve for AISI 310 at 297, 195, and 76 K.*

(Paper 75C2–318)

JOURNAL OF RESEARCH of the National Bureau of Standards—C. Engineering and Instrumentation
Vol. 75C, No. 2, April-June 1971

# A Program in Refractory Metal Thermocouple Research*

**G. W. Burns and W. S. Hurst**

**Institute for Basic Standards, National Bureau of Standards, Washington, D.C. 20234**

**(February 8, 1971)**

A refractory metal thermocouple research program, directed towards establishing the parameters that are necessary to achieve reliable, long term, high temperature thermocouple performance, is outlined. A description of special apparatus for exposing bare-wire thermoelements to high temperatures in vacuum and in high purity gaseous environments is given, and the design and performance of an ultra-high-vacuum, high-temperature furnace system are described. Bare-wire W–3 percent Re and W–25 percent Re thermoelements were exposed at 2400 K in argon, hydrogen or vacuum, and experienced a shift in their emf-temperature relationship upon initial exposure. After the initial shift, the thermoelements exposed in the gaseous environments experienced no significant further change in their emf-temperature relationship for periods up to 1000 hours. The thermoelements exposed in vacuum continually drifted in their emf-temperature relationship as a result of the preferential loss of Re by evaporation.

Key words: EMF-temperature relationship; furnace; high temperature; refractory metals; thermocouple; thermoelements; sensor; ultra high vacuum; W-Re alloys.

## 1. Introduction

The temperature measuring systems required in the technology of nuclear power systems and energy conversion devices have resulted in increased demands on the capabilities of high temperature thermocouple sensors. In particular, the design and development of propulsion and space power systems are requiring reliable thermocouple sensor operation at temperatures between 1800 and 2400 K for thousands of hours. Almost without exception, ceramic insulated, metal sheathed, W-Re thermocouple type sensors of various designs are employed in these applications.

However, for commercial thermocouple sensors currently available, the experience has been that thermocouple reliability for extended periods is generally unpredictable, even in relatively low temperature, non-nuclear environments [1,2,3].[1] For example, Sandefur et al. [1] report that W-Re type thermocouple sensors used in irradiation capsules sometimes lasted throughout the irradiation, whereas at other times, under exactly the same conditions, supposedly identical sensors failed at the beginning of irradiation.

It is reasonable to expect that the performance and reliability of thermocouple sensors could be improved by exercising more care in their design and construction. Some substantial improvements might be realized through more careful selection, processing, and handling of materials, inasmuch as previous studies [4,5] have already shown that small amounts of impurities may greatly influence the performance of W-Re type thermocouples. Thermodynamic consideration of the chemical stability of materials commonly used in configuring high temperature thermocouple sensors indicate that if gaseous reaction products are confined and materials are pure, little chemical reaction will take place [4]. Thus, reasonable thermoelectric stability should occur in non-nuclear environments if the thermocouple materials are sufficiently pure and the thermocouple sheath maintains the necessary integrity. Furthermore, some of the failures in presently available sensors are of a mechanical nature, and often occur during the first few hours of use. These failures result from such effects as gas leakage at thermocouple sheath seals, cracked sheaths, and breakage of the thermocouple hot junction upon initial heating. With improved fabrication techniques, it should be possible to reduce the failure rate from this cause.

Accordingly, a new refractory metal thermocouple research program was initiated at the National Bureau of Standards and is directed towards establishing those parameters that are necessary to achieve reliable, long term thermocouple sensor performance. An investigation with carefully processed and well characterized materials in controlled environments has been undertaken to accomplish this objective.

For this program the sensor materials have been limited to W-Re alloy thermoelements, high purity sintered beryllium oxide (BeO) insulators, and Ta or W-Re alloy sheaths. The studies have been confined to thermoelements of 0.25 mm diam or less and sheaths with 1.6 mm o.d. or less. The experimental approach has been to study first the performance of each component of the sensor separately, then in a two component interaction, and finally as a complete assembly. Thus, extensive studies were first performed to investigate the behavior of bare-wire (noninsulated) thermoelements in various gaseous

* Work supported by NASA-Lewis Research Center, under Interagency Agreement, NASA Order Numbers C-30968-B and C-61545-B.

[1] Figures in brackets indicate the literature references at the end of this paper.

environments and in vacuum. Studies were then begun with BeO-insulated thermoelements in these same environments. Yet to be performed are sheath evaluation, BeO-sheath interaction studies, and finally, evaluation of the performance of completely assembled thermocouple sensors. The temperature range of interest has been 2000 to 2400 K, although bare wire studies have been extended to as high as 3000 K. This paper describes the experimental techniques and apparatus being used in the program, and presents a few of the preliminary results that have been obtained.

## 2. Test Apparatus and Procedures

### 2.1. Studies of Bare-Wire Thermoelements

A typical apparatus for exposing bare-wire thermoelements at high temperatures in a gaseous environment or in vacuum is illustrated in figure 1. Four units of similar design are used for this purpose. The unit illustrated consists of a double-wall, water-cooled stainless steel chamber,

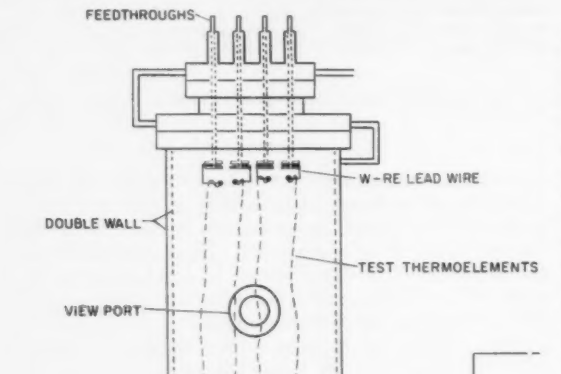


FIGURE 1. *Test chamber for thermal exposure of bare-wire thermoelements.*
The 1 cm all-metal valve, gas manifold and ionization gage are not shown.

25 cm in diameter by 65 cm high. Several ports are provided, equipped with standard ultra-high-vacuum-type flanges that seal with copper gaskets. At the top of the chamber, a special 30 cm diam water-cooled flange, equipped with a 15 cm diam access port, is sealed with a gold O-ring to a mating flange on the chamber. From 12 to 16 metal-to-ceramic sealed electrical feedthroughs are provided on the water-cooled flange installed on the access port. Mounted on 3.8 cm diam ports around the lower portion of the chamber are a 2.5 cm bakeable all-metal valve for roughing of the system, a Bayard-Alpert type ionization gage, and a 1 cm bakeable all-metal valve that is connected to a 1 cm diam stainless steel gas manifold. A Corning[2] type 7056 glass window is provided on the centrally located 3.8 cm diam port. Connected to the chamber by a 15 cm diam port is a 200 liter/s ion pump.

To create the desired test environments, the chamber is first evacuated to a pressure in the $10^{-3}$ torr[3] range with molecular sieve sorption pumps. Then, with ion pumping, pressures of $5 \times 10^{-9}$ torr and lower are achieved within 24 h, following a mild bakeout of the chamber and ion pump at about 400 K. Static gas environments are obtained by backfilling the evacuated test chamber to about 1 atm pressure from a cylinder of high purity compressed gas through the stainless steel gas manifold. A stainless steel gas transfer regulator and a stainless steel Bourdon tube gage are included in the manifold to facilitate gas pressure regulation. For tests in vacuum, the pressure is maintained at less than $1 \times 10^{-8}$ torr with the thermoelements at test temperature.

The test thermoelements, which are usually 90 to 100 cm in length, are hung vertically within the chamber from the electrodes, as shown in figure 1. They are welded to a short length of 0.5 mm diameter lead wire of nominally the same alloy, and the lead wire is then clamped between copper washers on the electrode. The thermoelements are cleaned with ether and during the mounting operation are handled using polyethylene gloves. As many as six thermoelements are mounted in the chamber and tested at the same time. During high temperature exposure tests, the thermoelements are heated electrically with alternating current (60 hertz). The current to each thermoelement is adjusted separately by manual regulation of a solid-state A-C current controller. The temperature of each thermoelement is determined and monitored during the exposure with a calibrated[4] visual optical pyrometer. Corrections are applied to account for the spectral transmittance of the glass window on the chamber and the spectral emittance of the thermoelements.

After exposure for specified periods of time, the test thermoelements are removed from the chamber and measurements are made of their thermal emf versus an unheated "as received" thermoelement from the same spool (lot) of wire. Measurements are typically made at 200 K intervals from 673 to 2073 K by heating the samples in argon in a high temperature resistance heated furnace [6]. For these tests, the temperature is determined with a W–3 percent Re versus W–25 percent Re thermocouple, with an estimated uncertainty in the temperature measurement of not more than $\pm$ 0.5 percent. In all tests the temperature of the reference junctions is maintained at 273.15 K in an ice bath, and the values of thermal emf are measured with a precision potentiometer having a resolution of 0.1 $\mu$V and a limit of error of not more than $\pm$ (0.015 percent of reading + 0.5 $\mu$V).

This procedure yields the relative changes in the thermal

[2] A trade name is identified in this paper in order to adequately specify the experimental procedure. Such identification does not imply recommendation or indorsement by the National Bureau of Standards.

[3] One torr = 133.322 newtons per square meter.

[4] Calibration performed by Radiation Thermometry Section at NBS. See NBS Monograph 41 for calibration procedure.

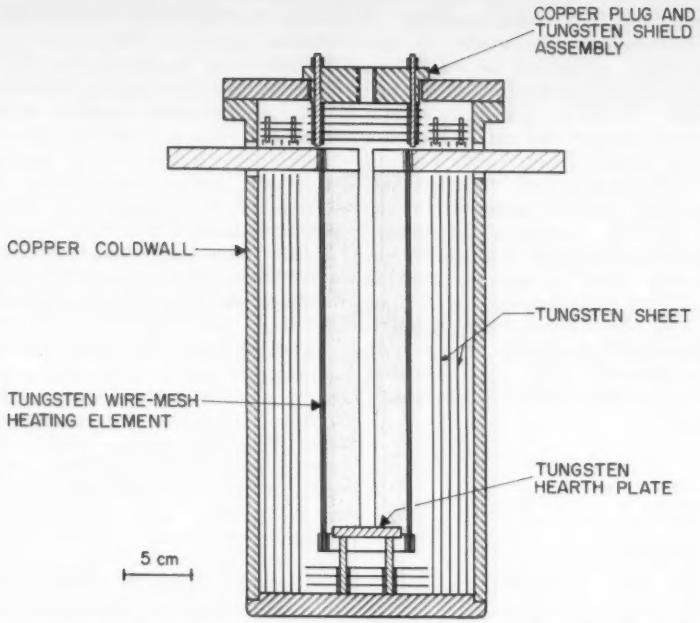


FIGURE 2. *Coldwall assembly and hot-zone of ultra-high-vacuum, high-temperature furnace.*
The copper tubing for water cooling of the coldwall is not shown.

emf-temperature relationship of the thermoelements [5] due to exposure. The error in the measurement of the relative changes by this procedure results primarily from: (a) the thermoelectric nonuniformity of the particular spool (lot) of wire; (b) the uncertainty in the measurement of the temperature; and (c) changes in the unheated "as received" thermoelement (and perhaps also the test thermoelement) that occur during the measurement of the emf-temperature relationship. In most cases, the contribution of (b) [6] and (c) to the overall uncertainty in the measurement can be shown to be small in comparison to the contribution of (a). The contribution of (a) was estimated from checks on the thermoelectric uniformity of each spool of wire. Based upon these checks and a reasonable estimate for the contribution of (b) and (c), the maximum uncertainty in the measurement of the relative change in the thermal emf of the test thermoelements is estimated to be $\pm$ 20 $\mu$V at 1273 K, and $\pm$ 30 $\mu$V at 2073 K. However, for the thermoelements exposed at 2400 K and above in vacuum, the contribution of (b) is more significant. This occurs not because of a larger uncertainty in the meaurement of the temperature (it remains about the same), but rather because the thermoelectric power of the test thermoelement versus the unheated "as received" thermoelement is often substantially larger. In these cases, the maximum uncertainty in the measurements is then estimated to be $\pm$ 30 $\mu$V at 1273 K, and $\pm$ 50 $\mu$V at 2073 K.

The change in the thermal emf–temperature relationship of a composite thermocouple in which both thermoelements have been exposed in the above manner may be obtained by combining the changes measured for the separately exposed thermoelements. It is convenient to express the change in thermal emf of the thermoelements and thermocouples at a given temperature in terms of an equivalent temperature change ($\Delta T$). We shall use the following convention in this paper: For the thermocouple, $\Delta T$ is obtained by dividing the change in the thermal emf of the thermocouple at a given temperature by the thermoelectric power ($dE/dT$) of the thermocouple at the same temperature; $\Delta T$ for the separate thermoelements is obtained similarly, except that for the W–25 percent Re thermoelement (negative element of thermocouple), a negative value for the thermoelectric power of the thermocouple is used, so that a positive change in emf results in a negative $\Delta T$. In this manner, changes occurring in the separate thermoelements are expressed in terms of their effect upon the thermocouple, and the algebraic sum of the $\Delta T$'s for each of the thermoelements equals the $\Delta T$ for the for the thermocouple.

### 2.2 Investigation of Insulator-Thermoelements and Insulator-Sheath Interactions, Sheath Integrity and Thermocouple Sensor Performance

An ultra-high-vacuum, high-temperature furnace system [7] is being used in these investigations. The furnace system incorporates many of the features of present day vacuum technology. All metal and metal-to-ceramic construction is utilized throughout, and all components are capable of sustaining repeated and extended bakeouts at

[5] The change in the emf-temperature relationship of a thermoelement is defined as the emf-temperature relationship of a thermocouple comprised of the thermoelement versus an unheated "as received" thermoelement from the same spool (lot) of wire, when the reference junctions are maintained at 273.15 K and the unheated "as received" thermoelement is designated as the negative leg of the thermocouple.

[6] Given by the product of the uncertainty in the measurement of the temperature and the thermoelectric power of the test thermoelement versus the unheated "as received" thermoelement.

[7] Built commercially to NBS specifications.

525 K without damage or loss of vacuum integrity. A high-speed, ultra-high-vacuum pumping system is employed, and facilitates rapid attainment of ultra-clean environments. Some of the principal features of the furnace are illustrated in figures 2 and 3. The furnace has a tungsten wire-mesh heating element 6.4 cm in diameter by 30.5 cm long, oriented with its central axis vertical. It is of single-phase design, having two semicylindrical tungsten wire-mesh segments that are connected at the bottom through a tungsten ring. Except at the bottom, the two segments are separated by a space of about 12 mm. The heating element is surrounded by tungsten radiation shields formed from 0.125 mm thick tungsten sheet. The heating element and shields are enclosed within a water-cooled copper coldwall assembly as shown in figure 2. The coldwall assembly is mounted within a stainless steel vacuum chamber (46 cm in diameter by 78 cm high), which is also water-cooled.

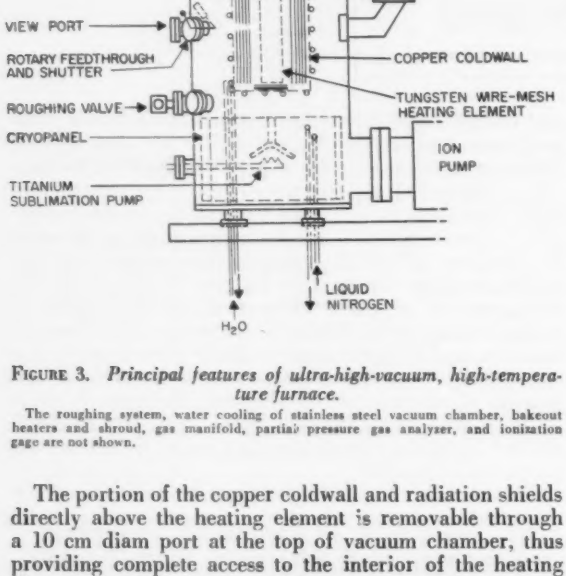


FIGURE 3. *Principal features of ultra-high-vacuum, high-temperature furnace.*

The roughing system, water cooling of stainless steel vacuum chamber, bakeout heaters and shroud, gas manifold, partial pressure gas analyzer, and ionization gage are not shown.

The portion of the copper coldwall and radiation shields directly above the heating element is removable through a 10 cm diam port at the top of vacuum chamber, thus providing complete access to the interior of the heating element for installing materials and experimental devices for test. An optical path is provided through the wire-mesh heating element, side radiation shields, and copper coldwall for viewing the interior of the heating element through a 3.8 cm diam viewing port on the side of the vacuum chamber. The view port is equipped with a Corning Type 7056 glass window. A stainless steel shutter within the vacuum chamber fully covers the view port when closed and does not obscure any part of the port when open. The shutter is actuated by a direct-drive rotary-motion feedthrough that is mounted on the vacuum chamber adjacent to the view port. Electrical connections between the heating element and a power transformer are made through two water-cooled, metal-ceramic sealed electrodes that extend into the chamber through ports on the vacuum chamber. The electrodes also serve to support the wire mesh heating element and maintain its electrical isolation from the tungsten shields and copper coldwall.

A sorption pump roughing system and a high speed, ultra-high-vacuum pumping system are used to evacuate the vacuum chamber. The roughing system, consisting of three molecular sieve type sorption pumps mounted on a stainless steel manifold, is connected to the vacuum chamber through a 3.8 cm bakeable metal-sealed valve. The high-speed, high-vacuum pumping system consists of a 400 liter/s sputter ion pump and an accessory (three filament cartridge type) titanium sublimation pump (TSP).

A cylindrical stainless steel shroud (cryopanel), cooled with liquid nitrogen, surrounds the TSP and enhances pumping. An optically-dense baffle is installed above the TSP and shields the upper chamber region from titanium deposition. The pressure within the chamber is measured with a nude Bayard-Alpert type ionization gauge. For bakeout, ceramic-insulated metal-clad heaters are attached to the exterior walls of the vacuum chamber and ion pump; these systems are surrounded by an aluminum bakeout shroud. The bakeout heater power controls are interlocked electrically with pressure and temperature sensing controls and permit unattended (automatic) bakeout of the chamber and ion pump at 525 K. To aid in studies of vacuum degassing of materials, a partial pressure gas analyzer is mounted on the side of the vacuum chamber. It is a cycloidal analyzer, using a crossed electrostatic and magnetic field, and is capable of mass number identifications from 2 to 100 atomic mass units (amu) down to pressures of $5 \times 10^{-12}$ torr.

If, after evacuating and baking the system, a gaseous environment is desired, high purity gas from a cylinder of compressed gas is introduced through a stainless steel manifold that is connected to the vacuum chamber by a 1 cm bakeable all-metal valve. The manifold is of design similar to that of the one described in section 2.1.

Power to the wire-mesh heating element is supplied through a 67-kVA Silicon Controlled Rectifier (SCR) type proportional power controller and a 47-kVA air-cooled stepdown transformer. Input line voltage to the power controller is 480 V, 60 Hz, single phase. The temperature within the hot zone is controlled by the indirect method of controlling the power supplied to the mesh heating element.

For automatically controlling the power at the desired level (set point), a closed loop control system is provided. The closed loop control utilizes a thermal watt converter type power sensor, which in conjunction with a high-response electronic controller, feeds back an appropriate control signal to the SCR proportional power controller. An adjustable set point on the electronic controller permits selecting a power level with a resolution of better than 0.1 percent. The controller has a 20 ms response and includes features such as adjustable gain, rate and reset time controls. At maximum gain settings, the control system has a sensitivity equivalent to about 2 W. The power controls are electrically interlocked with other controls and automatically shut off the heating element power if the cooling water flow drops below a safe operating level or if the pressure in the vacuum chamber rises above

an adjustable preset value. In certain applications, it may be advantageous to control directly the furnace hot-zone temperature by utilizing the output of a thermocouple sensor or an automatic photoelectric pyrometer. This type of control is also possible if minor modifications to the input circuitry of the electronic controller are made.

When the furnace is at ambient temperature (no power), base pressures of less than $5 \times 10^{-11}$ torr may be achieved within 20 h, (including a 10 h bakeout of the chamber and the pumping system at 525 K). The furnace is designed to produce hot-zone temperatures to 3000 K while maintaining the pressure in the $10^{-8}$ torr range; when the furnace chamber is filled with a high-purity inert gas or hydrogen gas at a pressure at 1 atm, it is designed to produce hot-zone temperatures in excess of 2700 K.

At elevated temperatures, the temperature in the hot-zone of the furnace responds very rapidly to changes in heating element power. Hence, precise automatic control of the power provides a reasonably sensitive and reproducible method for controlling the hot-zone temperature. With the furnace chamber filled with 1 atm pressure of argon, a temperature stability — over a period of 1000 h — of $\pm$ 4 K at 2073 K has been achieved. Over a 24 h period, the temperature stability has been typically $\pm$ 2 K at 2073 K, and for shorter periods (20 to 30 min), $\pm$ 0.5 K. Temperature stability was ascertained from measurements made with an automatic photoelectric optical pyrometer and with W–3 percent Re versus W–25 percent Re thermocouples.

The furnace is presently being used for vacuum degassing of materials, insulator — W/Re wire interaction studies in argon, and testing and evaluating the performance of BeO insulated thermocouples. For vacuum degassing and processing of sintered BeO tubing, the insulating parts have been supported in the hot-zone of the furnace with a W-Re wire basket that was formed by interweaving 0.125 and 0.25 mm diam wires. Studies of the chemical behavior of W-Re thermocouple wire that is insulated with sintered BeO insulating tubing are being performed in high purity argon ($<$ 10 ppmv total impurities) at about 1 atm pressure and temperatures in the 2000 to 2400 K range. For these studies, W–3 percent Re and W–25 percent Re wires of 0.25 mm diam are inserted into degassed, sintered, double-bore BeO insulating tubing of 0.3 mm bore and 1.1 mm o.d. The insulated wire is then suspended from the top shield assembly for exposure in the hot-zone of the furnace.

For testing and evaluating the performance of BeO-insulated W-Re type thermocouples, a tantalum blackbody enclosure is suspended in the hot-zone of the furnace. One design that has been used successfully in the 1800 to 2400 K range is shown in figure 4. The cylindrical tantalum enclosure is 2.5 cm in diam by 8 cm long, and has a 0.5 mm thick wall and a 1 mm diam blackbody opening. It is supported within the furnace hot-zone by a 6.35 mm diam tantalum tube that is attached (heli-arc welded) to the top shield assembly. This design closely approximates an ideal blackbody if the walls of the enclosure are at a uniform temperature. Using calculations derived by DeVos [7], it is estimated that the effective emittance of this blackbody enclosure is greater than 0.997.

Thermocouples for test are inserted through the 6.35 mm diam tantalum supporting tube so that their measuring junctions are within the blackbody enclosure. The thermocouple wires lead out of the vacuum chamber through metal-glass feedthroughs at the top of the chamber and the wire exits are sealed with a solvent-free epoxy resin. The metal-glass feedthroughs are mounted on a 15 cm o.d. ultra-high-vacuum flange that seals to a mating flange on the 10 cm diam loading port.

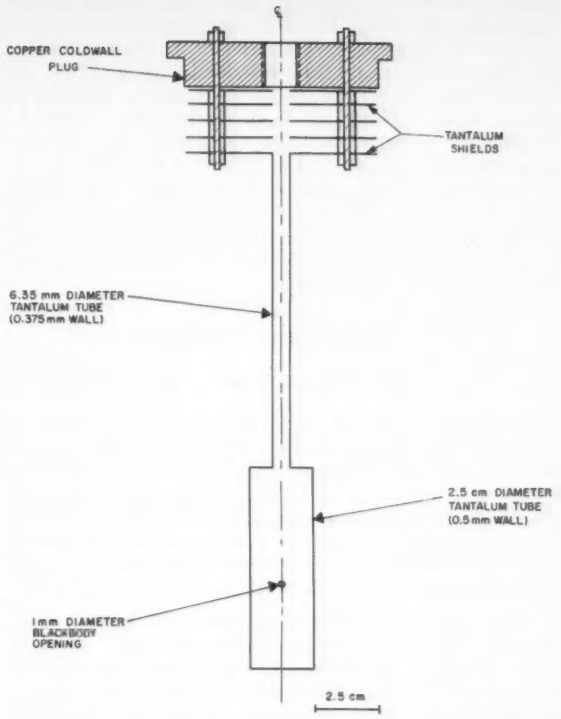
COPPER COLDWALL PLUG
TANTALUM SHIELDS
6.35 mm DIAMETER TANTALUM TUBE (0.375 mm WALL)
2.5 cm DIAMETER TANTALUM TUBE (0.5 mm WALL)
1 mm DIAMETER BLACKBODY OPENING
2.5 cm

FIGURE 4. *Tantalum blackbody enclosure for high-temperature furnace.*

The temperature of the tantalum blackbody enclosure is determined with a visual optical pyrometer, and also with an automatic photoelectric pyrometer by sighting on the blackbody opening. The pyrometers used in this work are of commercial design and are calibrated [8] by relating the pyrometer lamp current to the brightness or blackbody temperature. In use, the pyrometer lamp current is determined by measuring the voltage drop across a 1 $\Omega$ standard resistor in series with the lamp. All voltage measurements, including the emf's of test thermocouples, are made with a precision potentiometer having a limit of error of less than $\pm$ (0.015% of reading $\pm$ 2 $\mu$V), or alternatively with a 6 digit digital voltmeter having an absolute voltage accuracy of ($\pm$ 0.004% of reading $\pm$ 2 $\mu$V).

Thus far more than 1200 h of reliable operation in the 1800 to 2400 K range has been accumulated with the Ta blackbody in an argon environment. Two sets of measurements have been made (in an argon atmosphere) with three W–3 percent Re versus W–25 percent Re thermo-

[8] Calibration performed by Radiation Thermometry Section at NBS. See NBS Monograph 41 for calibration procedure.

couples inserted at different immersion depths in the blackbody enclosure. Different thermocouples were used for each set of measurements. The measurements indicate that the vertical temperature distribution over the central 5 centimeters of the blackbody enclosure is uniform to within about 2 kelvins at temperatures above 1800 K. Below 1800 K the temperature distribution becomes progressively less uniform, and at 1300 K a temperature gradient of about 2 K/cm exists over the central 5 centimeters of the enclosure. The improved temperature uniformity at high temperatures is apparently a result of the increasing predominance of the radiative heat flux in the system as the temperature is increased.

## 3. Results and Discussion

### 3.1. Studies Completed

Studies on the effects of thermal exposure of bare 0.25 mm diam W–3 percent Re and W–25 percent Re thermoelements in environments of vacuum, argon and hydrogen have been completed [8]. In these studies, thermoelements were exposed for periods ranging from 1 to 1000 h at 2400 K in high vacuum ($< 1 \times 10^{-8}$ torr) and in high purity argon and hydrogen environments (at 1 atm). Some tests in vacuum at 2200 and 2600 K were also conducted.

In the argon and hydrogen environments, both thermoelements typically experienced a change (shift) in their emf-temperature relationship during the first hour of exposure at 2400 K. Subsequent exposure for periods up to 1000 h was found to produce no further significant changes (drift) in the emf-temperature relationship. Typical curves showing the change in the emf-temperature relationship of W–3 percent Re and W–25 percent Re thermoelements after exposure in argon at 2400 K for periods of 1, 50, 100, 250, 500 , 750, and 1000 h are given in figure 5. The changes all fell within the shaded region, and no trend of the data with increasing exposure time was apparent. Similar results were obtained with thermoelements from the same wire lots after being exposed in hydrogen at 2400 K, except that the shift in the emf-temperature relationship of W–3 percent Re thermoelement averaged slightly less (about 120 $\mu$V at 2073 K). In the case of W–25 percent Re thermoelement there was no discernible difference between the argon and hydrogen results.

Three different lots of 0.25 mm diam W–3 percent Re versus W–25 percent Re thermocouple wires from the same supplier have been examined thus far, and the magnitude of the initial shift in the thermal emf varies somewhat between lots. Table 1 gives the changes in the emf-temperature relationship (equivalent $\Delta T$) at 2073 K for the thermoelements and thermocouples from the three lots after thermal exposure in argon for 1 and 50 h at 2400 K. It is noted that the shift for all lots is essentially complete after an exposure for 1 h. Further, the thermocouples from the three different lots exhibit positive shifts equivalent to about 0.1 percent, 0.3 percent, and 1 percent at 2073 K.

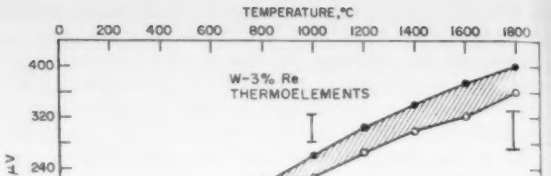


FIGURE 5. *Change in the emf-temperature relationship of W–3% Re and W–25% Re thermoelements from one lot after exposure in argon at 2400 K for periods up to 1000 hrs.*

Shaded region indicates range of values obtained for thermoelements exposed for 1, 50, 100, 250, 500, 750, and 1000 hours. Bars designate the estimated uncertainty in measurements at the indicated temperature.

It is well known that commercial W-Re thermocouple materials will experience some shift in their emf-temperature relationship on initial heating to elevated temperatures [5,9]. However, these results clearly demonstrate that thermocouple wire can be supplied which will exhibit only a very small initial shift (0.1% to 0.2%). As with most W-Re thermocouple wire sold in this country, the thermocouple materials used in this work were thermally conditioned by the supplier with a heat treatment that tends to minimize the shift and yet retain desirable mechanical properties.

Many engineering applications require that temperature be measured with an accuracy of only a few percent. For these applications, the shift in the "as supplied" wire is

TABLE 1. *Average change in the emf-temperature relationship (equivalent $\Delta$ T) at 2073 K of the thermoelements and thermocouples from three different lots after exposure at 2400 K in argon (1 atm)*

$\Delta$T in Kelvins

| | Lot 1 | | | Lot 2 | | | Lot 3 | | |
|---|---|---|---|---|---|---|---|---|---|
| Exposure Time (Hours) | W-3% Re Element | W-25% Re Element | Thermo-couple | W-3% Re Element | W-25% Re Element | Thermo-couple | W-3% Re Element | W-25% Re Element | Thermo-couple |
| 1 | +6 | −4 | +2 | +23 | −5 | +18 | +9 | −3 | +6 |
| 50 | +7 | −4 | +3 | +24 | −7 | +17 | +8 | −2 | +6 |

sufficiently small so that its effects may be neglected, and no special aging of the wire by the user is necessary. Furthermore, in typical thermocouple applications, high temperature exposure of the thermocouple will result in thermocouple wire that is not fully thermally conditioned along its entire length. For a given wire lot, the shift would then, in general, be less than the shift reported here. Nevertheless, the occurrence of such shifts tends to restrict the accuracy obtainable. For those cases where the ultimate in performance and accuracy is desired, additional thermal aging to eliminate the shift will probably prove desirable. This can be accomplished in such a manner that afterwards, the wires will possess sufficient room temperature ductility for fabrication purposes. Closer control of the thermal conditioning process in order to minimize the shift in the "as supplied" wire has been recently reported by one supplier [10].

Exposure of the bare thermoelements in high vacuum ($< 1 \times 10^{-8}$ torr) at temperatures above 2200 K results in a continual change (drift) in their emf-temperature relationship. Changes that occurred in the emf-temperature relationship of the thermoelements after exposure for periods of 50, 250, and 500 h at 2400 K are given in figures 6 and 7. The drift in the emf-temperature relationship of the thermoelements in high vacuum is strongly dependent upon the temperature of exposure. At 2600 K, an exposure of only 50 h produces about the same drift as an exposure of 500 h at 2400 K, while at 2200 K the drift after exposure for 500 h is negligible.

The drift in the emf-temperature relationship of both thermoelements in high vacuum has been shown to be the result of a preferential loss of Re from the alloys by evaporation. This was confirmed by electron probe microanalysis of the exposed thermoelements. Hence, any processing of the bare thermoelements in vacuum should be confined to temperatures of 2200 K or below to avoid changes in alloy composition. Furthermore, bare-wire

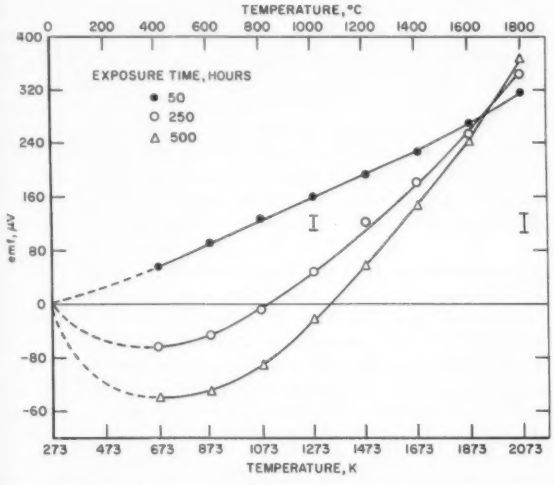


FIGURE 6. *Change in the emf-temperature relationship of W–3% Re thermoelements from one lot after thermal exposure for 50, 250, and 500 h at 2400 K in vacuum ($< 1 \times 10^{-8}$ torr).*

Bars designate the estimated uncertainty in measurements at the indicated temperature.

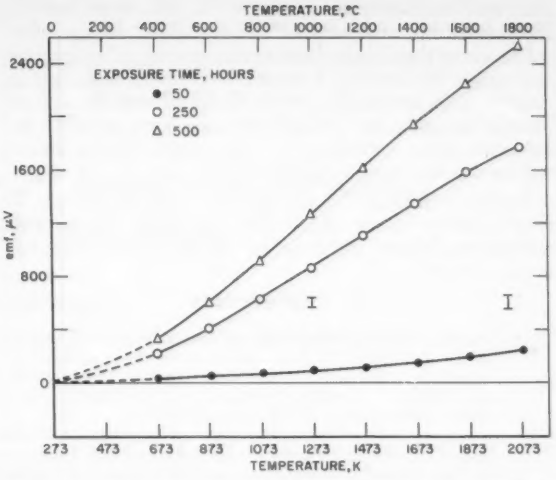


FIGURE 7. *Change in emf-temperature relationship of W–25% Re thermoelements from one lot after thermal exposure for 50, 250, and 500 h at 2400 K in vacuum ($< 1 \times 10^{-8}$ torr).*

Bars designate the estimated uncertainty in measurements at the indicated temperature.

W–3 percent Re versus W–25 percent Re thermocouples could be expected to drift in calibration with use in high vacuum at temperatures above 2200 K. However, since the conditions and methods of exposure for thermocouples in actual use are different from those in the present studies, the results presented are only considered as indicative of expected material behavior and are not generally valid for predicting the magnitude of the drift for thermocouples in actual use. These results indicate that the thermal emf of a bare-wire thermocouple will decrease with exposure in high vacuum at 2400 K or above, due primarily to the preferential loss of Re from the W–25 percent Re thermoelement. At 2400 K, the rate of change in the calibration might typically be on the order of a few tenths kelvin per hour.

### 3.2. Current and Planned Studies

Work now in progress includes studies to establish suitable time-temperature parameters for thermally conditioning W–3 percent Re and W–25 percent Re thermocouple wire before use. Tests to evaluate the bare thermoelements in high purity helium and nitrogen environments at 2400 K are also being performed. In addition, the behavior and performance of other commercially available W-Re type thermocouples (W–5% Re versus W–26% Re and W versus W–26% Re) are being investigated.

In progress also are studies with high purity ($> 99.8\%$) sintered double-bore beryllium oxide insulating tubing in the 2000 to 2400 K range. Preliminary results have indicated that material transport from the W-Re thermoelements to the inner bore of BeO tubing may occur in a high purity argon environment if the insulating tubing is not well degassed prior to use. In some cases, poor degassing technique has resulted in chemical reactions between the BeO and W-Re thermoelements. However, there are indications that, if the BeO insulating tubing is

first well degassed, the insulator-thermoelement material incompatibility problems will be negligible during subsequent use in high purity inert environments in the temperature range of interest. Tests are in progress with BeO insulated W–3 percent Re versus W–25 percent Re thermocouples in argon to establish the long term stability and behavior of this combination. The results of these studies will be reported in subsequent papers.

Studies will begin within the next year to evaluate Ta sheath performance, sheath-BeO insulator interactions, and the capabilities and behavior of fully sheathed thermocouple sensors.

## 4. References


[1] Sandefur, N. L., Carpenter, F. D., Grenda, R. J., and Steibel, J. S., Reliability of high temperature thermocouples in irradiation capsules, National Symposium on Developments in Irradiation Testing Technology (Conf-690910), Sandusky, Ohio, Sept. 9–11, 1969, pp. 551–582.

[2] Heckelman, J. D., A retractable-replaceable thermocouple for in-pile experiments, National Symposium on Developments in Irradiation in Irradiation Testing Technology (Conf-690910), Sandusky, Ohio, Sept. 9–11, 1969, pp. 652–668.

[3] Schwarzer, D. E., High temperature thermal cycling drift test of $W_{95}$-$Re_5$ versus $W_{74}$-$Re_{26}$ thermocouples, National Symposium on Developments in Irradiation Testing Technology. (Conf-690910), Sandusky, Ohio, Sept. 9–11, 1969, pp. 307–329.

[4] Droege, J. W., Miller, N. E., Schimek, M. E., Wood, V. E., and Ward, J. J., Refractory metal thermocouples in nuclear and high-temperature applications, Report No. BMI-X-10246, Battelle Memorial Institute, Columbus, Ohio (November, 1968).

[5] Walker, B. E., Ewing, C. T., and Miller, R. R., Instability of refractory metal thermocouples, Rev. of Sci. Instr. **36**, No. 6, 816–825 (June, 1965).

[6] Thomas, D. B., A furnace for thermocouple calibrations to 2200 °C, J. Res. Nat. Bur. Stand. (U.S.), **66C** (Eng. and Instr.), No. 3, 255–260 (July-Sept., 1962).

[7] DeVos, J. C., Evaluation of the quality of a blackbody, Physica **XX**, No. 10, 669–689 (Oct. 1954).

[8] Burns, G. W., and Hurst, W. S., An investigation of W–3% Re and W–25% Re thermoelements in vacuum, argon and hydrogen, Report No. NASA CR–72639, National Aeronautics and Space Administration, Cleveland, Ohio (March, 1970).

[9] Hall, Jr., B. F., and Spooner, N. F., Application and performance data for tungsten-rhenium alloy thermocouples, National Aeronautic and Space Engineering and Manufacturing Meeting, Los Angeles, Calif., Sept. 23–27, 1963, Paper 750C (Society of Automotive Engineers, Inc., New York, N. Y.)

[10] Tseng, Y., Schnatz, S., Zysk, E. D., Tungsten 3 rhenium vs tungsten 25 rhenium thermocouple—some recent developments, Engelhard Industries Technical Bulletin **XI**, No. 1, 12–18 (June, 1970).


(Paper 75C2–319)

JOURNAL OF RESEARCH of the National Bureau of Standards—C. Engineering and Instrumentation
Vol. 75C, No. 2, April-June 1971

# Polarization Measurements as Related to Corrosion of Underground Steel Piling

**W. J. Schwerdtfeger**

**Institute for Materials Research, National Bureau of Standards, Washington, D.C. 20234**

(April 14, 1971)

Most of this paper is devoted to the author's evaluation of polarization measurements made by the Corps of Engineers (Lower Mississippi Valley Division) on steel pipe specimens exposed to the soil at four dam sites as related to the corrosion of steel piling (underground) observed at the sites. As the polarization measurements were made periodically on weighed specimens for periods as long as seven years, the Corps' data offered an excellent opportunity for evaluating the accuracy and practicability of a polarization technique for measuring corrosion rates. Reasonable agreement between calculated and actual corrosion on the specimens made it possible to estimate maximum anticipated corrosion on the piling after 50 years of exposure.

Confidence gained in the value of polarization measurements made on short length pipe specimens led the author to make measurements on actual piling. Instantaneous corrosion rates were measured on two driven pipe piles, 72 ft (22 m) and 19 ft (5.8 m) in length, both of which had been exposed for 12 years. One month later, the short pile was extracted and examined. Relatively low corrosion rates calculated from the polarization data were verified by the appearance of the pile and by the limited extent of the pitting.

Key words: Corrosion; corrosion rate; disturbed soil; instantaneous rate; pit depth; pitting factor; polarization; steel piling; undisturbed soil; weight loss.

## 1. Introduction

Corrosion observed on structural steel piling exposed to underground environments based on visual inspection and measurements of pit depth has been described by Romanoff [1].[1] His inspections were made in cooperation with the Corps of Engineers (Lower Mississippi Valley Division) and the American Iron and Steel Institute. During the course of an investigation at four dam sites, where piling had been examined, Romanoff decided to expose steel pipe specimens, arranged in groups of four, to the same underground environments nearby. One specimen of each group was wired to enable periodic monitoring of instantaneous rates of corrosion by polarization measurements. The groups of specimens were removed from each site at intervals of 1, 2, 4, and 7 years.

The buried specimens, exposed to back-filled trenches, served a two-fold purpose. Romanoff [1] reported that steel exposed to excavated soils was subject to more severe corrosion than that which he observed on driven piling for a given environment. Thus, the steel specimens would provide the opportunity for comparing corrosion under the two conditions of exposure (driven or buried). Secondly, they offered an excellent chance for evaluating the accuracy and practicability of a polarization technique for measuring corrosion. The method was evaluated by comparing the cumulative metal losses (based on Faraday's law) of the wired specimens with their actual weight losses.

Past work has demonstrated that instantaneous rates of corrosion on pipe specimens in situ can be measured by a polarization technique and averaged for periodic intervals in calculating metal losses resulting from corrosion for a given period of exposure [2]. As exposure time for some of the Corps of Engineers' specimens extended over a period of 7 years, an excellent opportunity prevailed for a further evaluation of the technique as applied to underground corrosion. Furthermore, it became possible to monitor corrosion rates at each of the four sites over a period of 7 years. By thus monitoring corrosion rates, the length of exposure time required to obtain reliable performance data of metals exposed to a given environment can be estimated.

Romanoff [1] concluded, based primarily on visual observation and experience, that iron exposed to soil in backfilled trenches is more severely corroded than when exposed to the same soil (undisturbed). Romanoff referred to undisturbed soil as that soil adjacent to driven piling below the backfilled soil. In order to further substantiate this conclusion, Romanoff exposed iron pipe specimens to excavated trenches in the same areas where driven piling had previously been visually examined. The Corps of Engineers, responsible for making the polarization measurements, also exposed iron rods, limited in number, by driving some of them into the soil and by exposing other identical rods to excavated soil nearby. The National Bureau of Standards prepared weighed pipe specimens for the burial program. The rod specimens were

[1] Figures in brackets indicate the literature references at the end of this paper.

prepared by the Corps of Engineers. The Corps furnished the Bureau with copies of the polarization curves obtained at the periodic intervals. During the period of 7 years, all specimens involved in four removals were sent to the Bureau for cleaning and determination of metal losses.

In a recent report [3] by the Corps of Engineers on the corrosion of underground steel piling, the results of measurements made on the pipe and rod specimens are included. Included in that report are the weight losses and maximum pit depths on all specimens, pipe and rod, unwired and wired. Estimated weight losses based on electrical measurements are summarized and discussed in relation to what was observed on nearby piling.

In this paper, the polarization curves submitted to NBS by the Corps of Engineers are evaluated by the Bureau. This accounts for any differences (averaging 9%) between the Corps estimated weight losses and the calculated weight losses tabulated herein. Stabilized corrosion rates, based on polarization measurements made on the wired seven-year pipe specimens in back-filled trenches, are expressed as average penetration and compared with the maximum corrosion observed on piling at the same sites exposed from 11 to 20 years.

Recently, the writer became aware of some isolated steel pipe piles located on the grounds of a sewage disposal plant. It was suggested that it might be of interest to make polarization measurements on one or more of the driven piles which were exposed to the soil for 12 years. The results of measurements and calculated rates of corrosion for two 12.75 in (32.5 cm) diam piles 72 ft (22 m) and 19 ft (5.8 m) long are described.

## 2. Experimental Procedure

### 2.1. Preparation of Pipe and Rod Specimens

Sixteen pipe specimens were prepared for burial at each of four sites. The specimens were cut from standard black iron pipe 1.5 in (3.8 cm) diam to lengths of 14 in (35.5 cm). Loose mill scale was removed and the specimens were deburred, degreased and weighed to the nearest 50 mg. The inside of the pipe was coated with heavy grease and rubber caps were placed over the open ends so as to confine corrosion to the outer surface area 0.5 ft$^2$ (4.6 dm$^2$) approx. One of each set of four specimens, constituting a set for removal, was equipped with an insulated copper wire soldered to the inside of the pipe and brought through a hole in the center of one of the rubber caps. The pipes were placed laterally in the trench about 12 in (30.5 cm) apart and buried horizontally about 3 ft (0.92 m) below the earth's surface. The wires to specimens terminated above ground in boxes mounted on wooden posts.

The number of rod specimens was limited to two at each of the four sites. One of the rods was exposed vertically positioned in back-filled soil and the other rod was driven off to the side about 18 in (46 cm) away. The rods were cut from hot-rolled steel 0.75 in (1.9 cm) diam to 3 ft. (0.92 m) lengths. They were cleaned and weighed as previously mentioned for the pipe specimens. Both rods were equipped with insulated copper wires terminating above ground. The top 5 in (12.7 cm) of each rod, including the wire connection, was coated with coal tar. This again left about 0.5 ft$^2$ (4.6 dm$^2$) of bare surface for exposure to the soil, the same as for the pipe specimens.

### 2.2. Polarization Measurements — Pipe and Rod Specimens

A galvanized steel pipe 1 in (2.54 cm) diam and five ft (1.5 m) long was driven at each site for use as an auxiliary electrode. Polarization measurements were made by the Corps of Engineers [3] at intervals of from 3 to 7 months approximately. When making polarization measurements in soil environments, it is usually necessary to use a bridge circuit because changes in measured potential caused by the IR drop through the soil may be sufficient to obscure changes due to actual polarization. The Holler bridge circuit, originally described by Holler [4] and more recently by Schwerdtfeger [5], was used by the Corps of Engineers at the test sites. For running the polarization curves, equal increments of current were applied at one minute intervals.

### 2.3. Removal of Corrosion Products from the Specimens

The pipe and rod specimens were returned to the Bureau for cleaning after exposure to the soils. They were scrubbed under hot running water to remove soil and loose corrosion products. The rubber caps were removed from the pipe specimens and grease inside the pipes was melted out by applying heat from a torch flame. Following degreasing, the specimens were immersed in a hot solution (150 °F) of 10 percent ammonium citrate neutralized with ammonium hydroxide. Length of immersion time varied with the degree of corrosion, being usually not over five hours. Ammonium hydroxide was added as required to keep the solution on the neutral to alkaline side. Specimens were intermittently scrubbed with a steel-bristle brush to remove corrosion products down to bare metal. The rod specimens were freed of corrosion products in the same way. Solder was melted and scraped from those specimens which had wire leads. Finally, all specimens were again weighed to the nearest 50 mg.

### 2.4. Polarization Measurements on Pipe Piling in Situ

Polarization curves were obtained on bare pipe piling driven 12 years previously on property of the Hiawatha Treatment Plant at Syracuse, N. Y. Measurements were made on two 12 in diam (30.5 cm) pipe piles, 72 ft (22 m) and 19 ft (5.8 m) in length. The auxiliary anode was a third pipe pile driven to a depth of 122 ft (37 m). The piles were separated by a distance of about 5 ft (1.5 m). The reference electrode was copper-copper sulfate placed on the earth's surface at a distance of about 50 ft (15.2 m) from the top of the pile being measured.

An adaptation of the Holler bridge (fig. 1) was used by the Bureau to obtain the polarization curves. It will be noted that terminals are provided for inserting other control resistors. $R_s$ and $R_x$, should specimen size or environmental conditions make that necessary. For running the curves on the piling, the 0.5 Ω balancing resistor $R_x$ was used and the other balancing resistors were set at zero. A 12-volt storage battery supplied the polarizing

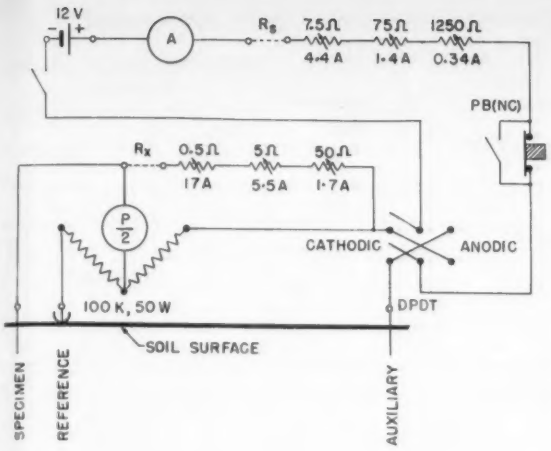


FIGURE 1. *Circuit used for obtaining polarization curves on piling.*

current. A potentiometer was used in the bridge circuit for measuring potentials. The polarization curves were obtained by applying equal increments of current at one minute intervals. The increments were previously determined by the applied current necessary to change the potential from 2 to 10 m$V$.

In addition to polarization, soil resistivity in the vicinity of the piling was measured at depths of 3, 12, and 30 ft (0.91, 3.7, 9.1 m) using the 4-pin Wenner method.

The 19 ft (5.8 m) pile was extracted for examination and measurement of depth of pits.

## 3. Results and Discussion

### 3.1. Corrosion Rates of Pipe Specimens in Back-Filled Trenches

In figure 2 are shown typical polarization curves obtained at periodic intervals on the seven-year pipe specimen at Sardis Dam. Corrosion rates at Sardis Dam were the lowest of the 4 sites. The cathodic curves are those having breaks indicated by $I_p$, while breaks in the anodic curves are shown by the currents $I_q$. Anodic curves are omitted for data obtained 8-10-60 and 5-1-61 because there was relatively little or no polarization, indicating a value for the current $I_q$ several times that of the current $I_p$. Typical polarization curves obtained on four-year pipe specimens at the 4 test sites are shown in figure 3. The curves were obtained a few months prior to removal of the specimens.

All electrical data obtained on the pipe specimens at the 4 sites are shown in tables 1 through 4. The method used in calculating corrosion currents and metal losses is described in the footnotes of the table. Actual weight losses, after chemical removal of corrosion products, are also shown for comparison. Agreement between actual and calculated values is reasonably good. The calculated values are based on the electrochemical equivalent for ferrous iron. With the exception of the Sardis site which is poorly aerated, where corrosion probably continues in

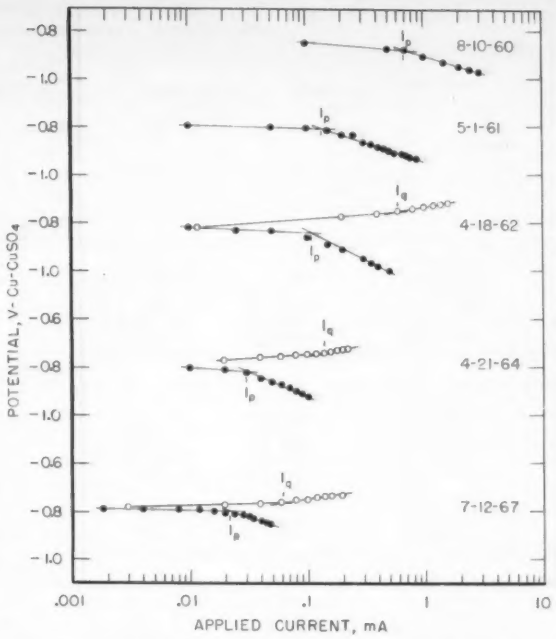


FIGURE 2. *Typical polarization curves of underground steel specimen (C8) during seven years of exposure at Sardis Dam site.*
● Cathodic ○ Anodic

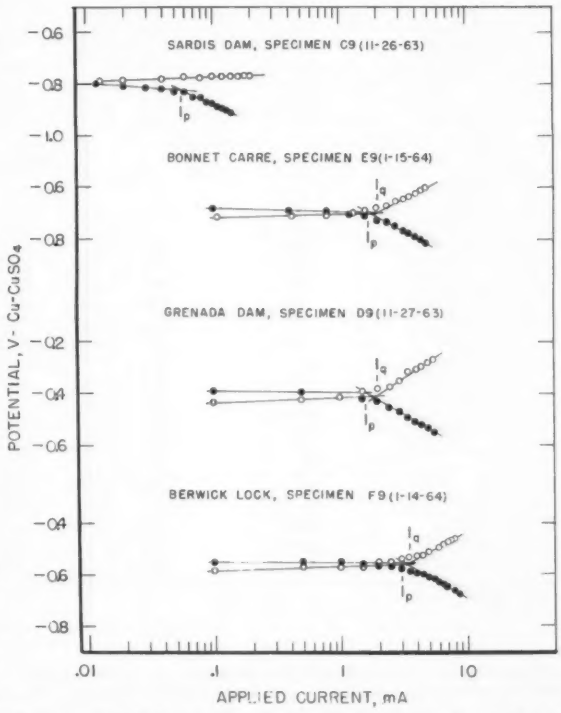


FIGURE 3. *Polarization curves of underground specimens Nos. 9 after 45 months of exposure at four soil sites.*
● Cathodic ○ Anodic

TABLE 1. *Total corrosion (weight loss) calculated from polarization curves of ferrous pipe specimens exposed up to 7 years in back-filled trenches at Berwick Lock*

| Date | Exposure time cumulative | Corrosion potential Ref-Cu-$CuSO_4$ | Polarizing Current[a] at break in curve | | Corrosion current | Weight loss | |
|---|---|---|---|---|---|---|---|
| | | | Cathodic $I_p$ | Anodic $I_q$ | $i_o$[b] | Calculated[c] cumulative | Actual |
| | days | V | mA | mA | mA | g | g |
| | Specimen F4 | | | | | | |
| 4-05-60 | 0 | | | | | | |
| 8-23-60 | 140 | −0.780 | 4.2 | $2I_p$[d] | 2.8 | 10 | |
| 11-16-60 | 225 | .735 | 2.7 | 4.2 | 1.6 | 15 | |
| 2-07-61 | 308 | .772 | 2.8 | 2.8 | 1.4 | 18 | |
| 5-10-61 | 400 | .762 | 2.9 | 4.1 | 1.7 | 21 | 19 |
| | Specimen F13 | | | | | | |
| 4-05-60 | 0 | | | | | | |
| 8-23-60 | 140 | −0.630 | 6.0 | $2I_p$[d] | 4.0 | 14 | |
| 11-16-60 | 225 | .640 | 3.0 | 3.6 | 1.6 | 20 | |
| 2-07-61 | 308 | .657 | 3.6 | 4.5 | 2.0 | 24 | |
| 5-10-61 | 400 | .580 | 5.4 | 7.4 | 3.1 | 30 | |
| 9-19-61 | 532 | .655 | 9.0 | 11.0 | 4.9 | 43 | |
| 1-17-62 | 652 | .625 | 10.0 | 14.0 | 5.8 | 59 | |
| 4-25-62 | 750 | .580 | 6.5 | 7.6 | 3.5 | 70 | 49 |
| | Specimen F9 | | | | | | |
| 4-05-60 | 0 | | | | | | |
| 8-23-60 | 140 | −0.718 | 5.6 | $2I_p$[d] | 3.7 | 13 | |
| 11-16-60 | 225 | .630 | 3.6 | 3.6 | 1.8 | 19 | |
| 2-07-61 | 308 | .700 | 3.1 | 4.4 | 1.8 | 23 | |
| 5-10-61 | 400 | .645 | 7.0 | 8.0 | 3.7 | 29 | |
| 9-19-61 | 532 | .665 | 6.8 | 7.5 | 3.6 | 40 | |
| 1-17-62 | 652 | .642 | 8.0 | 11.0 | 4.6 | 53 | |
| 4-25-62 | 750 | .577 | 8.0 | 9.4 | 4.3 | 64 | |
| 8-29-62 | 876 | .564 | 7.6 | 9.6 | 4.2 | 78 | |
| 1-16-63 | 1016 | .620 | 9.0 | 9.0 | 4.5 | 93 | |
| 5-15-63 | 1135 | .415 | 6.0 | 4.5 | 2.6 | 103 | |
| 9-18-63 | 1261 | .552 | 3.5 | 3.5 | 1.7 | 110 | |
| 1-14-64 | 1379 | .575 | 2.7 | 3.2 | 1.5 | 115 | |
| 4-28-64 | 1483 | .533 | 4.0 | 4.0 | 2.0 | 119 | 67 |
| | Specimen F8 | | | | | | |
| 4-05-60 | 0 | | | | | | |
| 8-23-60 | 140 | −0.628 | 7.4 | $2I_p$[d] | 4.9 | 17 | |
| 11-16-60 | 225 | .638 | 3.0 | 3.7 | 1.7 | 24 | |
| 2-07-61 | 308 | .635 | 5.2 | 4.3 | 2.3 | 28 | |
| 5-10-61 | 400 | .635 | 11.5 | 10.0 | 5.3 | 37 | |
| 9-19-61 | 532 | .660 | 7.5 | 6.5 | 3.5 | 51 | |
| 1-17-62 | 652 | .553 | 10.0 | 10.0 | 5.0 | 64 | |
| 4-25-62 | 751 | .578 | 6.8 | 6.6 | 3.3 | 74 | |
| 8-29-62 | 877 | .587 | 13.0 | 13.0 | 6.5 | 90 | |
| 1-16-63 | 1017 | .613 | 13.0 | 12.0 | 6.2 | 112 | |
| 5-15-63 | 1136 | .417 | 4.5 | 4.0 | 2.1 | 124 | |
| 9-18-63 | 1262 | .560 | 4.5 | 5.2 | 2.4 | 131 | |
| 1-14-64 | 1380 | .553 | 3.7 | 5.0 | 2.1 | 138 | |
| 4-28-64 | 1484 | .500 | 4.5 | 4.5 | 2.2 | 143 | |
| 9-09-64 | 1618 | .337 | 3.4 | 3.4 | 1.7 | 150 | |
| 12-17-64 | 1717 | .556 | 2.0 | 2.0 | 1.0 | 153 | |
| 5-04-65 | 1856 | .450 | 1.2 | 2.4 | 0.8 | 156 | |
| 1-11-66 | 2180 | .531 | 1.2 | 1.4 | 0.6 | 161 | |
| 5-17-66 | 2235 | .530 | 0.6 | 1.0 | 0.4 | 162 | |
| 10-25-66 | 2396 | .545 | 0.7 | 1.4 | 0.5 | 164 | |
| 7-25-67 | 2669 | .328 | 0.9 | 0.7 | 0.4 | 167 | 125 |

[a] See figure 2.

[b] $i_o = \frac{I_p\, I_q}{I_p + I_q}$.

[c] From Faraday's law, Weight loss (grams) $= Kti_o$, where $K$ = electrochemical equivalent $2.8938 \times 10^{-4}$ g/c, $t$ = time (s) for the period between successive readings, $i_o$ = average current (amperes) for a period. Approximately, weight loss (mg) $= 25\ t\ i_o$, where $t$ = days between successive measurements, $i_o$ = average current (mA) between successive measurements. The values of $i_o$ at the beginning and at the end of exposure are taken as the initial and final values, respectively, as calculated.

[d] Breaks are indefinite. Values are based on relative cathodic and anodic polarization and/or values of $I_q$ before or after.

TABLE 2. *Total corrosion (weight loss) calculated from polarization curves of ferrous pipe specimens exposed up to 7 years in back-filled trenches at Bonnet Carre Spillway*

| Date | Exposure time cumulative | Corrosion potential Ref-Cu-$CuSO_4$ | Polarizing Current[a] at break in curve | | Corrosion current | Weight loss | |
|---|---|---|---|---|---|---|---|
| | | | Cathodic $I_p$ | Anodic $I_q$ | $i_0$[b] | Calculated[c] cumulative | Actual |
| | days | V | mA | mA | mA | g | g |
| | Specimen E4 | | | | | | |
| 4-06-60 | 0 | | | | | | |
| 8-24-60 | 140 | −0.800 | 3.0 | 7.0 | 2.0 | 7 | |
| 11-17-60 | 225 | .780 | 2.9 | 7.3 | 2.1 | 11 | |
| 2-08-61 | 308 | .770 | 2.6 | 2.5 $I_p$[d] | 1.9 | 15 | |
| 5-11-61 | 400 | .780 | 3.0 | 2.5 $I_p$ | 2.1 | 20 | 12 |
| | Specimen E13 | | | | | | |
| 4-06-60 | 0 | | | | | | |
| 8-24-60 | 140 | −0.822 | 2.7 | 2 $I_p$[d] | 1.8 | 6 | |
| 11-17-60 | 225 | .786 | 2.3 | 2.5 $I_p$[d] | 1.7 | 10 | |
| 2-08-61 | 308 | .775 | 2.8 | 2.5 $I_p$ | 2.0 | 14 | |
| 5-11-61 | 400 | .790 | 2.8 | 2.5 $I_p$ | 2.0 | 18 | |
| 9-20-61 | 532 | .790 | 2.8 | 2.5 $I_p$ | 2.0 | 25 | |
| 1-18-62 | 652 | .777 | 2.7 | 6.7 | 1.9 | 31 | |
| 4-26-62 | 750 | .770 | 3.0 | 8.5 | 2.2 | 36 | 21 |
| | Specimen E9 | | | | | | |
| 4-06-60 | 0 | | | | | | |
| 8-24-60 | 140 | −0.806 | 2.8 | 2 $I_p$[d] | 1.9 | 7 | |
| 11-17-60 | 225 | .790 | 3.2 | 2.5 $I_p$[d] | 2.3 | 11 | |
| 2-08-61 | 308 | .780 | 2.9 | 2.5 $I_p$ | 2.1 | 16 | |
| 5-11-61 | 400 | .800 | 3.5 | 2.5 $I_p$ | 2.5 | 21 | |
| 9-20-61 | 532 | .799 | 3.1 | 2.5 $I_p$ | 2.2 | 29 | |
| 1-18-62 | 652 | .790 | 3.1 | 7.8 | 2.2 | 35 | |
| 4-26-62 | 750 | .800 | 3.0 | 8.4 | 2.2 | 41 | |
| 8-30-62 | 876 | .771 | 6.4 | 7.2 | 3.4 | 50 | |
| 1-17-63 | 1016 | .750 | 4.4 | 5.7 | 2.5 | 60 | |
| 5-16-63 | 1135 | .545 | 3.0 | 3.0 | 1.5 | 66 | |
| 9-17-63 | 1259 | .650 | 2.4 | 2.5 | 1.2 | 70 | |
| 1-15-64 | 1379 | .710 | 1.7 | 2.0 | 0.92 | 73 | |
| 4-29-64 | 1483 | .690 | 2.1 | 2.8 | 1.2 | 76 | 41 |
| | Specimen E8 | | | | | | |
| 4-06-60 | 0 | | | | | | |
| 8-24-60 | 140 | −0.812 | 2.8 | 2 $I_p$[d] | 1.9 | 7 | |
| 11-17-60 | 225 | .790 | 3.2 | 2 $I_p$ | 2.1 | 11 | |
| 2-08-61 | 308 | .775 | 3.6 | 9.0 | 2.6 | 10 | |
| 5-11-61 | 400 | .795 | 4.6 | 2 $I_p$[d] | 3.1 | 22 | |
| 9-20-61 | 532 | .790 | 3.5 | 9.0 | 2.5 | 32 | |
| 1-18-62 | 652 | .787 | 3.4 | 8.0 | 2.4 | 39 | |
| 4-26-62 | 751 | .780 | 4.2 | 12.0 | 3.1 | 45 | |
| 8-30-62 | 877 | .684 | 8.6 | 9.0 | 4.4 | 57 | |
| 1-17-63 | 1016 | .680 | 4.9 | 5.6 | 2.6 | 69 | |
| 5-16-63 | 1135 | .565 | 1.7 | 3.5 | 1.1 | 74 | |
| 9-17-63 | 1259 | .628 | 1.5 | 3.1 | 1.0 | 77 | |
| 1-15-64 | 1379 | .640 | 1.6 | 1.9 | 0.9 | 80 | |
| 4-29-64 | 1483 | .620 | 2.0 | 2.0 | 1.0 | 83 | |
| 9-10-64 | 1617 | .600 | 1.9 | 2.1 | 1.0 | 86 | |
| 12-18-64 | 1716 | .559 | 1.4 | 1.9 | 0.8 | 88 | |
| 5-05-65 | 1855 | .488 | 1.3 | 1.9 | 0.8 | 91 | |
| 1-12-66 | 2107 | .638 | 1.1 | 0.8 | 0.5 | 95 | |
| 5-18-66 | 2234 | .600 | 0.8 | 1.4 | 0.5 | 96 | |
| 10-26-66 | 2395 | .563 | 0.9 | 1.2 | 0.5 | 98 | |
| 7-26-67 | 2668 | .530 | 1.1 | 1.1 | 0.6 | 102 | 71 |

[a] See figure 2.

[b] $i_0 = \frac{I_p I_q}{I_p + I_q}$.

[c] From Faraday's law, Weight loss (grams) $= K\, t\, i_0$, where $K$ = electrochemical equivalent $2.8938 \times 10^{-4}$ g/c, $t$ = time (s) for the period between successive readings, $i_0$ = average current (amperes) for a period. Approximately, weight loss (mg) $= 25\, t\, i_0$, here $t$ = days between successive measurements, $i_0$ = average current (mA) between successive measurements. The values of $i_0$ at the beginning and at the end of exposure are taken as the initial and final values, respectively, as calculated.

[d] Breaks are indefinite. Values are based on relative cathodic and anodic polarization and/or values of $I_q$ before or after.

TABLE 3. *Total corrosion (weight loss) calculated from polarization curves of ferrous pipe specimens exposed up to 7 years in back-filled trenches at Grenada Dam*

| Date | Exposure time cumulative | Corrosion potential Ref-Cu-$CuSO_4$ | Polarizing Current[a] at break in curve | | Corrosion current[b] $i_0$ | Weight loss | |
|---|---|---|---|---|---|---|---|
| | | | Cathodic $I_p$ | Anodic $I_q$ | | Calculated[c] cumulative | Actual |
| | days | V | mA | mA | mA | g | g |
| | Specimen D4 | | | | | | |
| 3-30-60 | 0 | | | | | | |
| 8-11-60 | 134 | −0.408 | 1.9 | 2.9 | 1.1 | 3.7 | |
| 11-02-60 | 217 | .403 | 2.0 | 2.2 | 1.0 | 5.9 | |
| 2-16-61 | 323 | .444 | 3.3 | 4.1 | 1.8 | 9.6 | |
| 5-03-61 | 399 | .437 | 4.0 | 8.3 | 2.7 | 14 | 17 |
| | Specimen D13 | | | | | | |
| 3-30-60 | 0 | | | | | | |
| 8-11-60 | 134 | −0.452 | 4.0 | 4.5 | 2.1 | 7 | |
| 11-02-60 | 217 | .483 | 2.2 | 4.0 | 1.4 | 11 | |
| 2-16-61 | 323 | .588 | 7.0 | 13.0 | 4.5 | 18 | |
| 5-03-61 | 399 | .560 | 7.5 | 9.7 | 4.2 | 27 | |
| 9-07-61 | 526 | .457 | 4.5 | 5.6 | 2.5 | 37 | |
| 1-26-62 | 667 | .473 | 5.0 | 6.4 | 2.8 | 47 | |
| 4-19-62 | 750 | .500 | 6.0 | 6.6 | 3.1 | 53 | 40 |
| | Specimen D9 | | | | | | |
| 3-30-60 | 0 | | | | | | |
| 8-11-60 | 134 | −0.467 | 2.6 | 2.7 | 1.3 | 4 | |
| 11-02-60 | 217 | .433 | 2.7 | 3.9 | 1.6 | 7 | |
| 2-16-61 | 323 | .630 | 4.3 | 6.0 | 2.5 | 13 | |
| 5-03-61 | 399 | .662 | 4.3 | 4.3 | 2.2 | 17 | |
| 9-07-61 | 526 | .495 | 4.8 | 5.6 | 2.6 | 25 | |
| 1-26-62 | 667 | .725 | 3.1 | 3.5 | 1.6 | 32 | |
| 4-19-62 | 750 | .725 | 2.4 | 2.6 | 1.2 | 35 | |
| 9-06-62 | 890 | .265 | 4.2 | 5.9 | 2.4 | 42 | |
| 12-12-62 | 987 | .169 | 2.4 | 2.5 | 1.2 | 46 | |
| 4-04-63 | 1100 | .501 | 4.2 | 4.2 | 2.1 | 51 | |
| 8-29-63 | 1247 | .550 | — | — | — | — | |
| 11-27-63 | 1337 | .425 | 2.5 | 2.1 | 1.1 | 60 | |
| 4-22-64 | 1483 | .610 | 2.0 | 2.0 | 1.0 | 64 | 63 |
| | Specimen D8 | | | | | | |
| 3-30-60 | 0 | | | | | | |
| 8-11-60 | 134 | −0.388 | 1.9 | 3.0 | 1.2 | 4 | |
| 11-02-60 | 217 | .390 | 2.2 | 2.5 | 1.2 | 6 | |
| 2-16-61 | 323 | .447 | 3.5 | 3.9 | 1.8 | 10 | |
| 5-03-61 | 400 | .457 | 4.6 | 5.2 | 2.4 | 14 | |
| 9-07-61 | 528 | .387 | 3.0 | 8.0 | 2.2 | 22 | |
| 1-26-62 | 669 | .437 | 3.8 | 5.5 | 2.2 | 30 | |
| 4-19-62 | 752 | .465 | 2.7 | 5.2 | 1.8 | 34 | |
| 9-06-62 | 892 | .230 | 3.0 | 4.0 | 1.7 | 40 | |
| 12-12-62 | 989 | .132 | 1.7 | 2.6 | 1.0 | 43 | |
| 4-04-63 | 1102 | .358 | 3.0 | 4.3 | 1.8 | 47 | |
| 8-29-63 | 1249 | .384 | 2.0 | 2.2 | 1.0 | 53 | |
| 11-27-63 | 1339 | .403 | 1.3 | 1.9 | 0.8 | 55 | |
| 4-22-64 | 1485 | .379 | 1.2 | 1.1 | 0.6 | 57 | |
| 8-26-64 | 1611 | .382 | 0.8 | 1.2 | 0.5 | 59 | |
| 1-13-65 | 1751 | .366 | 0.5 | 0.8 | 0.3 | 60 | |
| 4-29-65 | 1858 | .359 | 0.5 | 0.7 | 0.3 | 61 | |
| 12-08-65 | 2081 | .390 | 0.3 | 0.4 | 0.2 | 62 | |
| 5-11-66 | 2235 | .373 | 0.3 | 0.5 | 0.2 | 63 | |
| 10-12-66 | 2389 | .127 | 0.2 | 0.3 | 0.1 | 63 | |
| 7-13-67 | 2663 | .406 | 0.4 | 0.4 | 0.2 | 64 | 55 |

[a] See figure 2.

[b] $i_0 = \frac{I_p \quad Iq}{I_p + Iq}$.

[c] From Faraday's law, Weight loss (grams) $= K\, t\, i_0$, where $K$ = electrochemical equivalent $2.8938 \times 10^{-4}$ g/c, $t$ = time (s) for the period between successive readings, $i_0$ = average current (amperes) for a period. Approximately, weight loss (mg) $= 25\, t\, i_0$, where $t$ = days between successive measurements, $i_0$ = average current (mA) between successive measurements. The values of $i_0$ at the beginning and at the end of exposure are taken as the initial and final values, respectively, as calculated.

TABLE 4. *Total corrosion (weight loss) calculated from polarization curves of ferrous pipe specimens exposed up to 7 years in back-filled trenches at Sardis Dam*

| Date | Exposure time cumulative | Corrosion potential Ref-Cu-$CuSO_4$ | Polarizing Current[a] at break in curve | | Corrosion current $i_0$[b] | Weight loss | |
|---|---|---|---|---|---|---|---|
| | | | Cathodic $I_p$ | Anodic $I_q$ | | Calculated[c] cumulative | Actual |
| | days | V | mA | mA | mA | g | g |
| | Specimen C4 | | | | | | |
| 3-29-60 | 0 | | | | | | |
| 8-10-60 | 134 | −0.821 | 0.54 | $\geqslant I_p$[d] | 0.54 | 1.8 | |
| 11-01-60 | 217 | .802 | .16 | 9 $I_p$[d] | .14 | 2.5 | |
| 2-15-61 | 323 | .800 | .11 | 9 $I_p$ | .10 | 2.8 | |
| 5-01-61 | 398 | .795 | .09 | 9 $I_p$ | .08 | 3.0 | 4.3 |
| | Specimen C13 | | | | | | |
| 3-29-60 | 0 | | | | | | |
| 8-10-60 | 134 | −0.815 | 0.86 | $\geqslant I_p$[d] | 0.86 | 2.9 | |
| 11-01-60 | 217 | .806 | .35 | 9 $I_p$[d] | .31 | 4.1 | |
| 2-15-61 | 323 | .800 | .25 | 9 $I_p$ | .22 | 4.8 | |
| 5-01-61 | 398 | .795 | .22 | 9 $I_p$ | .20 | 5.2 | |
| 9-06-61 | 526 | .799 | .32 | 9 $I_p$ | .29 | 6.0 | |
| 1-25-62 | 667 | .803 | .16 | 9 $I_p$ | .14 | 6.7 | |
| 4-18-62 | 750 | .800 | .20 | 9 $I_p$ | .18 | 7.1 | 6.0 |
| | Specimen C9 | | | | | | |
| 3-29-60 | 0 | | | | | | |
| 8-10-60 | 134 | −0.815 | 0.58 | $\geqslant I_p$[d] | 0.58 | 1.9 | |
| 11-01-60 | 217 | .808 | .28 | 9 $I_p$[d] | .25 | 2.8 | |
| 2-15-61 | 323 | .805 | .11 | 9 $I_p$ | .1 | 3.3 | |
| 5-01-61 | 398 | .800 | .11 | 9 $I_p$ | .1 | 3.5 | |
| 9-06-61 | 526 | .800 | .09 | 9 $I_p$ | .08 | 3.7 | |
| 1-25-62 | 667 | .806 | .10 | 9 $I_p$ | .09 | 4.0 | |
| 4-18-62 | 750 | .812 | .10 | 9 $I_p$ | .09 | 4.2 | |
| 9-05-62 | 890 | .800 | .08 | 9 $I_p$ | .08 | 4.5 | |
| 12-11-62 | 987 | .770 | .13 | 9 $I_p$ | .12 | 4.8 | |
| 4-03-63 | 1100 | .804 | .09 | 9 $I_p$ | .08 | 5.0 | |
| 8-28-63 | 1247 | .830 | .06 | 9 $I_p$ | .06 | 5.3 | |
| 11-26-63 | 1337 | .797 | .06 | 9 $I_p$ | .05 | 5.4 | |
| 4-21-64 | 1483 | .800 | .04 | 9 $I_p$ | .03 | 5.6 | 4.6 |
| | Specimen C8 | | | | | | |
| 3-29-60 | 0 | | | | | | |
| 8-10-60 | 133 | −0.828 | 0.68 | $\geqslant I_p$[d] | 0.68 | 2.3 | |
| 11-01-60 | 216 | .810 | .27 | 9 $I_p$[d] | .24 | 3.2 | |
| 2-15-61 | 322 | .810 | .14 | 9 $I_p$ | .13 | 3.7 | |
| 5-01-61 | 397 | .802 | .14 | 9 $I_p$ | .13 | 3.9 | |
| 9-06-61 | 525 | .805 | .13 | 0.4 | .10 | 4.3 | |
| 1-25-62 | 666 | .808 | .12 | .8 | .11 | 4.6 | |
| 4-18-62 | 749 | .808 | .11 | 1.2 | .10 | 4.8 | |
| 9-05-62 | 889 | .799 | .10 | 1.0 | .09 | 5.2 | |
| 12-11-62 | 986 | .782 | .08 | 0.8 | .07 | 5.4 | |
| 4-03-63 | 1099 | .790 | .05 | 0.3 | .04 | 5.6 | |
| 8-28-63 | 1246 | .830 | .04 | 9 $I_p$[d] | .04 | 5.7 | |
| 11-26-63 | 1336 | .792 | .04 | 0.1 | .03 | 5.8 | |
| 4-21-64 | 1481 | .790 | .03 | .1 | .02 | 5.9 | |
| 8-25-64 | 1607 | .799 | .03 | 3 $I_p$[d] | .02 | 5.9 | |
| 1-12-65 | 1747 | .790 | .02 | 0.1 | .02 | 6.0 | |
| 4-28-65 | 1854 | .800 | .02 | .6 | .02 | 6.1 | |
| 12-07-65 | 2078 | .787 | .01 | .4 | .01 | 6.1 | |
| 5-10-66 | 2232 | .790 | .02 | .5 | .01 | 6.2 | |
| 11-11-66 | 2417 | .790 | .02 | .5 | .01 | 6.2 | |
| 7-12-67 | 2660 | .797 | .02 | .6 | .02 | 6.3 | 4.8 |

[a] See figure 2.

[b] $i_0 = \dfrac{I_p I_q}{I_p + I_q}$.

[c] From Faraday's law, Weight loss (grams) $= K t\, i_0$, where $K$ = electrochemical equivalent $2.8938 \times 10^{-4}$ g/c, $t$ = time (s) for the period between successive readings, $i_0$ = average current (amperes) for a period. Approximately, weight loss (mg) $= 25\, t\, i_0$, where $t$ = days between successive measurements, $i_0$ = average current (mA) between successive measurements. The values of $i_0$ at the beginning and at the end of exposure are taken as the initial and final values, respectively, as calculated.

[d] Breaks are indefinite. Values are based on relative cathodic and anodic polarization and/or values of $I_q$ before or after.

the ferrous state, the use of the ferric equivalent might be more valid. The use of the ferric equivalent would reduce the calculated weight losses by one-third.

The corrosion potentials at Sardis (table 4) were continuously around 0.8 V, while at other sites the potentials fluctuated and were generally more positive. The high water table at Sardis probably accounted for the relatively high electronegative potentials indicative of a deficiency in oxygen. Poor aeration could also account for the low corrosion rates at the Sardis site.

### 3.2. Comparison of Corrosion on Pipe Specimens and on Piling in the Same Soils

Cumulative weight losses based on polarization curves obtained on the seven-year specimens at the 4 sites are plotted against time in figure 4. These losses after 3.7 years of exposure are converted to corrosion rates expressed as weight loss and average penetration (reduction in cross section) for each site. Corrosion rates are tabulated in table 5 for comparison with corrosion observed on piling at the sites. The maximum reduction in thickness shown for the piling is not an overall average based on weight loss but is based on the average depth of the 25 deepest pits measured in the most corroded spots over an area 1 $in^2$ (6.5 $cm^2$) on the piles and includes both sides of the piling wall. Had the maximum reduction in thickness been based on metal loss for a larger area, such as that of the pipe specimen 72 $in^2$ (4.6 $dm^2$), the percentages shown in table 5 would be considerably lower.

The corrosion data (table 5) pertaining to the pipe specimens, under conditions conducive to maximum rates of corrosion, show that corrosion is not a serious problem on piling in these particular locations. Pitting is not a limiting factor as it is on pipe lines. Thus, for example, at Berwick Lock (the most corrosive site) the average penetration on the pipe specimens after 3.7 years of exposure was at a rate of about 0.00078 in/yr (20 micrometers/yr). This means that on the piling of 0.375 in (0.95 cm) metal thickness, if corrosion were to occur on both sides in the same area at this rate only 10 percent of the metal thickness would be gone in 24 years. This corrosion would be in the area subject to the severest corrosion, that is, at the water table or in the excavated soil. In these areas on piling, the Corps of Engineers [3] considers a 35 percent reduction in cross section over a 50-year period as an acceptable maximum. At Berwick Lock, even taking into consideration the higher corrosion rate on specimens during the first 3.7 years, the average reduction in wall thickness over a 50-year period would still be under 30 percent, assuming that piling corroded at the same rate.

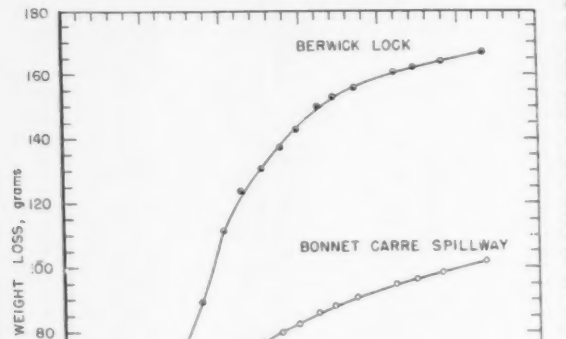


FIGURE 4. *Weight loss-time curves, based on polarization curves, obtained on iron specimens (Nos. 8) buried at four back-filled trench sites.*

### 3.3. Polarization Measurements on Driven and on Buried Steel Rods

Electrical measurements on the rods are tabulated in tables 6 through 9. During early exposure, corrosion currents on the buried rods were larger than on the driven rods. As time went on, corrosion currents tended to equalize, except perhaps at Bonnet Carre and at Berwick Lock where corrosion rates on the buried rods appear to be significantly greater than those on the driven rods.

The potentials of the driven rods are apparently less affected by oxygen than are the potentials of the buried rods. A deficiency of oxygen tends to make the corrosion potentials more electronegative. It is interesting to correlate potential changes with pitting on the rods. As reported by the Corps of Engineers [3], except at Sardis Dam, it was observed that the pits were several times deeper on the buried rods than on the driven rods. Such differences were greatest at Bonnet Carre and at Berwick Lock where the differences in corrosion potentials between buried and driven rods was also greatest, the buried rods having potentials which fluctuated to more positive values. The data [3] indicate that the pitting factor (ratio of maximum pit-depth to average penetration) is greater on buried structures than on driven structures. At Sardis Dam this difference was negligible because of the high water table. The data suggest that future experiments along similar lines should be carried out with longer rods.

### 3.4. Corrosion Rates of Pipe Piles as Calculated from Polarization Curves

The Hiawatha Treatment Plant processes sewage for the area of metropolitan Syracuse, N. Y., where the water table is said to be about 10 ft (3 m) from the ground surface. Soil resistivities in the vicinity of the test piles as measured by the 4-pin method at pin spacings of 3 ft (0.91 m), 12 ft (3.7 m), and 30 ft (9.1 m) were respectively, 10,300, 3450 and 800 Ω-cm.

Preliminary polarization indicated that current increments of 40 mA would be satisfactory for obtaining the cathodic polarization curve on the 72 ft (22 m) pile (fig.

TABLE 5. *Comparison of maximum corrosion on driven steel piles with the normal corrosion on steel pipe specimens buried in nearby backfilled trenches*

TABLE 5. *Comparison of maximum corrosion on driven steel piles with the normal corrosion on steel pipe specimens buried in nearby backfilled trenches*

| Location | Type of piling | Portion of pile inspected | | Exposure at time of inspection | Soil | | | Effect of soil on piling | | | | | | Effect of soil on pipe specimens. Corrosion rates from polarization curves based on the weight loss for the last 3.3 years of 7 years of exposure | | | |
|---|---|---|---|---|---|---|---|---|---|---|---|---|---|---|---|---|---|
| | | | | | | | | Surface with mill scale intact | | | Reduction in thickness in the most corroded spot [d] | | | Weight loss | | Average penetration | |
| | | Above water table | Below water table | | Type | Resistivity [a] | pH [b] | Above water table | In water table zone | Below water table | Above water table | In water table zone | Below water table | | | | |
| | | *ft* | *ft* | *yr* | | *Ω-cm* | | *percent* | *percent* | *percent* | *percent* | *percent* | *percent* | *oz/ft²/yr* | *mdd* [e] | *mpy* [f] | *micro-meters/yr* |
| Berwick Lock, Berwick, La. (westside) | Arch sheet Width, 19.625 in. Thickness, 0.375 in. | 4 By excavation | 1 | 11 | Fill-silty clay over natural clay | 800-1500 | 8.1-8.5 | 60 | 60 | 60 | 8 | nil | nil | 0.51 | 4.3 | 0.78 | 20 |
| Berwick Lock (eastside) | Arch sheet Width, 19.625 in. Thickness, 0.375 in. | 2.5 By excavation | 1 | 11 | Fill-clay over natural clay | 750-1610 | 7.9-8.1 | 40 | 40 | 75 | 11 | 8 | nil | | | | |
| Bonnet Carre Spillway, New Orleans, La. | H, 12 in. Thickness, 0.607 in. | 2 Pile extracted | 120 | 17 | Sand, organic silt and clay mixture | 400-1050 | 6.7-8.1 | 95 | 0 | 95 | nil | nil | nil | 0.43 | 3,6 | 0.66 | 17 |
| Granada Dam, Granada Miss. (northside) | Arch sheet Width, 19.625 in. Thickness, 0.375 in. | 14 Pile extracted | 0 | 12 | Fill-sandy loam and silt over natural shale and organic clay | 4000-15,400 | 3.6-4.9 | 50 | (c) | (c) | 8 | (c) | (c) | | | | |
| Granada Dam (northside) | Arch sheet Width, 15 in. Thickness, 0.375 in. | 5.5 By excavation | 0 | 11 | Fill-clay, sand and silt loam mixture | 2300-16,500 | 4.0-4.4 | 20 | (c) | (c) | 16 | (c) | (c) | | | | |
| Granada Dam (southside) | Arch sheet Width, 15 in. Thickness, 0.375 in. | 5.5 By excavation | 0 | 11 | Fill-sandy loam over natural silty sand | 2400-8000 | 4.4-6.9 | 60 | (c) | (c) | 19 | (c) | (c) | 0.17 | 1.4 | 0.26 | 7 |
| Sardis Dam, Sardis, Miss. | Arch sheet Width, 15 in. Thickness, 0.375 in. | 2 By excavation | 3 | 20 | Fill-sandy loam over natural clay | 3000-50,000 | 5.4-6.0 | 90 | 90 | 90 | nil | nil | 4 | 0.021 | 0.18 | 0.032 | 0.8 |

[a] Resistivity varied with depth and water content. Maximum values shown were measured in situ by the Wenner 4-pin method and the minimum values are as measured in the laboratory under saturated conditilns.

[b] Removed from the site in sealed containers and measured in the laboratory.

[c] Entire piling was well above the water table.

[d] The reduction in thickness is based on the average of 25 measurements in the most severely corroded spot (area of spot, about 1 in; 6.5 cm;) observed.

[e] mdd, milligrams per square decimeter per day.

[f] mpy, mils per year. One mil — .001 in (25 micrometers, approx.)

TABLE 6. *Comparative corrosion (weight loss) on steel rods (driven and buried) exposed about 5 years at Berwick Lock*

Periodic corrosion rates are based on polarization measurements.

| Date | Exposure time cumulative | Corrosion potential Ref-Cu-CuSO4 | | Polarizing current at break in polarization curve[a] | | | | Corrosion[b] current | | Weight loss[c] calculated cumulative | |
|---|---|---|---|---|---|---|---|---|---|---|---|
| | | Driven No. 21 | Buried No. 22 | Driven | | Buried | | Driven No. 21 | Buried No. 22 | Driven No. 21 | Buried No. 22 |
| | | | | Cathodic $I_p$ | Anodic $I_q$ | Cathodic $I_p$ | Anodic $I_q$ | | | | |
| | days | V | V | mA | mA | mA | mA | mA | mA | g | g |
| 6-20-62 | 0 | −0.805 | −0.787 | 1.8 | $>I_p$[d] | 2.4 | $>I_p$[d] | 1.8 | 2.4 | | |
| 8-29-62 | 70 | .811 | .811 | 1.7 | 12 | 2.6 | 8.0 | 1.5 | 2.0 | 2.8 | 3.8 |
| 1-16-63 | 210 | .773 | .785 | 1.9 | 10 | 3.3 | 18 | 1.6 | 2.8 | 8.0 | 12 |
| 5-15-63 | 329 | .768 | .765 | 2.1 | 2.6 | 3.9 | $>I_p$[d] | 1.2 | 3.9 | 12 | 22 |
| 9-18-63 | 455 | .800 | .770 | 2.5 | 10 | 3.2 | 3.8 | 2.0 | 1.7 | 17 | 31 |
| 1-14-64 | 573 | .795 | .739 | 1.0 | 1.0 | 1.6 | 2.0 | 0.5 | 0.89 | 21 | 35 |
| 4-28-64 | 677 | .814 | .722 | 1.5 | 4.0 | 1.7 | 2.3 | 1.1 | .98 | 23 | 37 |
| 9-09-64 | 811 | .790 | .660 | 0.95 | 1.3 | 0.95 | 1.4 | 0.55 | .57 | 26 | 40 |
| 12-17-64 | 910 | .795 | .655 | .65 | 0.65 | .75 | 1.1 | .33 | .45 | 27 | 41 |
| 5-04-65 | 1049 | .777 | .610 | .70 | .90 | .70 | 0.90 | .39 | .39 | 28 | 42 |
| 9-01-65 | 1169 | .795 | .617 | | | | | | | | |
| 1-11-66 | 1301 | .790 | .603 | .43 | .43 | .65 | .78 | .22 | .35 | 30 | 45 |
| 5-17-66 | 1427 | .793 | .601 | .63 | .63 | .70 | .70 | .31 | .35 | 31 | 46 |
| 10-25-66 | 1588 | .790 | .595 | .37 | .40 | .60 | .45 | .19 | .26 | 32 | 47 |
| 7-25-67 | 1861 | .760 | .620 | .27 | .45 | .56 | .33 | .17 | .21 | 33 | 49 |
| Actual weight loss | | | | | | | | | | 20 | 28 |

[a] See figure 2.

[b] $i_0 = \frac{I_p I_q}{I_p + I_q}$.

[c] From Faraday's law, Weight loss (grams) $= K t i_0$, where $K$ = electrochemical equivalent $2.8938 \times 10^{-4}$ g/C, $t$ = time (s) for the period between successive readings, $i_0$ = average current (amperes) for a period. Approximately, weight loss (mg) $= 25 t i_0$, where $t$ = days between successive measurements, $i_0$ = average current (mA) between successive measurements. The values of $i_0$ at the beginning and at the end of exposure are taken as the initial and final values, respectively, as calculated.

[d] Breaks are indefinite. Values are based on relative cathodic and anodic polarization and/or values of $I_q$ before or after.

TABLE 7. *Comparative corrosion (weight loss) on steel rods (driven and buried) exposed about 5 years at Bonnet Carre Spillway*

Periodic corrosion rates are based on polarization measurements.

| Date | Exposure time cumulative | Corrosion potential, Ref-Cu-CuSO4 | | Polarizing current at break in polarization curve[a] | | | | Corrosion[b] current | | Weight loss[c] calculated cumulative | |
|---|---|---|---|---|---|---|---|---|---|---|---|
| | | | | Driven | | Buried | | | | | |
| | | Driven No. 21 | Buried No. 22 | Cathodic $I_p$ | Anodic $I_q$ | Cathodic $I_p$ | Anodic $I_q$ | Driven No. 21 | Buried No. 22 | Driven No. 21 | Buried No. 22 |
| | days | V | V | mA | mA | mA | mA | mA | mA | g | g |
| 6-21-62 | 0 | −0.817 | −0.781 | 2.2 | $\geqslant I_p$[d] | 3.0 | $\geqslant I_p$[d] | 2.2 | 3.0 | | |
| 8-30-62 | 70 | .820 | .807 | 2.8 | 5 $I_p$[d] | 4.0 | 5 $I_p$[d] | 2.3 | 3.3 | 3.8 | 5.6 |
| 1-17-63 | 210 | .801 | .780 | 2.5 | 15 | 3.8 | 13 | 2.1 | 2.9 | 12 | 16 |
| 5-16-63 | 329 | .784 | .710 | 2.5 | 5 $I_p$[d] | 4.0 | 8.0 | 2.1 | 2.7 | 18 | 25 |
| 9-17-63 | 453 | .810 | .679 | 1.9 | 1.9 | 2.0 | 3.0 | 0.95 | 1.2 | 22 | 31 |
| 1-15-64 | 573 | .785 | .651 | 1.7 | 3.0 | 1.8 | 1.8 | 1.1 | 0.90 | 25 | 34 |
| 4-29-64 | 677 | .799 | .630 | 1.6 | 3.0 | 1.9 | 2.5 | 1.1 | 1.1 | 28 | 37 |
| 9-10-64 | 811 | .805 | .608 | 1.8 | 1.8 | 2.2 | 2.2 | 0.90 | 1.1 | 32 | 40 |
| 12-18-64 | 910 | .783 | .590 | 1.2 | 1.2 | 1.4 | 1.9 | .60 | 0.81 | 33 | 42 |
| 5-05-65 | 1049 | .780 | .529 | 1.6 | 3.0 | 1.1 | 1.8 | 1.1 | .68 | 36 | 45 |
| 9-02-65 | 1169 | .796 | .582 | | | | | | | | |
| 1-12-66 | 1301 | .792 | .563 | 1.0 | 0.80 | 0.70 | 0.70 | 0.44 | .35 | 41 | 48 |
| 5-18-66 | 1427 | .797 | .525 | 0.80 | 1.3 | 1.4 | 1.4 | .50 | .70 | 43 | 50 |
| 10-26-66 | 1588 | .785 | .503 | .70 | 0.70 | 0.85 | 0.60 | .35 | .35 | 44 | 52 |
| 7-26-67 | 1861 | .785 | .538 | .85 | .85 | 1.1 | 1.1 | .42 | .55 | 47 | 55 |
| Actual weight loss | | | | | | | | | | 27 | 48 |

[a] See figure 2.

[b] $i_0 = \frac{I_p I_q}{I_p + I_q}$.

[c] From Faraday's law, Weight loss (grams) $= K t i_0$, where $K$ = electrochemical equivalent $2.8938 \times 10^{-4}$ g/C, $t$ = time (s) for the period between successive readings, $i_0$ = average current (amperes) for a period. Approximately, weight loss (mg) $= 25 t i_0$, where $t$ = days between successive measurements, $i_0$ = average current (mA) between successive measurements. The values of $i_0$ at the beginning and at the end of exposure are taken as the initial and final values, respectively, as calculated.

[d] Breaks are indefinite. Values are based on relative cathodic and anodic polarization and/or values of $I_q$ before or after.

TABLE 8. *Comparative corrosion (weight loss) on steel rods (driven and buried) exposed about 5 years at Grenada dam*

Periodic corrosion rates are based on polarization measurements.

| Date | Exposure time cumulative | Corrosion potential, Ref-Cu-$CuSO_4$ | | Polarizing current at break in polarization curve[a] | | | | Corrosion[b] current | | Weight loss[c] calculated cumulative | |
|---|---|---|---|---|---|---|---|---|---|---|---|
| | | Driven No. 21 | Buried No. 22 | Driven | | Buried | | Driven No. 21 | Buried No. 22 | Driven No. 21 | Buried No. 22 |
| | | | | Cathodic $I_p$ | Anodic $I_q$ | Cathodic $I_p$ | Anodic $I_q$ | | | | |
| | days | V | V | mA | mA | mA | mA | mA | mA | g | g |
| 5-15-62 | 0 | −0.821 | −0.665 | 2.5 | > $I_p$[d] | 7.4 | > $I_p$[d] | 2.5 | 7.4 | | |
| 9-06-62 | 114 | .710 | .502 | 4.7 | 7.0 | 6.0 | 7.0 | 2.8 | 3.2 | 7.6 | 15 |
| 12-12-62 | 211 | .603 | .550 | 5.8 | 6.6 | 5.0 | 5.6 | 3.1 | 2.7 | 14 | 22 |
| 4-04-63 | 324 | .735 | .635 | 6.6 | 10.0 | 6.3 | 6.7 | 4.0 | 3.3 | 24 | 31 |
| 8-29-63 | 471 | .695 | .568 | 3.0 | 3.0 | 4.0 | 4.0 | 1.5 | 2.0 | 34 | 40 |
| 11-27-63 | 561 | .651 | .515 | 1.9 | 1.9 | 1.9 | 1.3 | 1.0 | 0.74 | 37 | 43 |
| 4-22-64 | 707 | .770 | .717 | 1.9 | 23 | 1.7 | 1.7 | 1.0 | .85 | 41 | 46 |
| 8-26-64 | 833 | .670 | .440 | 1.8 | 3 $I_p$[d] | 2.0 | 2.0 | 1.4 | 1.0 | 44 | 49 |
| 1-13-65 | 973 | .691 | .499 | 1.4 | 1.4 | 1.4 | 1.4 | 0.70 | 0.70 | 48 | 52 |
| 4-29-65 | 1068 | .740 | .560 | 1.1 | 0.90 | 1.0 | 0.8 | .50 | .44 | 49 | 54 |
| 9-16-65 | 1208 | .546 | .325 | | | | | | | | |
| 12-08-65 | 1291 | .525 | .311 | 0.50 | .86 | 0.78 | .72 | .32 | .37 | 52 | 56 |
| 5-11-66 | 1445 | .595 | .450 | .90 | .50 | .80 | .75 | .32 | .39 | 53 | 57 |
| 10-12-66 | 1599 | .428 | .257 | .80 | .90 | .54 | .54 | .42 | .27 | 54 | 58 |
| 7-13-67 | 1873 | .543 | .480 | .65 | .65 | .45 | .70 | .32 | .27 | 57 | 60 |
| Actual weight loss | | | | | | | | | | 59 | 64 |

[a] See figure 2.

[b] $i_0 = \frac{I_p I_q}{I_p + I_q}$.

[c] From Faraday's law, Weight loss (grams) = $K\,t\,i_0$, where $K$ = electrochemical equivalent $2.8938 \times 10^{-4}$ g/C, $t$ = time (s) for the period between successive readings, $i_0$ = average current (amperes) for a period. Approximately, weight loss (mg) = $25\,t\,i_0$, where $t$ = days between successive measurements, $i_0$ = average current (mA) between successive measurements. The values of $i_0$ at the beginning and at the end of exposure are taken as the initial and final values, respectively, as calculated.

[d] Breaks are indefinite. Values are based on relative cathodic and anodic polarization and/or values of $I_q$ before or after.

TABLE 9. *Comparative corrosion (weight loss) on steel rods (driven and buried) exposed about 5 years at Sardis Dam*

Periodic corrosion rates are based on polarization measurements.

| Date | Exposure time cumulative | Corrosion potential Ref-Cu-$CuSO_4$ | | Polarizing current at break in polarization curve[a] | | | | Corrosion[b] current | | Weight loss[c] calculated cumulative | |
|---|---|---|---|---|---|---|---|---|---|---|---|
| | | | | Driven | | Buried | | | | | |
| | | Driven No. 21 | Buried No. 22 | Cathodic $I_p$ | Anodic $I_q$ | Cathodic $I_p$ | Anodic $I_q$ | Driven No. 21 | Buried No. 22 | Driven No. 21 | Buried No. 22 |
| | days | V | V | mA | mA | mA | mA | mA | mA | g | g |
| 5-16-62 | 0 | −0.791 | −0.797 | 0.91 | $\geq I_p$[d] | 1.1 | $\geq I_p$[d] | 0.91 | 1.1 | | |
| 9-05-62 | 112 | .773 | .772 | .60 | 9 $I_p$[d] | 1.0 | 9 $I_p$[d] | .54 | 0.9 | 2.0 | 2.8 |
| 12-11-62 | 209 | .767 | .765 | .52 | 9 $I_p$[d] | 0.52 | 9 $I_p$[d] | .47 | .47 | 3.3 | 4.4 |
| 4-03-63 | 322 | .790 | .787 | .50 | 9 $I_p$[d] | .48 | 9 $I_p$[d] | .45 | .43 | 4.6 | 5.7 |
| 8-28-63 | 469 | .772 | .716 | .70 | 9 $I_p$[d] | .50 | 9 $I_p$[d] | .63 | .45 | 6.6 | 7.3 |
| 11-26-63 | 559 | .760 | .740 | .54 | 1.5 | .44 | 0.52 | .40 | .24 | 7.8 | 8.1 |
| 4-21-64 | 705 | .778 | .770 | .47 | 1.4 | .38 | .56 | .35 | .23 | 9.1 | 9.0 |
| 8-25-64 | 831 | .645 | .620 | .40 | 0.45 | .52 | 1.0 | .21 | .34 | 10 | 9.9 |
| 1-12-65 | 971 | .763 | .762 | .35 | .35 | .29 | 0.20 | .18 | .12 | 11 | 11 |
| 4-28-65 | 1066 | .791 | .780 | .50 | .85 | .30 | .50 | .32 | .19 | 11 | 11 |
| 9-15-65 | 1206 | .610 | .624 | | | | | | | | |
| 12-07-65 | 1289 | .625 | .642 | .33 | .33 | .45 | .38 | .16 | .21 | 13 | 12 |
| 5-10-66 | 1443 | .755 | .721 | .35 | .40 | .42 | .68 | .19 | .26 | 13 | 13 |
| 10-11-66 | 1597 | .657 | .631 | .35 | .35 | .52 | .62 | .18 | .28 | 14 | 14 |
| 7-12-67 | 1871 | .745 | .637 | .25 | .25 | .32 | .32 | .13 | .16 | 15 | 16 |
| Actual weight loss | | | | | | | | | | 31 | 31 |

[a] See figure 2.

[b] $i_0 = \frac{I_p I_q}{I_p + I_q}$.

[c] From Faraday's law, Weight loss (grams) $= K t i_0$, where $K$ = electrochemical equivalent $2.8938 \times 10^{-4}$ g/C, $t$ = time (s) for the period between successive readings, $i_0$ = average current (amperes) for a period. Approximately, weight loss (mg) $= 25 t i_0$, where $t$ = days between successive measurements, $i_0$ = average current (mA) between successive measurements. The values of $i_0$ at the beginning and at the end of exposure are taken as the initial and final values, respectively, as calculated.

[d] Breaks are indefinite. Values are based on relative cathodic and anodic polarization and/or values of $I_q$ before or after.

FIGURE 5. *Polarization curves of a bare pipe pile, 12.75 in O.D. × 72 ft. long (32.5 cm × 22m) after underground exposure for 12 years at the Hiawatha treatment plant, Syracuse, N. Y.*

5). The following day, the anodic curve was also obtained by using the same increments of applied current. Both curves are shown plotted on rectangular coordinates in order to verify changes-in-slope (breaks). Based on the Pearson equation [2], the total corrosion current on the bare metallic piling surface was calculated to be 215 mA, or a corrosion rate of 0.9 mA/ft² (0.097 mA/dm²). Upon learning that one of the other piles in the vicinity (about 5 ft or 1.5 m away) was of the same diameter but only 19 ft (5.8 m) long, the thought occurred that the average corrosion rate of the shorter pile ought to be greater than that of the long pile because a larger percentage of the short one was probably exposed to excavated soil during installation. Time permitted running a cathodic curve on the 19 ft (5.8 m) pile, applied current increments (10 mA) being estimated in the same manner as previously (fig. 6). Time did not permit obtaining the anodic polarization curve; however, it seemed reasonable to assume that the $I_p/I_q$ ratio would be similar to what was previously observed for the long pile. Based on this assumption, the average corrosion current was calculated to be 79 mA and the corrosion rate 1.3 mA/ft² (0.14 mA/dm²). Because of the limited data, it could be argued that the corrosion rates of the two piles might not be significantly different, and rightly so. Nevertheless, the second pile measurements add validity to the corrosion rate calculated for the long pile. Validation of the corrosion rate was further emphasized when the continuous application of 400 mA to the long pile for one hour caused a change in potential of 50 mV, confined strictly to polarization. This indicated that the pile (fig. 5) was being cathodically protected and that the current at the break, about 300 mA, was in excess of the corrosion current (calculated to be 215 mA).

On the basis of soil resistivity as measured in the area where the piles are located, it appears that the greater portion of the 72 ft (22 m) pile is driven into soil having a resistivity of 800 Ω-cm or less. To further validate the corrosion rate measurements made on the piling other information can be mentioned. The corrosion rates of plain ferrous pipe specimens, based on actual weight loss-time curves involving hundreds of specimens after five years of exposure in 28 soil sites having resistivities between 500 and 3000 Ω-cm, averaged 1.6 mA/ft² [6] (0.17 mA/dm²). The specimens had been buried in back-filled trenches (disturbed soils).

One month after making the polarization measurements, the 19 ft (5.8 m) pile was extracted and cleaned for the measurement of pit depths. It was found that 40 to 50 percent of the pile surface was still covered by mill scale after 12 years of exposure. Pitting on the remaining surface was scattered. By far, most of the pitting was in the upper 9 ft (2.75 m). Thirty-four pits ranging in depth from 50 to 100 mils (1.3 to 2.6 mm) were found in the upper 9 ft (2.75 m), most of the other pits being less than 30 mils (0.77 mm). In the lower 10 ft (3.05 m) of the pile, ten pits ranging from 30 to 90 mils (0.77 to 2.3 mm) were observed. Pits less than 30 mils (0.77 mm) were not recorded.

Assuming that piling at the Syracuse Plant corrodes at the rate of 1.3 mA/ft² (0.14 mA/dm²) for 50 years, the average reduction in metal thickness is of interest. A current density of 1.0 mA/ft² (0.11 mA/dm²) is approximately equivalent to an overall reduction in wall thickness of 0.5 mils/yr (13 micrometers/yr). Thus, the corrosion current density of 1.3 mA/ft² (0.14 mA/dm²) for 50 years would cause a reduction in pipe wall thickness of about 33 mils (0.85 mm). As the wall thickness of the pipe under discussion is 0.375 in (9.5 mm), the overall reduction in thickness for 50 years would be less than 9 percent. As previously mentioned, the Corps of Engineers [3] considered a 35 percent loss in cross section as the acceptable maximum for 50 years. Were a similar rate of corrosion taking place on two surfaces (for example on H piling), the reduction in wall thickness would still be within the acceptable maximum.

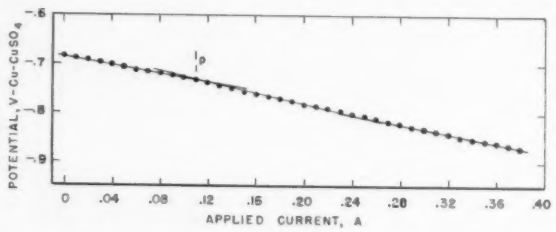


FIGURE 6. *Polarization curve of a bare pipe pile, 12.75 in O.D. × 19 ft. long (32.5 cm × 5.8 m), after exposure underground for 12 years at Hiawatha treatment plant, Syracuse, N. Y.*

## 4. Conclusions

Polarization curves obtained by the Corps of Engineers (Lower Mississippi Valley Division) on four wired pipe specimens at each of four underground test sites were evaluated by the National Bureau of Standards for accuracy in the calculation of metal loss attributable to corrosion and as a means of estimating corrosion on piling which had been previously examined and exposed to the same environments. At each test site one specimen (wired) along with three identical steel unwired specimens were removed after 1, 2, 4 and 7 years of exposure. The Corps of Engineers periodically had made cathodic and anodic polarization measurements on the wired specimens at intervals varying from 2 to 7 months. Using the changes-in-slope (breaks) in the curves plotted on semi-logarithmic coordinates, the calculated instantaneous rates of corrosion were converted to total metal losses by averaging rates for the intervals. The calculated metal losses were in reasonable agreement with the actual weight losses of the wired specimens and also with the weight losses of the unwired specimens.

The relatively stable rates of corrosion which were observed after about four years of exposure of the wired 7-year pipe specimens are expressed as average penetration (reduction in metal thickness) and compared with the corrosion visually observed on piling in the same area or soil environment. On the basis of a criterion mentioned by the Corps of Engineers and using average penetration rates at the most corrosive of the four sites it was concluded that the corrosion taking place on the bare piling was not a serious problem from the standpoint of loss in structural strength.

Corrosion which had taken place in five years on driven steel rods was compared with the corrosion on identical rods exposed concurrently in nearby excavated soil. The corrosion potentials, measured periodically on the rods in connection with polarization runs, seem to bear some relation to the maximum pit depths reported by the Corps of Engineers. Pits were several times deeper on the buried rods than on the driven rods at the two most corrosive sites where the buried rods fluctuated in corrosion potential to values more electropositive than those of the driven rods. While rod specimens were limited in number, one driven and one buried at each of the four sites, the data do indicate that pitting is deepest on the metal in contact with excavated soil above the water table. The differences in weight losses of driven and buried rods were not always significant; however, the metal losses on the driven rods were generally less.

Cathodic and anodic polarization curves were obtained on two 12 in (32.5 cm) diam pipe piles, 72 ft (22 m) and 19 ft (5.8 m) in length, driven 12 years previously at a sewage disposal plant. The 72 ft (22 m) pile was exposed to soil varying in resistivity from 800 Ω-cm for the greater part to 10,300 Ω-cm near the surface. Instantaneous corrosion rates were calculated from the curves. Based on the pipe wall thickness 0.375 in (0.95 cm) the average reduction in wall thickness of the short pile over a period of 50 years would be less than 9 percent. The polarization curves indicated that the long pile was corroding at a lower rate than the short one; however, as only two piles were involved, the difference may be insignificant. About one month later, the short pile was extracted and examined for general corrosion and pitting. It was found that about 40-50 percent of the surface was still covered with mill scale. Most of the pits under 30 mils (0.77 mm) in depth were in the upper 9 ft (2.75 m) of the pile with 34 pits ranging in depth from 50 to 100 mils (1.3 to 2.6 mm). Only two pits were 100 mils (2.6 mm) deep.

---

The author is deeply indebted to his former associate Melvin Romanoff (deceased) who made the arrangements with the Corps of Engineers to carry out the visual inspection of piling at the dam sites and the electrical measurements on pipe specimens at the sites.

The financial support of the American Iron and Steel Institute is gratefully acknowledged.

Deserving special recognition is E. Harold Ardahl, U.S. Army Engineer District, Lower Mississippi Valley Division, Vicksburg, Miss., who carried out all electrical measurements on the pipe and rod specimens and together with Mr. Romanoff made physical inspections on excavated and extracted piles at the dam sites.

The author extends his thanks to O. W. Wade, Consultant, who instigated making polarization measurements on isolated piling at the Hiawatha Treatment Plant, Syracuse, N. Y. and for his assistance in performing the measurements. Mr. Wade later evaluated the corrosion on one of the extracted piles.

## 5. References

[1] Romanoff, Melvin, Corrosion of steel pilings in Soils, Nat. Bur. Stand. (U.S.), Monogr. 58, 23 pages (Oct. 1962).

[2] Schwerdtfeger, W. J., A study by polarization techniques of the corrosion rates of aluminum and steel underground for sixteen months, J. Res. Nat. Bur. Stand. (U.S.), **65C** (Eng. and Instr.), No. 4, 271–276 (Oct.-Dec. 1961).

[3] Corps of Engineers-Lower Mississippi Valley Division, Vicksburg, Miss., Report on Corrosion of Underground Steel Piling, December 1969.

[4] Holler, H. D., Studies on galvanic couples 1. Measurement of electromotive force and internal resistance of cells during current flow, J. Electrochem. Soc. **97**, 271 (Sept. 1950); Corrosion **7**, 52 (Feb. 1951).

[5] Schwerdtfeger, W. J., Current and potential relations for the cathodic protection of steel in a high resistivity environment, J. Res. Nat. Bur. Stand. (U.S.) **63C** (Eng. and Instr.). No. 1, 37–45 (July-Sept. 1959).

[6] Schwerdtfeger, W. J., Soil resistivity as related to underground corrosion and cathodic protection, J. Res. Nat. Bur. Stand. (U.S.), **69C** (Eng. and Instr.), No. 1, 71–77 (Jan.-Mar. 1965).

(Paper 75C2–320)

JOURNAL OF RESEARCH of the National Bureau of Standards—C. Engineering and Instrumentation
Vol. 75C, No. 2, April-June 1971

# Publications of the National Bureau of Standards*

## Selected Abstracts

Achenbach, P. R., **Building research at the National Bureau of Standards,** *Nat. Bur. Stand. (U.S.), Bldg. Sci. Ser. O, 59 pages (Oct. 1970) 60 cents, SD Catalog No. C13.29/2:0.*

Key words: Building materials; building performance; building research; building systems; building technology; history.

The history of building research and technology at the National Bureau of Standards is as long as the history of the institution itself. The participation of the Bureau in the application of science and engineering to building materials and components played an early and important role in the development of steel and reinforced concrete as structural materials; in the understanding of the physics and chemistry of cement, lime and gypsum; in the evaluation of the fire properties of building components; in safe plumbing practices; in laboratory evaluation of the effects of weather on deterioration of building materials; and in measurement of the heat and sound transmission properties of building materials and constructions. The central and continuing objectives of the building research program are shown to be the development of new technical information and new measurement methods for building materials, components, and systems, and the application of this knowledge to the specifications for Federal procurement, to the national standards of the building industry, and to the building code structure of the nation. The Bureau has served as a major technical resource in three large-scale national efforts to accelerate the construction of economical and effective buildings for housing and commercial purposes. One of these efforts is currently in progress and is characterized by an emphasis on the design of buildings to meet the performance requirements of the user rather than through the specification of the properties of the materials used.

Adler, I., Walter, L. S., Lowman, P. D., Glass, B. P., French, B. M., Philpotts, J. A., Heinrich, K. F. J., Goldstein, J. I., **Electron microprobe analysis of Apollo 11 lunar samples,** *(Proc. Apollo 11 Lunar Science Conf., January 1970, Houston, Texas), Geochim. Cosmochim.* **34,** *Suppl. 1, 87–92 (January 30, 1970).*

Key words: Analysis; electron probe; lunar samples; microanalysis; minerals; rocks.

Plagioclase feldspar, clinopyroxene and ilmenite in a polished thin section of a "Type A" crystalline rock were analyzed. The clinopyroxene grains are compositionally variable and both high Ca and low Ca phases are present. The plagioclase is compositionally homogeneous. The ilmenite is chemically homogeneous except for occasional, small areas of high local chromium concentration. Accessory minerals are: apatite (containing Cl, F, Y and Ce), troilite and metallic iron.
Glassy spherules from the lunar soil are mostly similar in composition to the crystalline rocks; however, some appear to have been monomineralic.
The crystalline rock has apparently formed by relatively rapid cooling of a silicate melt under conditions of low oxygen partial pressure. Many components of the soil appear to have formed by meteoritic impact.

Ahern, A. J., **Homogeneity of ion sensitive emulsions and precision of ion beam measurements in spark source mass spectrometry,** *(Summary), Proc. 16th Annual Conf. on Mass Spectrometry and Allied Topics, May 12–17, 1968, Pittsburgh, Pa., sponsored by ASTM Committee E14, pp. 273–276 (1968).*

Key words: Accuracy; circumvention; emulsions; homogeneity; ions; mass; platinum; precision; replicate; spark; spectrometry.

The precision and accuracy with which materials can be trace characterized by spark source mass spectrometry is determined in part by the precision with which ion beams can be measured with ion sensitive emulsions. Consequently, the homogeneity of the emulsion becomes an important factor. Replicate mass spectra of platinum extending over Q2 emulsions show that the sensitivity fluctuations about an average may be <5% standard deviation in a 5 cm length, or there may be as much as a 30% change in sensitivity over this distance.

Anderson, H. J., Brenner, A., **Chemical vapor deposition of rhenium,** *Proc. 2nd Intern. Conf. on Chemical Vapor Deposition, Los Angeles, Calif., May 1970, pp. 356–366 (1970).*

Key words: Chemical vapor deposition; rhenium; rhenium coatings; rhenium oxychlorides.

The chemical vapor deposition (CVD) of rhenium from a variety of compounds was investigated. The reduction of perrhenyl chloride and rhenium oxytetrachloride with hydrogen resulted in the production of deposits which ranged from bright to powdery, the latter being obtained at a temperature above 600°C. The bright deposits were cracked and exfoliated from the substrate. The only ductile deposits were obtained by thermal decomposition of $ReOCl_4$ at about 1200 °C, which process has been previously described by Russian workers.

Andrews, J. R., **Improved bias supply for tunnel-diode picosecond pulse generators,** *IEEE Trans. Instr. Meas.* **IM–19,** *No. 3, 171–175 (August 1970).*

Key words: Jitter; picosecond; pulse generator bias supply; tunnel diode.

An improved bias supply for tunnel diode picosecond pulse generators is described. The supply is stable with temperature and in a commercial 35 picosecond (nominal) risetime sampling oscilloscope system has produced a 4:1 reduction in time base jitter and a 2.5:1 reduction in time base drift. Also described is a tunnel diode pulse generator which when used with the bias supply produces a stable pulse having a flat top sag of no more than 2% in one microsecond.

Armstrong, R. W., Waters, H. P., **Testing programs and research on restraint systems,** *Proc. Intern. Engineering Congress, Detroit, Michigan, January 13–17, 1969, Report No. 690247, pp. 1–48 (Society of Automotive Engineers, New York, N. Y., 1969); Abstract in SAE Trans.* **78,** *102 (1969).*

Key words: Anthropomorphic dummies; auto seat tests; deceleration; human kinematics; human tests; restraint geometry; restraint systems; seat belt; sled tests; webbing abrasion; webbing degradation.

Extensive research in the field of occupant restraints has been made by the Office of Vehicle Systems Research at the National Bureau of Standards. Portions of that research, consisting of human dynamic sled tests at Holloman Air Force Base, tests of restraint systems on the NBS sled, and a variety of strength and degradation tests of seat belts are reported. The geometry of

restraint systems in 1968 production automobiles is documented. Results of 75 human tests reported indicate the nature of human kinematic response to deceleration in seat belts and the forces the seat belt might be expected to withstand. Requirements for dynamic tests of seat belts have been investigated as well as degradation tests for improvement of the Federal Standards for Seat Belts for Use in Motor Vehicles.

Armstrong, R. W., Waters, H. P., Stapp, J. P., **Human muscular restraint during sled deceleration,** *Proc. 1968 Stapp Car Crash Conf., October 22–23, 1968, Detroit, Michigan, Report No. 680793, pp. 440–462 (Society of Automotive Engineers, New York, N. Y., 1969); Abstract in SAE Trans.* **77,** *179 (1969).*

Key words: Occupant restraint systems-seat-belts; seat-biomechanics-biodynamics-kinematics-acceleration (mechanical)-human engineering.

The value of the restraint by legs and arms of a human have been generally disregarded in the development of restraint systems for occupants of an automobile. As part of a series of tests on humans in automobile restraints conducted for the National Bureau of Standards by the 6571st Aero-Medical Research Laboratory, Holloman Air Force Base, New Mexico, measurements were made of the forces exerted on a foot rest during 15 G decelerations. Calculations revealed that for "Lap Belt Only" configuration, 26% of the subject's kinetic energy absorbed was attributed to the seat belt and 42% attributed to the restraint by the legs.

Arthur, M. G., **Impulse spectral intensity calibration at the National Bureau of Standards,** *Proc. Electromagnetic Compatibility Symp., Ft. Monmouth, N. J., June 19–20, 1969, pp. 133–138 (U.S. Army Electronics Command Hdq., Ft. Monmouth, N. J., 1969).*

Key words: Fourier transform; impulse; impulse generator; impulse spectral intensity; impulse standards.

The National Bureau of Standards, in its Radio Standards Engineering Division, is working on standards and measurement techniques of impulsive signals. This work includes a study of impulse spectral intensity, the development of methods of measuring it, and the development of standard impulsive signal generators. These tasks are not yet completed, but certain useful accomplishments have been made.
An authoritative definition of impulse spectral intensity is lacking. Even so, two techniques are being developed at NBS for measuring the amplitude of the frequency spectrum of an impulsive signal. One technique involves the measurement of power spectral density, from which the spectrum amplitude is computed. The other technique involves the measurement of the relative amplitude of the spectrum, and makes use of the results of the first technique to obtain the actual spectrum amplitude. Also under development are two different types of precision impulse generators to be used as reference standards. Since none of this work is completed, no NBS calibration services for impulse spectral parameters are presently available.

Bagg, T. C., **Factors dictating characteristics of systems utilizing microforms,** *J. Micrographs* **3,** *No. 3, 143–146 (1970); ABFM Format* **1,** *No. 2, 1–2 (May 1970).*

Key words: Document storage and retrieval; microform-microfilm systems.

There is a wide variety of microform formats and equipment available for handling microimages. The systems designer therefore has the opportunity to select those procedures and equipment which will assure the fulfillment of the system's requirements. This paper will briefly discuss some questions he must answer before establishing the most effective design.
Each application of microforms has its particular requirements; therefore the questions can serve only as guidelines.
It cannot be over emphasized that the most useful systems are the simplest that will produce legible output images.

Baird, R. C., **Recent theoretical and experimental results of the determination of antenna pattern and gain from near-field measurements, (Summary),** *Proc. Conf. Precision Electromagnetic Measurements, National Bureau of Standards, Boulder, Colo., June 2–5, 1970, CPEM Digest, p. 60 (1970).*

Key words: Gain; microwave antennas; near-field measurements; patterns.

Recent results based on a new method of determining antenna pattern and gain from near-field measurements are summarized. A brief description of the method covering the important new features (such as the ability to correct for the effects of the measuring probe) is included. Preliminary results of measurements made on three different horn antennas (gains = 6.8 dB, 21 dB, 47 dB) are presented. The accuracy of the method appears to be at least as good as conventional far-field measurements and may be significantly better for many antennas. Some potential applications of the method are mentioned and references of publications containing more complete discussions are given.

Baird, R. C., Newell, A. C., Wacker, P. F., Kerns, D. M., **Recent experimental results in near-field antenna measurements,** *Electronic Letters* **6,** *No. 11, 349–351 (May 28, 1969).*

Key words: Antenna gain; antenna pattern; calculated far-field patterns; near-field measurements; new antenna theorems.

Recent experimental results on determination of antenna pattern and effective gain from near-field measurements are described. Two new antenna measurement theorems were applied. Measurements were made on an electrically large horn-lens, a standard-gain horn, and a nominal duplicate of the measuring antenna. Some comparisons with direct far-field measurement results were made.

Barnes, J. A., **Frequency measurement errors of passive resonators caused by frequency-modulated exciting signals,** *IEEE Trans. Instr. Meas.* **IM-19,** *No. 3, 147–152 (August 1970).*

Key words: Frequency; resonance; standards.

The condition of resonance for a signal with FM is defined in this paper as the condition of maximum power transfer by the resonant device. It is shown that if the width of the signal spectrum is small compared to the resonator's line width, then the frequency error is proportional to the third moment of the instantaneous signal frequency about its mean.
One expects that this treatment should at least give the leading term for a precise treatment of atomic resonances. Experimental results with a cesium beam frequency standard confirm this expectation and add caution to the idea that higher Q atomic resonances make better absolute frequency standards.

Barnes, J. A., Chi, A. R., Cutler, L. S., Healey, D. J., Leeson, D. B., McGunigal, T. E., Mullen, J. A., Smith, W. L., Sydnor, R., Vessot, R. F. C., Winkler, G. M. R., **Characterization of frequency stability,** *Nat. Bur. Stand. (U.S.), Tech. Note 394, 50 pages (Oct. 1970) 60 cents, SD Catalog No. C13.46:394.*

Key words: Allan variance; frequency; frequency stability; sample variance; spectral density; variance.

Consider a signal generator whose instantaneous output voltage $V(t)$ may be written as

$$V(t) = [V_0 + \epsilon(t)] \sin [2\pi\nu_0 t + \varphi(t)]$$

where $V_0$ and $\nu_0$ are the nominal amplitude and frequency respectively of the output. Provided that $\epsilon(t)$ and $\varphi(t) = \frac{d\varphi}{dt}$ are sufficiently small for all time, $t$, one may define the fractional instantaneous frequency deviation from nominal by the relation

$$y(t) \equiv \frac{\dot{\varphi}(t)}{2\pi\nu_0}.$$

A proposed definition for the measure of frequency stability is the spectral density $S_y(f)$ of the function $y(t)$ where the spectrum is

considered to be one-sided on a per hertz basis.
An alternative definition for the measure of stability is the infinite time average of the sample variance of two adjacent averages of $y(t)$; that is, if

$$\bar{y}_k = \frac{1}{\tau}\int_{t_k}^{t_{k+\tau}} y(t)dt,$$

where $\tau$ is the averaging period, $t_{k+1} = t_k + T$, $k = 0, 1, 2\cdots$, $t_0$ is arbitrary, and $T$ is the time interval between the beginnings of two successive measurements of average frequency; then the second measure of stability is

$$\left\langle \sigma_y^2(\tau) \equiv \frac{(\bar{y}_k - \bar{y}_{k-1})^2}{2} \right\rangle,$$

where [ ] denotes infinite time average and where $T = \tau$.
In practice, data records are of finite length and the infinite time averages implied in the definitions are normally not available; thus estimates for the two measures must be used. Estimates of $S_y(f)$ would be obtained from suitable averages either in the time domain or the frequency domain. An obvious estimate for $\sigma_y^2(\tau)$ is

$$\sigma_y^2(\tau) \approx \frac{1}{m}\sum_{k=1}^{m} \frac{(\bar{y}_{k+1} - \bar{y}_k)^2}{2}.$$

Parameters of the measuring system and estimating procedure are of critical importance in the specification of frequency stability. In practice, one should experimentally establish confidence limits for an estimate of frequency stability by repeated trials.

Berger, M. J., **Beta-ray dosimetry calculations with the use of point kernels,** *(Proc. Symp. Medical Radionuclides: Radiation Dose and Effects, Oak Ridge Association Universities, Oak Ridge, Tennessee), Atomic Energy Commission Report CONF-691212, pp. 63–86 (June 1970).*

Key words: Absorbed dose; beta-ray; dosimetry; nuclear medicine; point kernel; radionuclide.

Work is described on the evaluation, compilation and use of point kernels in beta-ray dosimetry. Such kernels describe the distribution of absorbed dose around point sources. By the superposition of such kernels one can determine the spatial pattern of absorbed dose in media in which a beta-emitting radionuclide is distributed in some specified fashion. The superposition method has the advantage of great economy. It is not completely realistic, however; its applicability is limited to media which are in effect unbounded and which are homogeneous in composition and uniform in density. Under the auspices of the MIRD Committee of the Society of Nuclear Medicine, point kernels have been compiled for 72 radionuclides. These results are theoretical and are based on information about the shapes of beta spectra (obtained from the ORNL Nuclear Data Group), data about electron stopping power and range values, and point kernels for monoenergetic sources calculated by Spencer.

Birky, M. M., **Simultaneous recording of near-field and far-field patterns of lasers,** *Appl. Opt.* **8,** *No. 11, 2249–2253 (November 1969).*

Key words: Laser; near-field and far-field diffraction; ruby and neodymium.

A technique has been developed to record simultaneously the near-field and far-field diffraction patterns of ruby and neodymium optical masers at several different intensities on each laser pulse. A ruby and neodymium rod have been studied.

Blaine, R. L., **A statistical study of the effects of trace elements on the properties of portland cement,** *Proc. 5th Intern. Symp. on the Chemistry of Cements, Tokyo, Japan, October 7–11, 1968,* **3,** *Part 3, 86–91 (December 31, 1969).*

Key words: Alkalies; concrete; durability; heat of hydration; portland cements; shrinkage; statistical evaluation; strength; sulfate expansion; trace elements.

A digital computer was used to find and evaluate significant relationships between the properties of a large number of portland cements and various independent variables which included chemical compounds, minor constituents, and trace elements. This article presents a review of the probable effects of minor constituents and trace elements on various properties including heat of hydration, sulfate expansion, compressive strength with different curing conditions, shrinkage, and durability. On the basis of the statistical study, $Na_2O$ or $K_2O$ were associated with most of the properties measured but not always to the same degree. Very few of the other individual trace elements had a highly significant relationship to the various properties measured, but when used in equations in addition to other commonly determined variables, there was usually a highly significant reduction in variance. The coefficients for Ba, Cu, SrO, P and Li were significant at the 0.01 probability level in some tests and at the 0.05 probability level in other tests. The coefficients for Cr, Ni, Rb, Ti, V, and Zr were significant at the 0.05 probability level in equations for some of the tests. The effects of the alkalies and trace elements were generally small compared to the effects of major constituents and other independent variables.

Borie, E., **Radiative corrections to back scattering,** *Phys. Rev. C,* **2,** *No. 2, 770–771 (August 1970).*

Key words: Anomalous moment; back scattering; electron; radiative correction.

It is shown that the anomalous magnetic moment of the electron contributes to the radiative correction to scattering by a charge, even at high energies, when the scattering angle is 180°. This effect increases the radiative correction slightly as compared with the usual Schwinger correction.

Boyne, H. S., Hall, J. L., Barger, R. L., Bender, P. L., Ward, J., Levine, J., Faller, J., **Absolute strain measurements with a 30-meter vacuum interferometer,** *(Proc. Conf. Laser Applications in the Geosciences, Huntington Beach, Calif., June 1969), Chapter in Laser Applications in the Geosciences, J. Gauger and F. F. Hall, Jr., Ed., pp. 215–225 (Western Periodicals, North Hollywood, Calif., 1970).*

Key words: Earth strain; earth tide; geophysics; laser strainmeter; seismograph.

We present details on the design and performance of a 30-meter interferometric strain gauge. We also discuss a practical method for recording absolute earth strain measurements by comparing length changes in the interferometer with an absolute wavelength standard.

Branscomb, L. M., **A fully integrated partnership between government laboratory and university,** *Proc. Education on Federal Laboratory-University Relationships Symp. sponsored by the Federal Council for Science and Technology and the American Council on Education, Washington, D. C., October 29–31, 1968, pp. 139–151 (May 1969).*

Key words: *Research management* principles embodied in *government-university collaboration* in the *Joint Institute for Laboratory Astrophysics.*

Invited talk to symposium "Education and Federal Laboratory-University Relationships" sponsored by the Federal Council for Science and Technology, at the Smithsonian Institution, Oct. 29–31, 1968.
The pattern of government laboratory-university collaboration inherent in the Joint Institute for Laboratory Astrophysics (JILA) is described, with emphasis on its advantages and shortcomings and the relevant management principles.

Branscomb, L. M., **Discussion,** *Can. J. Chem.* **47,** *No. 10, 1703–1941 (May 15, 1969).*

Key words: Aeronomy; editorial comments.

This manuscript contains the edited comments on invited papers by A. Dalgarno, A. V. Phelps, and E. E. Ferguson which will appear in Transactions of the IAGA (International Association of Geomagnetism and Aeronomy) Symposium on Laboratory Measurements of Aeronomic Interest, September 3–4, 1968, York University, Toronto, Canada. The Transactions are to be published in the Canadian Journal of Chemistry.

Brauer, G. M., **Pyrolysis-gas chromatographic techniques for polymer identification,** *Chapter 2. Thermal Characteristics Techniques in Techniques and Methods of Polymer Evaluations, P. Slade Ed., II, 41–105 (Marcel Dekker Publ., New York, N. Y., 1970).*

Key words: Chromatographic analysis of degradation products; polymer characterization; polymer identification; pyrolysis-gas chromatography of polymers; pyrolytic techniques.

Pyrolytic techniques used in conjunction with gas chromatography are very useful for elucidating the structure of macromolecules. These methods are a powerful tool in the qualitative characterization of the gross structure, the study of the thermal stability of polymers and the identification of their pyrolysis products, but have also found an increasing number of applications for the quantitative analysis of copolymeric systems and in studies of the kinetics of polymer degradation. The shape of the pyrograms is dependent on the structural characteristics such as the degree of branching or crosslinking, stereoregularity, crystallinity and monomer sequence length distribution in block and graft copolymers. Thus the pyrolysis-gas chromatographic technique opens up new avenues in studying the ultimate arrangement of monomeric units within the polymer chain.

Brauer, G. M., Huget, E. F., Termini, D. J., **Plastic modified o-Ethoxybenzoic acid cements as temporary restorative materials,** *J. Dental Res.* **49,** *No. 6, 1487–1494 (November-December 1970).*

Key words: Dental restorative materials; EBA cements; plastic reinforced restoratives; restorative materials; temporary dental cements.

To improve the stress-bearing characteristics, powdered polymers of relatively low elastic moduli were incorporated into the powder component of EBA cements. Acrylic and vinyl copolymers appeared to be the most suitable additives for achieving reinforcement. The resultant products exhibited significant increases in tensile strength.
These materials possess excellent manipulative qualities. Limited clinical evaluation indicates that some of the polymer-reinforced materials, on the basis of their demonstrated mechanical and palliative properties, appear to be highly useful as long duration temporary restoratives.

Brenner, A., Anderson, H. J., **Chemical vapor deposition of rhenium,** *Proc. Interfinish 1968 7th International Metal Finishing Conf., May 5–9, 1968, Hanover, Germany, pp. 28–31 (1968).*

Key words: Carbonyl; chemical vapor deposition; electrodeposition; hexafluoroacetylacetone; rhenium coatings; trifluorophosphine.

Methods of depositing rhenium coatings are reviewed, and a brief account is given of work now in progress at NBS on the deposition of rhenium. The electrodeposition of rhenium from an aqueous perrhenate bath does not yield a satisfactory coating; work at NBS with various rhenium compounds in both aqueous and nonaqueous solutions did not lead to a better plating process. The chemical vapor deposition (CVD) of rhenium is more promising, particularly the reduction of rhenium hexafluoride with hydrogen. At NBS work has been done with the CVD of rhenium from the carbonyl, the hexafluoroacetylacetone derivative, and work is in progress with the trifluorophosphine derivatives.

Brown, D. W., Lowry, R. E., Wall, L. A., **Radiation-induced copolymerization of tetrafluoroethylene and 3,3,4,4,5,5,5-heptafluoropentene-1 under pressure,** *J. Polymer Sci. Part A-1,* **8,** *No. 9, 2441–2452 (1970).*

Key words: Amorphous polymer; copolymerization, fluoropolymers; glass temperature; high pressure; radiation-induced; tetrafluoroethylene; 3,3,4,4,5,5,5,-heptafluoropentene-1.

An investigation was made of the gamma-ray induced copolymerization of tetrafluoroethylene and 3,3,4,4,5,5,5-heptafluoropentene-1. At 22°C and 5000 and 10,000 atm the polymerization rate changes little between 0 and 75 mole percent tetrafluoroethylene. Above 90 mole percent the rate increases greatly. Molecular weights vary in a fashion similar to the variation in the rates. Between 10,000 and 15,000 atm the viscosity of the pentene increases by a factor of $10^8$. A rate maximum occurs in this pressure range; polymerization continues long after irradiation is ended. Both reactivity ratios favor the pentene.
Several copolymer properties were studied. The polymers are amorphous and soluble in perfluoro-ethers, -alkanes, and -aromatics if they contains less than 80% tetrafluoroethylene. The glass temperatures of the amorphous polymers decrease and the thermal and radiation stability increases as the tetrafluoroethylene content increases.

Bullis, W. M., Scace, R. I., **Measurement standards for integrated circuit processing,** *Proc. IEEE* **57,** *No. 9, 1639–1646 (September 1969).*

Key words: ASTM standards; integrated circuits; microelectronics; semiconductor devices; semiconductor materials; semiconductor process control; silicon.

Both yield and quality of silicon monolithic integrated circuits depend on adequate control at all stages of their manufacture. Such control depends on measurement at each step beginning with the selection of the substrate wafer, process chemicals, and parts, through the fabrication, assembly, and packaging of the finished circuit. American Society for Testing and Materials Committee F-1 on Materials for Electron Devices and Microelectronics has developed standards for tests which have been widely used in the exchange of materials at various interfaces in the electron device industry. Many of these standards can be readily adapted for in-process control as well as for materials and parts acceptance tests. These standards and the process by which they were developed are reviewed and the importance of both industrial participation and the technical support activities of the National Bureau of Standards in this development is indicated. The need for additional standards is emphasized.

Casella, R. C., **Possible failure of the Pomeranchuk theorem —shrinkage of the forward elastic peak,** *Phys. Rev. Letters* **24,** *No. 25, 1463–1466 (June 22, 1970).*

Key words: Asymptotics; cross section; diffraction shrinkage; high energy; pomeranchuk theorem.

If one elects to interpret recent Serpukhov data as indicating failure of the Pomeranchuk Theorem, then elastic cross sections of the asymptotic form $(d\sigma/dt)_{t=0} \times F[\log^2 s)t]$ are suggested for such processes (e.g., $K^{\pm}p$) at large $s$ and small $|t|$. A prominent special case is $F(x) = \exp(Ax)$.

Cezairliyan, A., McClure, J. L., Morse, M. S., Beckett, C. W., **Measurement of heat capacity of tantalum in the range 1900–3000 K by a pulse heating method,** *Proc. 5th Symp. Thermophysical Properties, Newton, Mass., September 30-October 2, 1960, C. F. Bonilla, Ed., pp. 385–390 (American Society of Mechanical Engineers, New York, N. Y., 1970).*

Key words: Heat capacity; high-speed measurements; high temperature; tantalum; thermodynamics.

A technique is described for the high-speed (millisecond resolution) measurement of heat capacity of electrical conductors at high temperatures (above 1900 K). Measurements on heat capacity of tantalum in the temperature range 1900 to 3000 K are reported and are compared with those in the literature. Duration of an individual experiment in which the specimen was heated from room temperature to close to its melting point is less than one second. Temperature measurements were made with a high-speed photoelectric pyrometer. Experimental quantities (voltage, current, temperature) were recorded with a high-speed digital

data acquisition system which has a time resolution of 0.4 ms. Estimated inaccuracy of heat capacity measurements in the above temperature range is 2 to 3 percent.

Champion, E. C., Marinenko, G., Taylor, J. K., Schmidt, W. E., **Determination of submicrogram amounts of chromium by coulometric titrimetry,** *Anal. Chem.* **42,** *11, 1210–1213 (September 1970).*

Key words: Chromium; coulometry; trace analysis.
An improved method has been developed for the determination of micro- and nanogram amounts of chromium by coulometric titrimetry. Sample containing 30 $\mu$g to 15 ng chromium may be analyzed with an uncertainty limit of one nanogram. The method is bias free within the uncertainty of the measurement due to random errors, and the end point determination is the limiting factor for further improvements of the method.

Chandler, H. H., Bowen, R. L., Paffenbarger, G. C., Mullineaux, A. L., **Clinical investigation of a radiopaque composite restorative material,** *J. Am. Dental Assoc.* **81,** *No. 4, 935–940 (October 1970).*

Key words: Clinical research (dental); composite restorations; diagnosis; physical properties of fillings; x-ray opaque.
A radiopaque composite restorative material was developed using a ternary eutectic dimethacrylate liquid formulation as the binder and a $BaF_2$-containing glass and fused silica as the reinforcing fillers. One hundred and ten restorations were placed using this newly developed material. The restorations will be observed over a prolonged period. They had sufficient radiopacity and yet were esthetically pleasing. Postoperative radiographs showed comparatively radiolucent areas in and around many of the restorations. These radiolucencies were usually caused by unfilled spaces at the tooth-restoration interface.

Chandler, R. F., Christian, R. A., **Comparative evaluation of dummy performance under $-G_x$ impact,** *Proc. 13th Stapp Car Crash Conf., Boston, Mass., December 2–4, 1969, Report No. 690798, pp. 61–75 (Society of Automotive Engineers, New York, N. Y., 1970); Abstract in SAE Trans.* **78,** *171–172 (1969).*

Key words: Automobiles; dummies; dynamic; impact; performance; restraints.

Comparative evaluation of a variety of anthropomorphic dummies undertaken by the Office of Vehicle Systems Research at the National Bureau of Standards indicates a wide range of dummy performance. Dynamic tests, which were conducted on the NBS Dynamic Seat Belt Tester, simulated an impact environment with the dummies restrained by lap belt alone, or combined lap and torso diagonal belts of the type used in American automobiles. A variety of dummies, varying in construction from the most rudimentary to the most sophisticated were tested. Test parameters included variations in impact velocity and $-G_x$ acceleration. Each dummy was tested with both types of restraints, and sufficient tests were made to demonstrate the ability of the dummy to reproduce its reaction performance.
These tests indicate that even when dummies are subjected to carefully controlled impacts with skilled technical personnel following identical procedures, it is difficult to reproduce test results. Techniques which were used to control dummy performance and modifications which were incorporated to improve reliability of the dummies are discussed.

Clark, A. F., Childs, G. E., Wallace, G. H., **Electrical resistivity of some engineering alloys at low temperatures,** *Cryogenics* **10,** *No. 4, 295–305 (August 1970).*

Key words: Aluminum alloys; copper alloys; cryogenics; electrical conductivity; iron alloys; nickel alloys; titanium alloys.
The electrical resistivities of several engineering alloys have been measured at 4K, 20K, 76K, 192K, and 273K. Specimens of aluminum, nickel, copper, titanium and iron alloys have been measured, some of them in different heat treated conditions. Most of the alloys have a smooth decrease in resistivity with decreasing temperature, but some unusual results are reported. Comparisons are made between different alloys and between different heat treatments of the same alloys.

Corliss, E. L. R., **Hearing aids,** *Nat. Bur. Stand. (U.S.) Monogr. 117, 26 pages (Oct. 1970) 35 cents, SD Catalog No. C13.44:117.*

Key words: Audition; communications; hearing, hearing aids; selection of hearing aids; speech communication.

This publication contains information, useful to the hard of hearing, on several topics relating to hearing and hearing aids. It is assumed that the individual has already consulted a physician on the diagnosis of his hearing loss, for this is the necessary first step in correcting any faulty hearing condition. The publication may also be of interest to teachers and others wishing to explore this field.
This publication represents an extensive revision of NBS Circular 534, Hearing Aids. It includes new material based upon research conducted at the National Bureau of Standards during the intervening years.

Cornog, D. Y., Cornog, J. R., **Human factors engineering in the sorting and handling of mail,** *Proc. NATO Advanced Study Institute on "Human Factors/Ergonomics," Mondello, Sicily, September 29, 1969, pp. 1–34 (January 21, 1970).*

Key words: Human factors; mail handling; mail processing; mail sorting; methodology.

A case study is used to illustrate both the technical and management aspects of human factors in a unique American organization —an organization which combines a government agency with the typical operations of a gigantic materials handling industry—the United States Post Office Department. Mail handling operations are described with an enumeration of the types of human factors problems to be found. The various approaches to solving human factors problems include: in-house Human Factors Engineering Laboratory research, field studies in postal installations, and contract research performed by industry, private research firms and university departments. Future human factors research in mail handling problem areas is discussed. Information is provided about data sources for American human factors research activities and personnel.

Costrell, L., **Development and current status of the standard nuclear instrument module (NIM) system,** *Nat. Bur. Stand. (U.S.), Tech. Note 556, 15 pages (Oct. 1970) 30 cents, SD Catalog No. C13.46:556.*

Key words: Instrumentation; instruments; modules; NIM; nuclear; standards.

The standard Nuclear Instrument Module (NIM) system described in AEC Report TID-20893 is widely used in laboratories throughout the world. This report presents a history of the development and reviews the current status of the NIM system.

Cruz, J. E., Jellison, J. C., **A digital technique for generating variable frequency multiphase waveforms,** *Rev. Sci. Instr.* **41,** *No. 7, 1098–1099 (July 1970).*

Key words: Digital; logic gating; quasi-sinusoid.

To drive a two or three phase synchronous motor over a wide frequency range has, until now, required complex electronic networks to keep the proper phase relationships.
In this paper a technique is described for driving a two phase synchronous motor over a frequency range of three decades. This method consists of using digital techniques for generation of the two driving waveforms, with constant phase between them, over the specified frequency range.
Discussion of the feasibility of automatic control of the speed of the motor and expansion of the digital logic to generate $n$-phase waveforms is presented.

Davis, D. D., **Transmission of time/frequency signals in the vertical interval,** *Proc. 108th Technical Conference and Equipment Exhibit, New York, N. Y., October 4–9, 1970, Article No. 43, p. 3 (Society of Motion Picture and Television Engineers, New York, N. Y., 1970).*

Key words: Frequency and time dissemination; television; verti-

cal interval signals.
An abstract will be prepared from the synopsis, by the Society of Motion Picture and Television Engineers, subject to the author's clearance.

Davis, D. D., Jespersen, J. L., Kamas, G., **The use of television signals for time and frequency dissemination,** *Proc. IEEE* **58,** *No. 6, 931–933 (June 1970).*

Key words: Frequency and time code; television; time.

Measurements of the three U. S. television networks show the path delay from Washington, D. C. to Denver, Colorado is stable to a few microseconds over a period of months. Stability over half-hour periods of ± 5 ns was measured by observing the phase of the 3.58 MHz color subcarrier. A time dissemination system to exploit the characteristics of television is described. On local broadcasts, timing information is recoverable to ±3 ns, corresponding to a frequency stability of $\pm 1 \times 10^{-12}$ for 1 hour averaging.

Diller, D. E., Hanley, H. J. M., Roder, H. M., **The density and temperature dependence of the viscosity and thermal conductivity of dense simple fluids,** *Cryogenics* **10,** *No. 4, 286–294 (August 1970).*

Key words: Density dependence; liquid state; simple fluids; temperature dependence; thermal conductivity; transport properties; viscosity.

This paper discusses the experimental information on the transport properties of dense simple fluids with emphasis on the compressed and saturated liquid states. Similarities and differences in the wide range density and temperature dependencies of the viscosity and thermal conductivity coefficients are summarized. The excess transport properties of argon, helium, hydrogen, oxygen, and carbon dioxide are graphically compared in the same reduced density and temperature ranges.

Durst, R. A., **Pick an ion, any ion,** *Ind. Res. pp. 36–39 (November 1970).*

Key words: Electrode monitoring; industrial monitoring; ion-selective electrodes; pollutant monitoring.

A brief discussion is given of the types of ion-selective electrodes and the basic principles of their operation. The advantages of these sensors for industrial and environmental pollution monitoring are given, such as, the continuous direct-reading nature of the measurement, fast response time, and portability. Examples of typical industrial and environmental monitoring applications are included, for example, sulfide ion in pulp processing, nitrogen oxides and fluoride in air pollution, and nitrate in soil slurries. Care is necessary in applying these sensors to complex systems where interferences could be a problem and ingenuity is required in modifying the analysis parameters to obtain reliable results. The specificity and sensitivity of these sensors to several serious pollutants will probably result in their future use in pollution-monitoring systems.

Engen, G. F., **A new method of characterizing amplifier noise performance (Summary),** *Proc. Conf. Precision Electromagnetic Measurements, National Bureau of Standards, Boulder, Colo., June 2–5, 1970, CPEM Digest, pp. 20–21 (1970).*

Key words: Amplifier noise; noise; noise measurement.

Although the use of a noise figure or noise temperature to characterize amplifier performance is a well-established practice, it is also recognized that this parameter provides only a partial description of the amplifier noise properties. In general, the noise figure (or temperature) depends upon the generator impedance and is thus a function of the signal source and amplifier combination.
Typically, the noise figure is measured by the Y-factor method using hot and cold noise sources which are nominally matched (reflectionless). The result of this measurement is of value as a figure of merit; however, if optimum performance is to be realized, the applications engineer must know whether to adjust the signal source impedance for maximum power transfer, minimum noise figure, or according to some other criteria, and the deterioration in performance which results if this is not done. It is the purpose of this paper to present an alternative method of characterizing amplifier noise performance in terms of parameters which provide ready answers of these questions. In addition, the measurement of these parameters via a simple extension of the Y-factor method will be described.

Farrar, T. C., **Pulsed and Fourier transform NMR spectroscopy,** *Anal. Chem.* **42,** *No. 4, 109A–112A (April 1970).*

Key words: Fourier transform; nuclear magnetic; pulsed resonance.

The development of pulsed and Fourier transform NMR spectroscopy is discussed. Some of the requirements of pulsed NMR spectrometers and of the ancillary signal averaging and data reduction devices are given.

Frederick, N. V., Scott, W. W., Jr., **A simple technique for metalizing boron nitride,** *Rev. Sci. Instr.* **40,** *No. 9, 1240 (September 1969).*

Key words: Boron nitride; ceramic; metallizing; ultrasonic; vacuum.

Boron nitride is a relatively new material, first developed about ten years ago. It is a refractory ceramic of noteworthy physical and dielectric properties. Successful metalization of boron nitride results in a product which should be very useful in the electronics industry.
A process is described for preparing the boron nitride surface which ultimately results in a strongly attached gold film surface which easily passes the accepted "scotch tape" test.

French, B. M., Walter, L. S., Heinrich, K. F. J., **Quantitative mineralogy of an Apollo 11 lunar sample,** *(Proc. Apollo 11 Lunar Science Conf., January 1970, Houston, Texas), Geochim. Cosmochim.* **34.** *Suppl 1, 433–444 (February 1970).*

Key words: Apollo 11; electron probe analysis; mineralogy; moon; petrography; rocks.

Petrography and mineral analyses of Sample 10017, collected by the Apollo 11 mission, are reported. They indicate formation by relatively rapid crystallization of a silicate melt. Major components are clinopyroxene, plagioclase and ilmenite. Minor components include troilite, native iron, and apatite. The mineral compositions indicate differentiation during magmatic crystallization, leading to Fe enrichment in the pyroxenes and to alkali enrichment in the feldspars. The mesostasis, the residual liquid produced during crystallization, is strongly enriched in K and Si, but strikingly low in Na; this may be due to volatilization during the later stages of crystallization. The compositional trends, similar to those in other lunar samples, indicate formation by relatively rapid magmatic crystallization, which developed significant chemical fractionation, at low oxygen fugacity and under virtually anhydrous conditions.

Gebbie, H. A., Kuhn, P., Bohlander, R. A., **Scattering by high cirrus: Its effect on submillimeter wave determination of atmospheric water vapor, Nature,** *Letter to Editor* **226,** *No. 5242, 71–72 (April 4, 1970).*

Key words: Fourier spectroscopy; high cirrus; submillimeter waves; water vapor.

Submillimeter waves and, by implication in this context, the use of the pure rotation band, offer important advantages for determining the distribution of water vapor with height in the atmosphere. The reasons are there. 1) We can readily resolve single rotation lines in this region by Fourier Spectoscopy using interferometers. The calibration for intensity of single lines is easily made and a range of lines with different absorption strengths can then be chosen to match the requirements of the inversion procedure used to construct the model radiating atmosphere. 2) The use of long wavelengths allows us to dispense with hot radiation sources and use, for example, the radiation exchange between a room temperature detector and cold sky.

Gills, T. E., Marlow, W. F., Thompson, B. A., **Determination of trace elements in glass by activation analysis using hydrated antimony pentoxide for sodium removal,** *Anal. Chem.* **42,** *1831–1833 (December 1970).*

Key words: Activation analysis; glass; hydrated antimony pentoxide (HAP); radiochemical separations; sodium; trace elements.

A method has been developed for the determination of a number of trace elements at the ppm and ppb levels in high-sodium glass by neutron activation analysis. For glass containing about 10 percent sodium, neutron irradiation at levels sufficient to allow determination of trace constituents results in production of 10 mCi or more of $^{24}Na$. If the $^{24}Na$ is allowed to decay before analysis, information about elements producing short-lived radioisotopes is lost. In the procedure described the radiosodium is removed by passing the dissolved glass through a column of hydrated antimony pentoxide (HAP). The effluent can be counted directly with a Ge(Li) or NaI(Tl) detector. The method has been applied to the analysis of NBS Standard Reference Material (SRM) glass which was found to contain 1 ppm of Cu and subppm levels of Mn, Au, Ga, Sb, La, Co, and Ir.

Glass, A. J., Guenther, T. H., Editors, **Damage in laser materials,** *Proceedings of a Symposium Sponsored by the American Society for Testing and Materials and by the National Bureau of Standards June 24–25, 1970, NBS, Boulder, Colorado, Nat. Bur. Stand. (U.S.), Spec. Publ. 341, 133 pages (Dec. 1970) $1.25, SD Catalog No. C13.10:341.*

Key words: Ferroelectric materials; glass; laser damage; lasers.

The second ASTM Symposium on Damage in Laser Materials was held at the National Bureau of Standards at Boulder, Colorado on June 24th and 25th, 1970. About 150 attendees heard papers by fourteen speakers, representing the major manufacturers of laser glass, government, industrial and university laboratories. Although the primary emphasis was on Nd:glass as a laser material, damage mechanisms and morphology in ruby, sapphire, and nonlinear optic materials were also considered. It was clear that substantial advances have been made in the last year in the production of damage-resistant laser glass for use in conventional Q-switched lasers. New diagnostic techniques have been developed, and in some cases, adopted as quality control procedures by the glass manufacturers. Theoretical understanding of the fundamental damage mechanisms is beginning to emerge, and material properties relevant to these damage mechanisms are beginning to be measured. It was equally clear that a great deal of effort remains to be expended to develop techniques suitable for nondestructive testing of laser materials, and that many properties of laser materials at high energy density are presently poorly understood.

Glaze, D. J., **Improvements in atomic cesium beam frequency standards at the National Bureau of Standards,** *IEEE Trans. Instr. Meas.* **IM–19,** *No. 3, 156–160 (August 1970).*

Key words: Atomic frequency standard; cesium beam; figure of merit; frequency accuracy; frequency multiplier; frequency precision; NBS–III; NBS–5; phase noise; quartz crystal oscillator; ramsey cavity; slave oscillator.

The National Bureau of Standards Frequency Standard, NBS–III, a cesium beam with a 3.66 meter interaction region, has been in operation since 1963. The last published (1966) accuracy capability for NBS–III was $1.1 \times 10^{-12}$ ($1\sigma$). With this performance NBS–III was used in the measurement of the frequency of the hyperfine separation of hydrogen. This was, and is, the most accurate published measurement of any physical quantity. A number of improvements are being made in NBS–III to improve its accuracy capability. In early 1966 the vacuum system was modified to use three commercial 200 liter per second ion pumps. The resulting ultimate pressure was improved by a factor of ten to about $10^{-8}$ torr ($1.3 \times 10^{-6}$ N/m$^2$). Several new solid-state, broadband frequency multiplier chains have been constructed with particular attention given to reduction of both power-line related sideband levels and random phase noise sideband levels. Reduction of the random phase noise by more than 20 dB compared to the previous state of the art has been obtained consistently. One of these frequency multiplier chains is presently in use in the 5 to 60 MHz section of the 9.192 . . . GHz excitation system. In addition a solid-state servo system has been employed to control the frequency of the 5 MHz slave oscillator. This servo system and the new frequency multiplier chain have improved both the reliability and long-term stability of NBS–III.
Comparisons were made between NBS–III and one of the commercial cesium standards in the NBS Clock Ensemble. The relative fractional frequency stability of $\sigma(N = 2,\ \tau = 1$ day, $T = 7$ days$) = 1 \times 10^{-13}$ was observed for nine weekly comparisons. Presently at NBS there are no hydrogen masers or thallium beams capable of being used in meaningful measurements against NBS–III. The very long-term frequency stability for this recently improved NBS–III system has not been evaluated fully. Due to the improvements in both electronics systems and evaluative techniques, however, an accuracy of $5 \times 10^{-13}$ ($1\sigma$) for a single evaluative experiment is reported. Substantial NBS effort is being expended toward improvement of the accuracy and figure of merit (presently 10) for NBS–III. New designs and associated components for improved beam optics have been completed. Improved, completely solid-state 5 MHz to 9.2 GHz frequency multipliers have been constructed, and testing is being conducted now. The modified NBS–III beam tube together with new electronic systems will be designated NBS–5. It is expected to be in operation in early 1970 and to exhibit a figure of merit in excess of 500.

Goldman, A. J., **Analysis of a capacity concept for runway and final-approach path airspace,** *Proc. Ion National Air Meeting on Air Traffic Control in the 1970's, Institute of Navigation, St. Louis, Mo., April 14–16, 1970, pp. 119–131 (1970).*

Key words: Air traffic control; airport; capacity concept; markov renewal process; runway.

This paper describes some highlights of a short-term analytical study leading: (a) to a "maximum throughput-rate" capacity concept in the context of a service facility handling a stream of customers of various types, and (b) to the specialization of this concept to a stream of IFR landings at a runway. The specialization is shown to be representable by a simple mathematical formula, of potential value (for example) in connection with cost-effectiveness analyses of proposed changes in ATC equipment or procedures. Directions for further research are identified, and the paper concludes with some general remarks on conceptual difficulties associated with the notion of "capacity."

Greenfeld, S. H., Warner, E. R., Reinhart, H. W., **Bibliographies on fabric flammability. Part 5. Testing and test methods,** *Nat. Bur. Stand. (U.S.), Tech. Note 498–2, 39 pages (Sept. 1970) 45 cents, SD Catalog No. C13.46:498–2.*

Key words: Bibliography of test methods; burning; burning rate; combustion; fire; fire retardant; flame; flame spread; gases; ignition; smoke.

This, the fifth of a series of bibliographies on fabric flammability, relates to test methods and testing of fabrics and products made from fabrics and related materials. Unlike the earlier bibliographies, which cited references to flammability of categories of fabric products, this one cuts across product lines and covers all of the products within the ranges defined in the 1967 amendment to the Flammable Fabrics Act. Approximately 300 citations are included.

Grosch, H. R. J., **A view of computers from the Bureau of Standards,** *Input* **6,** *No. 2, 3–7 (1970).*

Key words: Activities of the Center for Computer Sciences; informal treatment; input.

A brief review is given of the activities of the Center for Computer Sciences at the National Bureau of Standards, in a popularized, informal treatment.

Guttman, C. M. DiMarzio, E. A., **Separation by flow. II. Application to gel permeation chromatography,** *Macromolecules* **3,** *No. 5, 681–691 (September–October 1970).*

Key words: Chromatography; gel filtration; gel permeation chromatography; macromolecules; separation by flow.

Models of a Gel Permeation Chromatography column are proposed in which there is flow through each of the beads as well as around them. Diffusion is allowed within and outside of the beads. By making general arguments on particle current flow, the volume elution is computed as a function of solute particle size for a simplified view of the column. The equation for the location of volume elution peaks thus derived show functional dependences on the particle radius and the column geometry very much like equations derived by previous workers for models in which there was no flow in the beads. The method of Herman's is extended to allow for flow within the beads. Two times characterize the system; the time for a particle to diffuse into and out of the bead and the time to flush the particle out of the bead. The width of the volume elution peak (in contradistinction to the work of Herman's) no longer becomes infinite as the diffusion coefficient goes to zero since the residence time within the bead is never larger than the flush time. Explicit formulae are given for the first three moments of the volume elution; it is shown that the elution volume for a monodispersed species is gaussian. In all cases systems with open pores which allow flow show better separation capabilities than those which do not allow flow.

Haar, L., Shenker, S. H., **A phenomenological equation of state,** *Proc. 5th Symp. Thermophysical Properties, Boston, Mass., September 30-October 2, 1970, C. F. Bonilla, Ed., pp. 223-226 (American Society of Mechanical Engineers, New York, N. Y., 1970).*

Key words: Compressibility factors; equation of state; high density; high temperature; pairwise potentials; redlich kwong; second virial coefficient; thermodynamics.

A simple phenomenological equation of state for high temperature gases is proposed. It is developed from considerations of the two body pair interactions, and it has no arbitrary parameters. The equation has been applied to two simple gases, nitrogen and argon. The results compare quite well with experimental data up to 10,000 bar and in the range of two to four times the critical temperature. Also included for comparison is the widely used Redlich Kwong equation. The present work compares favorably with the Redlich Kwong at the lowest temperature; however, as temperature is increased the present work becomes increasingly more accurate, whereas the corresponding states equation tends to degrade with temperature.

Halford, D., **Frequency stability of quality quartz crystal oscillators: Performance and some critical applications,** *Proc. Intern. Colloq. Chronometrie, Paris, France, September 16-20, 1969, Serie A, pp. A-11-1-A-11-3 (September 1969).*

Key words: Atomic frequency standards; cesium beam; flicker noise; frequency stability; frequency standards; hydrogen maser; long baseline interferometry; quartz crystal oscillators; time standards.

For time intervals, tau, of one second or less, the short-term fractional frequency stability of high quality quartz crystal oscillators is superior to all other known frequency sources. For time intervals in the range of 1 to 10 seconds, these quartz crystal oscillators are at least as good as all other devices, such as hydrogen maser oscillators and rubidium gas cell frequency standards. For time intervals in the range from 10 to 1000 seconds, only hydrogen maser oscillators and the best cesium beam frequency standards are capable of frequency stabilities which exceed those of the best quartz crystal oscillators.

The stability of good quartz crystal oscillators has been found to be at least as good as 2 parts in $10^{13}$ for time intervals, tau, in the vicinity of 10 seconds, and is not much different for tau equal to 100 seconds.

This superb stability of quartz crystal oscillators, together with their other desirable features, indicates their use in several critical applications. These include long baseline interferometry, stable frequency reference for the cavity tuning servo in the hydrogen maser frequency standard, and stable frequency reference for evaluating the accuracy capability of cesium beam frequency standards, as well as the slaved oscillator in even the finest atomic frequency standards.

At the Colloque, I will discuss the measured frequency stability of commercially available quartz crystal oscillators, and some of their critical applications (accomplished and proposed). I will also mention some possibilities of achieving fractional frequency stabilities in the few parts in $10^{14}$ range with quartz crystal oscillators in the future. The nature of the flicker of frequency noise of quartz crystal oscillators will be discussed.

Hellwig, H., **The hydrogen storage beam tube, a proposal for a new frequency standard,** *Metrologia* **6,** *No. 2, 56-60 (April 1970).*

Key words: Atomic beam tube; cavity pulling; frequency stability; frequency standard; hydrogen maser.

The basic design features and the frequency stability and accuracy capabilities of a proposed new frequency standard are projected. The hydrogen storage beam tube combines the virtues of the hydrogen maser with those of beam tubes eliminating most of the problems associated with these devices. The projected frequency stability for one second averaging is better than $10^{-14}$. The long term stability should be equally good. Ways for investigating the wall shift are discussed.

Hellwig, H., Allan, D. W., Glaze, D. J., Vessot, R. F. C., Levine, M., Zitzewitz, P. W., Peters, H. E., **Measurement of the unperturbed hydrogen hyperfine transition frequency (Summary),** *Proc. Conf. Precision Electromagnetic Measurements, National Bureau of Standards, Boulder, Colo., June 2-5, 1970, CPEM Digest, pp. 72-73 (1970).*

Key words: Frequency accuracy; hydrogen maser; wall shift.

We report the results of a joint experiment which was aimed at the determination of the frequency of the $H^1$ hyperfine transition ($F = 1$, $mF = 0$) $\longleftrightarrow$ ($F = 0$, $mF = 0$). In terms of the frequency of the $Cs^{133}$ hyperfine transition ($F = 4$, $mF = 0$) $\longleftrightarrow$ ($F = 3$, $mF = 0$), defined as 9192 631 770 hertz, we obtain for the unperturbed hydrogen transition frequency the value

$$\nu_H = 1420\ 405\ 751.\ 769\ \text{Hz}.$$

This result is the mean of two independent evaluations which differ by only $2 \times 10^{-3}$ Hz. One elevation is based on the wall shift experiments at Harvard University, the other is a result of a new measurement using many storage bulbs of different sizes at the National Bureau of Standards. We will describe the experimental procedures and the applied corrections. We will compare our results with previously published values and discuss the error limits of our experiments.

Henderson, M., Berry, P. L., **Progress of federal library automation,** *Drexel Library Quart.* **6,** *Nos. 3 & 4, 249-263 (July-October 1970).*

Key words: Automatic data processing; automation of library functions; federal libraries; federal library committee; library automation; system design for libraries; task force on automation.

Progress in automation for Federal libraries other than the three National libraries is the concern of the Federal Library Committee's Task Force on Automation. Its mission is to review automation developments in Federal libraries, to encourage compatible systems design, and to provide liaison between Federal libraries and other groups involved in automation of library functions and services. To fulfill this mission the Task Force has undertaken a phased program with four objectives: to review library automation developments; to define library functions not yet automated, but which would benefit from automation; to develop a generalized system design for functions of the Federal library community; and to establish a study and design sequence, for stepwise implementation of the system within that community. The first objective has been realized through the medium of two studies; the third phase, about to get underway, will work toward the longer-range objectives while building on and extending the earlier studies.

Hoer, C., Agy, D., **A broadhurst resistive coupler,** *Proc. Conf. Precision Electromagnetic Measurements (Summary), National*

*Bureau of Standards, Boulder, Colo., June 2–5, 1970, CPEM Digest, pp. 18–19 (1970).*

Key words: Coupler; directional coupler; directivity; impedance measurements; power measurements.

A new lumped circuit directional coupler is described for the 1 to 30 MHz frequency range. Directivity greater than 50 dB is achieved for coupling ratios of 30, 40, and 50 dB. Greater directivity can be achieved over a narrower frequency range, and the coupler can be tuned for essentially infinite directivity at a fixed frequency. The couplers, although resistive, can pass 100, 300, or 1000 Watts for the coupling ratios of 30, 40, and 50 dB respectively with less than 0.01 dB change in coupling ratio. The coupling ratios are constant with frequency to ±0.25dB. Equations and curves are given for obtaining component values needed to design a resistive divider type coupler with any coupling from 3 to 60 dB.

Holt, H. K., **Theory of gas lasers and its appplication to experiment,** *Phys. Rev. A,* **2,** *No. 1, 233–249 (July 1970).*

Key words: Collisions; gas laser; line widths; power output; theory; tuning curves.

The semi-classical theory of gas lasers has been reformulated using rate equations to describe the density matrix time behavior. The solution to these equations, in the form of a Fourier series, is applicable to arbitrarily high laser intensities. A calculation of the effect of phase-changing collisions is also included. The results are compared to experimental data taken with a He-Ne laser operating at a wavelength of 1.15 $\mu$m.

Homan, D. N., Zapf, T. L., **Two-stage guarded inductive voltage division for use at 100 kHz,** *Proc. 1969 Instrument Society of America Conf., Houston, Texas, October 27–30, 1969, pp. 69–614 (1969).*

Key words: Divider; inductive voltage divider; ratio; voltage divider; voltage ratio.

A single decade inductive voltage divider having output tap corrections less than $5 \times 10^{-7}$ of input at a frequency of 100 kHz is described and evaluated experimentally and theoretically. The divider is a two-stage device, and is guarded section by section as well. These two techniques greatly reduce errors caused by unequal leakage inductance and inter-winding capacitances which otherwise cause quite large errors at 100 kHz. Design and construction details are presented for the dividers and for the bridge circuit used to make the measurements of the output tap corrections to the divider.

Hosler, W. R., **Low resistance contacts on semiconducting oxides,** *Solid-State Electron.* **13,** *517–519 (1970).*

Key words: (U) Contact resistance; (U) $TiH_2$; (U) oxide semiconductors; (U) soldering.

A method using $TiH_2$ as a flux for a contacting metal in producing low resistance small area contacts in $KTaO_3$, $SrTiO_3$, $TiO_2$ and $BaTiO_3$ has been devised. The resulting contact resistances have been found to be near zero for $KTaO_3$ and to be greatly decreased for the other materials in comparison with conventional contacts.

Howett, G. L., **Achromatic-point prediction,** *J. Opt. Soc. Am.* **60,** *No. 7, 951–958 (July 1970).*

Key words: Achromatic; appearance; brightness; chromatic adaptation; chromaticity; color; least squares; luminance; model; neutral perception; vision.

This paper constitutes a mathematical elaboration, into a form permitting direct predictions of data, of the empirical discoveries of Helson and Michels concerning the "effect of chromatic adaptation on achromaticity." An equation is developed permitting the chromaticity of a test spot that appears achromatic against an extended chromatic background to be predicted from the background chromaticity and the luminance ratio of spot to background. The technique for numerical solution of the equation is detailed, and a family of curves allowing approximate solution by interpolation is presented. The most interesting numerical finding is that if the luminance of the achromatic spot is no greater than that of the background, the achromatic chromaticity always lies more than ¾ of the way along the line directed from the absolute (black-background) neutral point to the background point, regardless of the color of the background. As part of a discussion of additional numerical methods useful in applying the model to data, general least-squares formulas are presented for the coordinates of the point best representing the common intersection of any set of given lines; and for the line, passing through a specified point, that best fits a set of given points by the criterion of perpendicular deviations.

Hubbell, J. H., **X-ray absorption 75 years later,** *Phys. Bull. No. 21, 353–357 (1970).*

Key words: Absorption corrections; attenuation coefficient; conference; crystallography; electron microprobe; fluorescence analysis; gamma rays; photons; röntgen; x-rays.

A Conference on X-Ray Absorption, organized jointly by the X-Ray Analysis Group, the Spectroscopy Group, and the Electron Microscopy and Analysis Group of the IPPS (Institute of Physics and the Physical Society) was held Nov. 14, 1969 in London. This article besides reporting this conference, reviews some early developments in x-ray attenuation coefficient measurements starting with Röntgen (1895) and presents a graph of present coverage and uncertainties of measurements for elements $Z = 1$ to 100 and photon energies 10 eV to 100 GeV. The eleven presentations at the conference included, in addition to a paper on the present status of x-ray absorption data, papers on: (1) theoretical interpretations of these data including atomic photoeffect, phonon scattering and absorber grain-size effects, (2) measurement techniques including use of synchrotron light and Vodar discharge tube as soft x-ray sources, and use and performance of various soft x-ray detectors, and (3) absorption data requirements in analysis applications including crystallography, fluorescence spectrometry, electron microprobe analysis, and x-ray reflection topography. Some possible directions of future experimental and theoretical work are indicated.

Hudson, R. P., **Conference Reports — Ultra-low temperatures 1970.** *Cryogenics* **10,** *No. 5, 445 (October 1970).*

Key words: Cryogenics; low temperature physics.

A survey is given of a recent symposium at the Naval Research Laboratory on physics below 0.3 K.

Hunt, C. M., Woolf, A. R., **Comparison of some different methods for measuring particle size using microscopically calibrated glass beads,** *Powder Technol.* **3,** *9–23 (1969).*

Key words: Air elutriation; air permeability; Andreasen pipette; calibrated glass beads; Coulter counter; electroformed sieves; microscopic size measurement; particle size measurement.

Measurements of particle size distribution by the microscope and by a number of other methods were compared using samples of glass beads from a single blended batch as the reference material. The other methods included a Coulter counter, electroformed sieves, the Andreasen pipette, and the Roller analyzer. Surface average particle size calculated from microscopic and Lea–Nurse air-permeability measurements were also compared. As an independent check of diameter measurements with the microscope, comparisons were made with an interferometer, using fibers drawn from a melt of the same glass. These comparisons afforded an opportunity to assess some of the sources of error in each of the methods.

Differences between the averages of results obtained with the microscope and those obtained with the Coulter counter, the Lea–Nurse apparatus, the Andreasen pipette as well as the interferometer were comparable in magnitude with the normal statistical variations inherent in the methods themselves. However, small systematic biases were observed. Agreement between results by the microscope and the Roller analyzer was satisfactory, although the latter is subject to greater uncertainties than the other methods

investigated. Disagreements were obtained with fine electroformed sieves, which passed more material than predicted from the size distribution by the microscope.

Hust, J. G., **Thermal anchoring of wires in cryogenic apparatus,** *Rev. Sci. Instr.* **41,** *No. 5, 622–624 (May 1970).*

Key words: Cryogenics; equipment design; thermal contact; heat transmission.

Thermal anchoring of wires to heat sinks in cryogenic equipment is discussed. An analysis is presented to relate the length of tempered wire required and measurable parameters of the system. The solution of the problem is included along with tabular values for typical situations.

Jennings, D. A., West, E. D., **A laser power meter for large beams,** *Rev. Sci. Instr.* **41,** *No. 1, 565–567 (April 1970).*

Key words: calorimetry; laser; laser calorimetry; laser power.

A power meter is described in detail for large or divergent laser beams, either CW or repetitively pulsed. The meter measures the flow of heat generated by the beam and is calibrated with an electrical heater wound just behind the absorbing surface. The meter is capable of power measurements of 1 to 30 W accurate to ± 2.5%.

Kasen, M. B., **The ccect of grain boundaries on tthe recovery of electrical properties during annealing,** *Scripta Met.* **4,** *575–580 (1970).*

Key words: Aluminum; electrical resistivity; grain boundaries; solute segregation; super-purity metals.

The change in residual resistivity at 4K has been studied as a function of annealing temperature during step-isochronal annealing of recrystallized, cold-worked, aluminum of two purities. The continued recovery of electrical properties and the eventual development of a resistivity minimum are shown to reflect the decreasing grain boundary area per unit volume as annealing progresses, combined with changes in the amount of solute segregated to the grain boundaries. The resistivity minimum is found to coincide with removal from solid solution of an amount of solute approximating that required to form ⅓ of a monolayer of segregate at the existing boundaries.

Kearsley, E. A., **Intrinsic errors for pressure measurements in a slot along a flow,** *(Proc. Fifth Intern. Congress on Rheology, Kyoto, Japan, October 1968), Trans. Soc. Rheology* **14:3,** *419–424 (1970).*

Key words: Hole pressure; nonlinear rheology; normal stresses; pressure error; second order fluid.

Any rectilinear flow dynamically possible for a Newtonian fluid is shown to be possible also for a second order fluid. The stress which satisfies the condition of equilibrium is explicity calculated. The component of stress normal to a wall bounding a shear flow is expressed in terms of the reading of a pressure gauge connected to a narrow slot in the wall, oriented in the direction of flow.

Kerns, D. M., **Correction of near-field antenna measurements made with an arbitrary but known measuring antenna,** *Electronics Letters* **6,** *No. 11, 346–347 (May 28, 1970).*

Key words: Antenna gain; antenna gain measurement; antenna measurements; antenna pattern; antenna pattern measurement; near-field antenna measurements.

We describe a technique of rigorously correcting for the effects of an arbitrary but known measuring antenna (or "probe") in determination of vectorial far-field antenna pattern and effective gain function from near-field measurements.

Kerns, D. M., **New method of gain measurement using two identical antennas,** *Electronics Letters* **6,** *No. 11, 348–349 (May 28, 1970).*

Key words: Antenna gain; antenna gain measurement; antenna measurements; antenna pattern; antenna pattern measurement; near-field antenna measurements.

A new method for the measurement of on-axis pattern and gain using two identical antennas is described. The antennas must obey reciprocity, but may be otherwise arbitrary; the usual requirements in the conventional two-antenna gain measurement method, that the polarization be known *a priori* and that the separation be large compared to the Rayleigh distance, are eliminated.

Kidnay, A. J., Hiza, M. J., **Physical adsorption in cryogenic engineering,** *Cryogenics* **10,** *No. 4, 271–277 (August 1970).*

Key words: Adsorbent-reaction; adsorption; heat transfer; isotherm; kinetics; mass transfer.

This article is a selective review of the literature on physical adsorption that is pertinent to Cryogenic Engineering. Included are tabulations of experimental adsorption isotherms on high surface area adsorbents, both for pure materials and mixtures, and a brief discussion of the more important techniques for correlating and predicting adsorption isotherms. Adsorption kinetics, heat and mass transfer in packed beds, and adsorbent bed reactivation techniques are also discussed.

Lance, H. W., **Report on metrology sessions at the 24th annual ISA conference,** *Appl. Opt.* **9,** *No. 6, 1497–1498 (June 1970).*

Key words: Education for metrology; measurements; measurement techniques; metrology.

This report is primarily about the ISA sessions on "Education for Metrology." These sessions described (1) metrology training programs in the military establishment and in industry—at least some of which are necessary because the nation's educational institutions largely neglect the subject of metrology—and (2) metrology courses being given or planned by a few universities. The latter verified the need for better measurement training, pointed the way toward revitalized courses, and hinted that the universities may be beginning to give more attention to this subject. The report also mentions selected papers from other sessions and summarizes briefly a Confernece on Measurement Education held in England in July, 1969.

Latanision, R. M., Westwood, A. R. C., **Surface- and environment-sensitive mechanical behavior,** *Chapter in Advances in Corrosion Sciences and Technology,* **1,** *51–145 (Plenum Press, New York, N. Y., 1970).*

Key words: Complex-ion embrittlement; dislocations; liquid metal embrittlement; surface; surface active agent.

The influences of surface structure and environment on the mechanical behavior of crystalline inorganic solids are reviewed and possible mechanisms discussed. In particular, the various roles of such factors as the atomic, electronic, and defect structure of the near-surface regions, the presence of adsorbed surface-active species, alloyed layers, oxide films, gaseous or liquid environments, etc. are considered in connection with the Roscoe, Rebinder, and Joffe effects, liquid-metal embrittlement, complex-ion embrittlement, hydrogen embrittlement, and other phenomena.

Ledbetter, H. M., **On the martensite crystallography of the cubic to orthorhombic transformation in Au-47.5 Cd,** *Scripta Met.* **4,** *No. 11, 931–937 (November 1970).*

Key words: Crystallography; gold-cadmium alloy; martensite; phase transformations; twinning.

Complete calculations of the geometrical features of the cubic to orthorhombic martensitic transformation in the Au-47.5 Cd alloy system have been made for both Type I and Type II transformation twinning. None of the usual crystallographic features are sufficiently sensitive to distinguish between these two possible modes of lattice invariant deformation. Alternatives are offered which

are believed to be experimentally simpler than those previously proposed.

Ledbetter, H. M., Reed, R. P., **On the martensite crystallography of Fe-Ni alloys,** *Mater. Sci. Eng.* **5,** *No. 6, 341–349 (June 1970).*

Key words: Crystallographic theory; iron-nickel alloy; martensite.

For the first time lattice parameter data and habit plane measurements are available for an alloy system whose crystallographic features change continuously with composition. This information has been produced for the plate-like martensitic transformation in Fe-base alloys containing between 29 and 35 wt. % Ni. This paper presents a critical examination of the data from the viewpoint of the theories of martensite crystallography. It is found that the current theories cannot explain the variation of the habit plane with composition without invoking a varying $\delta$ (1.000 to 1.013), $\delta$ being an isotropic dilatation parameter. In addition to the habit plane, several quantities have been calculated as a function of composition; the volume change, the magnitude of the lattice invariant deformation, the magnitude and direction of the shape change, and the orientation relationship. The effects of errors in lattice parameter and of thermal expansion are considered.

McSparron, D. A., Mohan, K., Raybold, R. C., Saunders, R. D., Zalewski, E. F., **Spectroradiometry and conventional photometry an interlaboratory comparison,** *Nat. Bur. Stand. (U.S.), Tech. Note 559, 197 pages (Nov. 1970) $1.50, SD Catalog No. C13.46:559.*

Key words: Barnes colorimeter; chromaticity coordinate; color correction; cool white fluorescent lamp; correlated color temperature; daylight fluorescent lamp; heterochromatic photometry; integrating sphere; intercomparison; luminous flux; photometry; spectroradiometry.

This report summarizes the results of a fluorescent lamp intercomparison carried out under the aegis of the National Bureau of Standards Photometry Section. The purpose of the intercomparison was to evaluate the interlaboratory precision obtainable in photometric and spectroradiometric measurements. The tests were also designed to disclose suspected systematic errors in measurement techniques.

The intercomparison consisted of five parts: (1) A homochromatic, photometric measurement of coöl white fluorescent lamps and a heterochromatic, photometric measurement of a daylight fluorescent lamp and an incandescent lamp utilizing cool white fluorescent lamps as standards, all within an integrating sphere. (2) Spectroradiometric measurement of the above mentioned lamps in an integrating sphere. (3) Spectroradiometric measurement of a 25 cm section of the fluorescent lamps in a baffled enclosure. (4) An experiment designed to reveal systematic errors in heterochromatic photometry. (5) Measurement of the x and y chromaticity coordinates with a Barnes colorimeter.

Marsden, C. P., **Tabulation of published data on electron devices of the U.S.S.R. Through March 1970,** *Nat. Bur. Stand. (U.S.), Tech. Note 526, 122 pages (Oct. 1970) $1.25, SD Catalog No. C13.46:526. Supersedes NBS Technical Note 441.*

Key words: Electron devices; electron tubes; semi-conductors; U.S.S.R.

This tabulation includes published data on U.S.S.R. electron devices as collected from publications, mostly handbooks, published by the various ministries and institutes of the U.S.S.R. Information is given on all active devices ranging from receiving to microwave devices, semiconductor devices, and miscellaneous devices such as, for example, photographic flash tubes and thermistors.

Marshall, R. D., Thom, H. C. S., Editors, *Proceedings of technical meeting concerning wind loads on buildings and structures held at the National Bureau of Standards, Gaithersburg, Maryland, January 27–28, 1969, Nat. Bur. Stand. (U.S.), Bldg. Sci. Ser. 30, 172 pages (Nov. 1970) $1.75, SD Catalog No. C13.29/2:30.*

Key words: Aerodynamic forces; atmospheric boundary layer; structural design; turbulence; wind effects; wind loads.

A technical meeting concerning wind loads on buildings and structures was held at the Gaithersburg Facility of the National Bureau of Standards on January 27 and 28, 1969. The meeting, jointly sponsored by the Building Research Division of the National Bureau of Standards and the Environmental Data Service of the Environmental Science Services Administration, was intended to promote the exchange of information between research workers and practicing engineers engaged in this important area of technology.

Thirteen papers covering four themes were presented. These themes were as follows: engineering problmes in the design of structures to resist wind loads; atmospheric considerations; experimental and theoretical determination of aerodynamic forces; and recent advances in design procedures and current deficiencies. Presentations were followed by a panel discussion which included a summary of each theme. The last session of the meeting was devoted to open discussion.

Mather, W. G., III, Kit, B. V., Bloch, G. A., Herman, M. F., **Man, his job and the environment: A review and annotated bibliography of selected recent research on human performance,** *Nat. Bur. Stand. (U.S.), Spec. Publ. 319, 107 pages (Oct. 1970) $1.00, SD Catalog No. C13.10:319.*

Key words: Bibliography; effort; environment; fatigue; human performance; human physiology; psychology; psychophysics; stress (physiological); stress (psychological); work.

Recent scientific literature was searched to review procedures currently being used to study human reactions to work and environmental stress. An ecological context is followed, considering task variables, environmental conditions, individual variations in subjects, and physiological, psycho-physical, psychological, and sociological responses. The different types of research reviewed included analyses of on-the-job performance, simulations of real-life situations, laboratory experiments with human and nonhuman subjects, and clinical studies. A methodological program is suggested for measuring the expenditure of effort in work situations. In addition to an extensive bibliography, detailed abstracts of 190 research reports are presented.

Meadow, C. T., Meadow, H. R., **Organization, maintenance and search of machine files,** *Chapter 7 in Annual Review of Information Science and Technology, C. A. Cuadra, Ed., pp. 169–191 (Encyclopedia Britannica, Chicago, Ill., 1970).*

Key words: Data management; data structures; file organization; information retrieval; information systems; programming languages.

This article reviews the most significant literature in the field of file organization and search procedures that appeared during 1969. Among the points noted are the differences between total information systems and data management support systems and the separate development of several instances of each. The most important development is the trend toward data independence—separation of the concepts of logical and physical data organization.

Melmed, A. J., Carroll, J. J., **Some initial observations of TiNi in the field-ion microscope,** *Appl. Phys. Letters* **17,** *No. 6, 247–249 (September 15, 1970).*

Key words: Atomic planes; field-ion microscope; liquid nitrogen; TiNi specimens.

It is demonstrated that TiNi specimens can be successfully imaged with the field-ion microscope at liquid nitrogen temperature, using hydrogen as the imaging gas. The material examined is shown to be structurally inhomogeneous, with regions of order in a less-ordered matrix. It is also shown that alternate atomic planes are different within an ordered region.

Moore, G. A., **Is quantitative metallography quantitative?** *Am. Soc. Testing Mater. Spec. Publ. 480, pp. 3–48 (1970).*

Key words: Morphometry; quantitative metallography; quantita-

tive microscopy; stereology.

While the basic principles of quantitative metallography have been firmly established, the practice of such measurements yields highly variable results. Simple laws define the statistical limitation on any measuring method. Serious errors arise from improper selection and preparation of specimens. Anticipated gradients must be encompassed by a planned sampling scheme which guarantees unbiased representation and permits measurement of actual variation in the material studied. Specimen preparation must give a truthful image of the structure. Any free choices by the operator introduce bias. The precision of measurement of one micrograph is primarily controlled by combination of a statistical uncertainty and an observational error at the edges of particles. The statistical uncertainty conforms to the ideal when the apparent particle size is small, but observation becomes inefficient as the average intercept width increases and the number of particles in the field decreases. Edge errors are maximum with small particles, and vary with the observer or the instrument used. Maximum precision is obtained when these two errors are approximately equal. While quantitative metallography is a statistical rather than exact process, and subject to serious or fatal errors when practiced crudely, carefully controlled measurements can yield several structural parameters with a precision adequate to satisfy any practical metallurgist.

Nargolwalla, S. S., Niewodniczanski, J., Suddueth, J. E., **Experimental sensitivities for 3-MeV neutron activation analysis,** *J. Radioanal. Chem.* **5,** *403–423 (1970).*

Key words: Absolute flux; Cockcroft-Walton neutron generator; sample attenuation corrections; sensitivity and gamma-ray spectra of the elements; 3-MeV neutron activation analysis.

The experimental sensitivity for 72 different elements using 3-MeV neutron activation has been investigated. Using a 200 kV Cockcroft-Walton neutron generator with a 3-MeV neutron flux of about $5 \times 10^5$ $n.cm^{-2}.s^{-1}$, gamma-ray spectra of 51 elements were obtained with a sufficient number of photopeak counts for sensitivity calculations using a photopeak integration method. A useful table summarizing the sensitivity results is given. That 3-MeV neutron activation analysis is practical, is demonstrated by experimental sensitivities obtained.

Neill, A. H., Jr., **High-energy light detector for use with pulsed ruby and glass lasers,** *Appl. Opt.* **9,** *No. 10, 2392–2393 (October 1970).*

Key words: Calorimeter; detector; energy; laser; power; ruby.

A portable solid state light detector capable of measuring up to 100 joules of laser energy in the conventional mode has been designed and tested. Details on construction and operation are presented along with results of calibration.

Newton, C. J., Ruff, A. W., Jr., **X-ray study of annealing in plastically deformed Ag-Sn alloys,** *Met. Trans.* **1,** *No. 10, 2833–2838 (October 1970).*

Key words: Isochronal annealing; silver-tin alloys; stacking fault; x-ray diffraction data.

The stacking fault probability, root-mean-square strain and effective domain size are determined for pure silver and three silver-tin alloys using x-ray diffraction data. Both isochronal and isothermal annealing experiments were conducted to determine the nature of the recovery of plastic deformation in the filed powder specimens. An abrupt recovery of the above quantities was observed during isochronal annealing at temperatures that increased with solute concentration. Three recovery stages were observed in Ag-9, at .% Sn annealed at 165°C for varying times. The principal stage is probably associated with recrystallization since both the stacking fault probability and rms strain recover together. An activation energy at 25 kcal/mol is determined for this stage.

Otoshi, T. Y., Stelzried, C. T., Yates, B. C., Beatty, R. W., **Comparisons of waveguide losses calibrated by the dc potentiometer, ac ratio transformer, and reflectometer techniques,** *IEEE Trans. Microwave Theory Tech.* **MTT-18,** *No. 7, 406–409 (July 1970).*

Key words: Comparison of results; dc potentiometer test set; dual channel system; modulated subcarrier; ratio transformer test set; small attenuation measurement; small insertion loss measurement; small reflection coefficient measurements.

Comparisons are made of the losses of two precision waveguide sections that were calibrated by three independent attenuation measurement methods. The loss measurement systems involved were the (1) dual-channel system which uses thermistors and a dc potentiometer test set, (2) dual-channel system which uses barretters and an ac ratio transformer test set, and (3) National Bureau of Standards reflectometer system which utilizes a quarter-wave short-circuit and an IF attenuation standards. Loss values of about 0.05 dB as calibrated by the three independent methods agreed to better than 1 percent. It is believed that the results of these calibrations are representative of the best that can be achieved with current state-of-the-art techniques and available instrumentation for low-loss waveguide measurements.

Peavy, S. T., Varner, R.N., Bremer, S. G., **A systems programmer's guide for implementing OMNITAB II,** *Nat. Bur. Stand. (U.S.), Tech. Note 550, 43 pages (Nov. 1970) 50 cents, SD Catalog No. C13.46:550.*

Key words: ANSI FORTRAN; double precision; general-purpose computer program; implementation of OMNITAB II; labeled common; machine independent; OMNITAB II; overlay; segmentation; system parameters; transportable computer programs.

OMNITAB II is a general-purpose program which permits direct use of a computer without prior knowledge of computer languages. Every effort has been made to produce a system as machine independent as possible to make implementation on any large computer configuration relatively easy. However, there are a few modifications which may have to be made.

This Technical Note provides assistance to the systems programmer, with the task of implementing OMNITAB II, by pointing out where difficulties may occur and how to cope with them. It furthermore outlines a method for segmenting the OMNITAB II system which is very large. It is a partial documentation of the OMNITAB program.

OMNITAB II is a large system requiring a large computer. Overlay and segmentation are virtually essential. A method for segmenting OMNITAB II is outlined. The method should be useful for many computers.

Pella, P. A., DeVoe, J. R., **The determination of tin in copper-base alloys by Mössbauer spectrometry,** *Anal. Chem.* **42,** *No. 14, 1833–1835 (December 1970).*

Key words: Alloys; analysis; internal standard; Mössbauer spectrometry; stannic oxide.

The Mössbauer spectrometric method was applied to the determination of *tin as stannic oxide in NBS SRM copper-base alloys.* The absorption intensity of $SnO_2$ was measured versus $\beta$-Sn as an internal standard absorbed. Stannic oxide was obtained by the dissolution of the alloys in nitric acid. This produces a precipitate contaminated by the coprecipitation of a number of elements. Through the use of an appropriate standard, it was shown that the Mössbauer technique can measure the $SnO_2$ concentration without interference. The results for alloys 52c, 184, and 37e were 7.82± .05% (7.85), 6.31± .06% (6.38), and 0.99± .01% (1.00), respectively, where the uncertainties are the relative standard deviation of the mean values and the numbers in parenthesis are the NBS certified values.

Prydz, R., Straty, G. C., Timmerhaus, K. D., **Properties of fluorine along the vapor-liquid coexistence boundary,** *J. Chem. Phys.* 53, *No. 2359-2363 (September 15, 1970).*

Key words: Critical point; fluorine; latent heats of vaporization; saturated liquid densities; saturated vapor densities; vapor pressure.

Saturated liquid and vapor data from the triple point to the critical point are reported. These data were derived from experimental PVT isochores and a vapor pressure equation. The critical point was extracted by fitting an equation to all experimental data within 20 percent of the critical temperature. Separate equations, each constrained to the new critical point, were fitted to the saturated liquid and vapor data. Latent heats of vaporization were calculated from the Clapeyron equation and compared to other published values. A vapor pressure equation based on the IPTS 1968 temperature scale is reported.

Radebaugh, R., Siegwarth, J. D., **Theory of $He^3$-$He^4$ dilution refrigerators,** *(Proc. 1970 Ultralow Temperature Symp., Washington, D.C., April 23-24, 1970; NRL Report 7133) pp. 63-81 (1970).*

Key words: Cryogenics; dilution refrigerator; fermi-dirac statistics; heat exchangers; helium-3; helium-4; liquid helium; mixtures; quantum fluid; thermodynamic properties.

A review is given concerning the theoretical analysis of the dilution refrigerator. The weakly interacting Fermi-Dirac gas model for $He^3$ dissolved in superfluid $He^4$ is developed in detail to give accurate and self consistent values for thermodynamic properties of the dilute solutions. These calculated properties, along with measured properties of pure $He^3$, are used to analyze the behavior of the dilution refrigerator in the continuous mode. The temperature which can be reached with a given number of perfect discrete heat exchangers is derived. The analysis of a typical discrete heat exchanger taking thermal conductivity of the liquids into account shows it behaves nearly like the extreme of small length to area ratio, $l/A << 1$ . The other extreme of zero liquid conductivity, or $l/A >> 1$, is shown to be much more efficient for the same liquid volume but is difficult to make with low flow impedance. The optimum ratio of dilute to concentrated liquid volumes is found to be 2.1 for the heat exchanger analyzed.

Radlinski, R. W., Price, J. L., **The brake pedal force capability of adult females,** *Nat. Bur. Stand. (U.S.), Tech. Note 557, 25 pages (Oct. 1970) 35 cents, SD Catalog No. C13.46:557.*

Key words: Automotive braking systems; brakes; brake pedal forces; Federal Motor Vehicle Safety Standards; pedal effort; women, strength of.

A survey of the brake pedal force capability of 105 women employees at the National Bureau of Standards, Washington, D.C., was performed utilizing two stationary passenger automobiles as test vehicles. Results showed that over 50 percent of the test subjects could not achieve an average sustained brake pedal force of 200 lb, a value which is considered an acceptable braking system input force under certain conditions of the current Federal Motor Vehicle Safety Standard (FMVSS No. 105) for passenger vehicle braking system performance.

Rasmussen, A. L., **Laser energy and power measurement with a double reflecting plate calorimeter,** *Rev. Sci. Instr.* **41,** *No. 10, 1479-1484 (October 1970).*

Key words: Calorimetry; laser, laser calorimetry; laser energy, laser power.

In a double reflecting plate calorimeter (DP), the energy from a laser beam is partially absorbed by mirrors. The rset is reflected through an exit where it is free to interact with some medium. Characteristic of calorimeter DP with a pair of aluminum plate mirrors are (1) wavelength range $\backsim$ 0.1 $\mu$ to $\backsim$ 1 $\mu$, (2) energy input range $\sim$ 0.1 J/cm$^2$ to $\backsim$ 50 J/cm$^2$ (pulsed normal mode) and estimated power $\backsim$ 100 to $\sim$ 1000 megawatts/cm$^2$ (pulsed Q swtched) depending upon energy density, (3) estimated error $\pm$ 2% over most of the ranges given, (4) 5 seconds for the plates to reach a uniform temperature and to make measurements, and 2 to 4 minutes required cooling time between inputs, and (5) both absorption and reflection determined from plate calorimetric data. The sensitivity and the wavelength, energy and power ranges may be increased by using different plate dimensions and materials. Data from an intercomparison between calorimeter DP and an NBS liquid cell calorimeter yield agreement of 0.55%, $S_m = 0.04\%$ at 0.6943 $\mu$. The light was plane polarized.

Reed, R. P., Arp, V. D., **Techniques for measuring stress, strain, and resistivity at 4K for very soft materials,** *Cryogenics Letter to Editor,* **9,** *No. 5, 362-364 (October 1969).*

Key words: Cryostat; electrical resistance; soft materials; strain extensometer.

Existing techniques for conducting low temperature tensile tests have not proven satisfactory for super-purity aluminum, primarily due to its extreme softness. The desire to concurrently measure specimen resistivity during 4K tests also provided experimental difficulties, since the specimens had to be electrically isolated from the metallic load assembly. This paper discusses there problems and describes the apparatus designed to provide sensitive and accurate data on stress, strain, and resistivity at 4K.

Risley, A. S., Allan, D. W., Peters, H. E., Johnson, E. H., Vessot, R. F. C., Levine, M., Gray, J. E., Shoaf, J H., Machlan, H. E. and Glaze, D. J., **Stability characteristics of some atomic frequency standards, (Summary),** *Proc. Conf. Precision Electromagnetic Measurements, National Bureau of Standards, Boulder, Colo., June 2-5, 1970, CPEM Digest, pp. 74-75 (1970).*

Key words: Allan variance; cesium beam; frequency stability; hydrogen maser; NBS frequency standard; time scale.

Over a period of three and one-half months a frequency stability comparison was made between seven commercial cesium beams and a NASA (Goddard Space Flight Center) hydrogen maser. Two of the prime purposes in bringing the NASA maser to Boulder were: (1) to determine the general effect upon the NBS Time Scale of including the H maser as a part and (2) to determine the stability of the H maser for sampling times $\tau$ longer than $10^3$ seconds.

Two of the major results of the time scale and NASA maser comparison were, first $\sigma_y$ ($N = 2$, $T = \tau$, $\tau = 1$ day) of the time scale—*including the maser*—was less than $1 \times 10^{-13}$, where $y = \delta v/\nu$. Second, the inclusion of the maser in the time scale improved the precision about 30 percent.
Another hydrogen maser (from the Smithsonian Astrophysical Observatory) and a new four-foot long cesium beam (NBS-X4) were used along with the NASA maser to measure stabilities $\delta_y(N = 2, T = \tau, \tau)$ ($\tau \sim 1$ day). The stabilities for both masers and for NBS-X4 were better than one part in 10.[15]

Ruff, A. W., Jr., **Measurement of stacking fault energy from dislocation interactions,** *Met Trans. 1, No. 9, 2391-2314 (Sept. 1970).*

Key words: Dislocations; dislocation nodes; dislocation ribbons; faulted dislocation dipoles; stacking faul energy; stacking fault tetrahedra.

The theories and methods applied to the determination of the stacking fault energy ($\gamma$) using techniques of direct observation of dislocation configurations are reviewed. The four principal methods, utilizing dislocation nodes, multiple ribbons, stacking fault tetrahedra, and faulted dipoles, are discussed in detail. Different theoretical treatments are compared wherever possible. Experimental procedures and quantitative measurement methods are reviewed. Detailed examples of the application of each method are given. For $\gamma/\mu b$ in the range of $2 \times 10^{-4}$ to $5 \times 10^{-3}$ ($\mu$ the shear modulus, b the Burgers vector), measurements on dislocation nodes or multiple ribbons in favorable cases should permit determinations of the stacking fault energy to a precision of 5%. For larger values of $\gamma/\mu b$ (up to $12 \times 10^{-3}$), measurements can be made on tetrahedra or faulted dipoles with less precision. Larger values of the stacking fault energy require high resolution studies of dislocations; these techniques are not yet well established. Possible sources of systematic bias are discussed. Two significant theoretical problems remain concerning the treatment of the dislocation core and the use of anisotropic elasticity. It is of prime importance to characterize as carefully as possible the materials studied if accurate results are desired.

Schneider, S. J., **Cooperative determination of the melting point of alumina,** *J. Pure Appl. Chem.* **21,** *No. 1, 117-122 (1970).*

Key words: $Al_2O_3$; alumina; IUPAC; melting point of $Al_2O_3$; melting point standards.

A task force on secondary standards, sponsored by the Commission on High Temperatures and Refractories, International Union of Pure and Applied Chemistry, has undertaken a program to investigate various inorganic non-metallic substances for use as high temperature reference materials. As part of this program a cooperative determination of the melting point of $Al_2O_3$ (alumina) was conducted by the task force. In all nine scientific groups, representing seven countries contributed experimental data. All work was performed utilizing a common supply of $Al_2O_3$ of nominal 99.9% purity. Experimental techniques varied depending upon the individual investigator. The value for the alumina point, as recommended by the task force is 2054 ± °C (IPTS 1968).

Selby, M. C., **The Bolovac and its applications, (Summary),** *Proc. Conf. Precision Electromagnetic Measurements, National Bureau of Standards, Boulder, Colo., June 2–5, 1970, CPEM Digest, pp. 14–15 (1970).*

Key words: Bolovac; current measurement (HF & MW); (HF & MW); microwave currents; microwave voltages; power measurement; voltage measurement (HF & MW).

The Bolovac is a new device for the standardization and measurement of TEM voltage, current and power through 18 GHz (potentially through 36 GHz). It can be used for attenuation measurement and as a near perfect impedance termination. It is the first and only anywhere practical means of calibrating microwave current indicators and of evaluating osciloscopes displaying 25-ps or shorter rise-time pulses.

The application of the Bolovac will revolutionize power measurements. It eliminates (1) "mismatch errors," the major present source of uncertainty in power measurement, (2) the measurement of complex reflection coefficients, (3) complex computations, (4) the use of "error-limit" charts, and (5) the measurement of "effective efficiency" and "calibration factor." Its application may radically increase optimum accuracy and measurement-time efficiency.

The Bolovac can be used as a source of voltage or as an absorption power meter. It needs no rf calibration. It has a 15 to 40 dB range depending on the desired precision and on whether one or more sensors (special bolometric disks) are used.

Sengers, J. M. H. L., **Scaling predictions for thermodynamic anomalies near the gas-liquid critical point,** *Ind. Eng. Chem. Fundamentals,* 9, *No. 3, 470–480 (November 9, 1970).*

Key words: Argon; carbon dioxide; classical equation; coexistence curve; critical exponents; critical point; lattice gas; power laws; rectilinear diameter; steam; thermodynamic; vapor pressure.

Most classical (or van der Waals type) equations of state of fluids show characteristic critical thermodynamic anomalies and symmetries that are common to them all. These characteristics are reduced from the Taylor expansion, in density and temperature, of these equations at the critical point. It is shown that the anomalies found experimentally are of a different nature, more similar to those predicted by the Ising model for the lattice gas. Consequences for data correlations in the critical region are discussed and examples of such correlations are presented.

Sharp, E. J., Weber, M. J., Cleek, G., **Energy transfer and fluorescence quenching in Eu- and Nd-doped silicate glasses,** *J. Appl. Phys.* **41,** *No. 1, 364–369 (January 1970).*

Key words: Energy transfer; Eu and Nd doped glass; fluorescence; fluorescence decay times; fluorescence quenching; laser glass; rare earth glass.

Radiative and nonradiative energy transfer and decay processes have been investigated in high silicate glasses co-doped with Eu and Nd. Energy transfer from Eu to Nd was established from an examination of the excitation spectra and the increased Eu decay rates in the presence of Nd. Measurements of the concentration dependence of the $Eu^{3+}$ fluorescence lifetimes reveal the presence of four distinct processes arising from various ion-ion interactions: (1) self-quenching of the $Nd^{3+}$ fluorescence, (2) self-quenching of the $Eu^{3+}$ fluorescence, (3) nonradiative energy transfer from $Eu^{3+}$ to $Nd^{3+}$ and (4) Eu quenching of the $Nd^{3+}$ fluorescence. This last process decreases the radiative quantum efficiency of the $^4F_{3/2}$ state of $Nd^{3+}$, thus limiting the attractiveness of Eu sensitization for Nd laser action.

Shinyayev, A. Ya., Butrymowicz, D. B., **Interdiffusion in and the phase diagram for vanadium-rich alloys of the V-Al system at pressures 0 to 47 kbar,** *Met Trans. 1, No. 7, 1905–1907 (July 1970).*

Key words: Alloys; aluminum; diffusion; high-pressure; phase-diagram; vanadium.

The V-Al system between 16 and 39 at. pct. Al was studied at 1400 °C under pressures of 0, 30, and 47 kbar. Electron microprobe analysis, x-ray diffraction, microhardness readings, and metallographic examination revealed only a single solid solution. Interdiffusion coefficients were determined as a function of composition and pressure. Concentration gradients were measured with an electron microprobe analyzer and the diffusion coefficients were calculated by the Matano analysis. At 1400 °C, the value of the interdiffusion coefficient varies from 1 to 12 × $10^{-9}$ $cm^2/s$., increasing with aluminum content and decreasing with increasing pressure.

Sieck, L. W., Searles, S. K., **High pressure photoionization mass spectrometry. Reactions of alkane and cycloalkane molecular ions with water vapor at thermal kinetic energies,** *J. Chem. Phys.* **53,** *No. 1, 2601–2604 (October 1, 1970).*

Key words: Hydrocarbons; ion-molecule reactions; mass spectrometry; Photoionization; proton transfer; water.

The reactions of alkane molecular ions ($RH_2^+$) with water vapor were found to proceed via a bimolecular mechanism in both ethane and propane. Parent ions from cyclohexane, cyclopentane, *i*-butane, *n*-butane, *i*-pentane, *n*-pentane and *n*-hexane were observed to react exclusively via a termolecular mechanism involving two water molecules: $RH_2^+ + 2H_2O \rightarrow H^+(H_2O)_2 + RH$. Thermal rate constants of 1.2 and 1.4 × $10^{-9}$ $cm^3$ molecule-second, respectively were derived for the bimolecular reactions of $C_2H_6^+$ and $C_3H_8^+$ with $H_2O$. The termolecular rate constants found in other $RH_2^+ - H_2O$ combinations were quite high, falling in the range $10^{-25}$ to $10^{-27}$ $cm^6$/molecule$^2$-second. The nature of the collision complex is discussed, and new limits are estimated for $\Delta Hf\ (H_3O^+)$.

Simson, B. G., Mandel, J., Brenner, F. C., **Research for a uniform quality grading system for tires. III. Breaking energy,** *Rubber Chem. Tech.* **43,** *No. 2, 356–369 (March 1970).*

Key words: Bias ply; breaking energy; passenger car; radial; tires; tire strength; winter.

A test procedure, designed to classify tires according to their average breaking energy has been applied to a sample of passenger car tires. Data are reported on 127 different tires of all grades and types over a range of sizes.
A scaling system is devised and applied to the data. It is found that the system leads to conclusions similar to those derived from the original data.

Spencer, L. V., Stanley, W., **On neutron penetration in duet systems with large cross section,** *Proc. Special Sessions on Gamma-Ray Production and Transport and on Civil Defense Shielding, American Nuclear Society pp. 199–221 (August 1969).*

Key words: Albedo; Civil Defense; ducts; neutron penetration; nuclear weapons data; structure shielding.

Neutron albedo data for non-hydrogenous wall materials in insensitive to variations of the total cross section with energy and, to some extent, to details of cross section angular distributions. As a result, it makes sense to explore models in which the differential albedo is factored into energy dependent and direction dependent parts. This approximation results in a factoring of the transport

equation for large enclosures into two parts, a one-velocity type of problem and a general problem of determining spectra for different orders of reflection. We extend this approach further to identify suitable parameters in terms of which data for elementary types of enclosure can be applied to configurations. These parameters are given, the procedure for combining duct sections is sketched, and calculations for a three-legged duct are compared with Monte Carlo data for such a duct.

Stein, P. G., **Image-analyzing microscopes,** *Anal. Chem.* **42,** *No. 13, 103A–107A (November 1970).*

Key words: Computers; digital logic; image processing; microscope; microspectrophotometry; pattern recognition.

Image Analyzing Microscopes—instruments that gather density and position data from specimens located in the object plane of a light microscope are reviewed and discussed. TV (vidicon) scanners with storage cathodes, image dissectors with non-storage cathodes, and mechanical scanners are compared, as are the types of processing logic needed for data analysis with each type of system.

Stein, P. G., Lipkin, L. E., Shapiro, H. M., **Spectre II: General-purpose microscope input for a computer,** *Science* **166,** *328–333 (October 17, 1969).*

Key words: Biological structure; biomedical instrumentation; computer; image processing; microscope; microspectrophotometry; pattern recognition.

This paper describes a system of instruments used in biological and medical research for microspectrophotometry and computer analysis of microscopic images. The apparatus includes an optical microscope, spectrophotometer, a scanner, and a motor driven stage and monochromator all controlled by a small general-purpose computer. A keyboard permits manual operation of the equipment under computer control.

The system was constructed with great flexibility to permit its use in the evaluation and design of special-purpose apparatus for specific biomedical applications. A discussion of design criteria and a comparison with existing input devices for microscopic image analysis is included.

Stevens, M. E., **Introduction to the Special Issue on Optical Character Recognition (OCR),** *Pattern Recog.* **2,** *No. 3, 147–150 (September 1970).*

Key words: Automatic pattern recognition; handprinted characters; OCR standards; optical character recognition.

A brief introduction, stressing some aspects of the state of the art and the state of the practice of optical character recognition (OCR), is provided for a special issue of the journal, Pattern Recognition.

Stevens, M. E., **Selected R & D requirements in the computer and information sciences,** *Proc. Fall Joint Computer Conf., Houston, Texas, November 17–19, 1970, pp. 159–168 (AFIPS Press, Montvale, N. J., 1970).*

Key words: Communications; information processing; languages; man-machine relationships; teleprocessing.

The paper presents an advance overview of a series of reports on R & D requirements in the computer and information sciences, based upon selective reviews of the literature. Examples of topics include: information acquisition, sensing and input, including pattern recognition; some overall systems design requirements with emphasis upon programming languages and advanced hardware technologies, and communication problems of machine-with-machine, man-with-machine, and man-with-man. Some of the possible contributions of the computer sciences to the more traditional library and information sciences are noted, but there are fundamental problems of human perception, learning, concept formation, and knowledge requiring interdisciplinary attack.

Straty, G. C., Prydz, R., **Fluorine compatible apparatus for accurate PVT measurements,** *Rev. Sci. Instr.* **41,** *No. 8, 1223–1227 (August 1970).*

Key words: Cryostat; fabrication techniques; fluorine, materials compatibility; P-V-T apparatus; P-V-T method.

A fluorine compatible apparatus, incorporating numerous safety features, is described. This apparatus has been used to make accurate determinations of the PVT properties of gaseous and liquid fluorine from 53.5 K (the triple point) to 300 K and to pressures of 20 $MN/m^2$ (3000 psi). The experimental method is similar to the isochoric one used previously in this laboratory for oxygen and hydrogen. A limited testing program, to determine the suitability of various materials for use with high pressure fluorine, is described and the test results tabulated. Some general fabrication techniques, suitable for construction of fluorine handling apparatus, are discussed.

Straty, G. C., Prydz, R., **The vapor pressure of liquid fluorine,** *(Proc. 1969 Cryogenic Engineering Conf., June 16–18, 1969, Univ. of California, Los Angeles, Calif.), Chapter in Advances in Cryogenic Engineering 15, Paper No. B-1, 36–41 (Plenum Press, Inc., New York, N. Y., 1970).*

Key words: Critical point pressure; fluorine; normal boiling point; vapor pressure data; vapor pressure equation.

This paper reports new vapor pressure measurements on liquid fluorine from the triple point to the critical point at 1 K intervals. Accuracies in both temperature and pressure approach a few hundredths of a percent. The data were fitted to a newly developed, non-analytic vapor pressure equation and compared graphically to earlier, inconsistent measurements available in the literature. Of this earlier data, the estimated P-T values above the normal boiling point and the value given for the critical pressure are in error by as much as 10 to 15 percent.

Swartzendruber, L. J., Bennett, L. H., **Clustering, cold work, and the Mössbauer effect doublet structure in Cu-Ni-Fe alloys,** *Physics Letters* **31A,** *No. 01, 581–582 (May 18, 1970).*

Key words: Alloys; clustering; cold work; Cu; Fe; magnetic moments; Mössbauer effect; Ni.

The doublet structure observed in the high temperature Mössbauer effect spectra of Cu-Ni-Fe alloys is a property of the random alloy and not due to metallurgical clustering. The structure of the doublet is distorted by cold work.

Thomas, A. M., **Further study of vacuum vane gauge criteria: Effects of port-vane geometry,** *J. Vacuum Sci. Technol.* **7,** *No. 4, 501–503 (July-August 1970).*

Key words: Monte Carlo method; port-vane geometry; vacuum vane gauge.

The force on a movable vane which covers the exit of a tube is related to the pressure at the tube entrance. This principle can be utilized in the construction of a "vane" gauge. The Monte Carlo method has previously been used to determine the correlation between the force on the vane and the pressure at the tube inlet. An extension of that work to a more complex and realistic geometry, which includes an elbow and a conical section, is presented here. This geometry represents the port structure of a gauge presently under construction in our laboratory. Details of the molecular motion, such as density and flux distributions throughout the system, were calculated. Under certain conditions, the geometry upstream of the port was shown to have negligible effect on the force imparted to the vane and a calibration curve is presented relating this force to the vane-to-port distance over a limited range.

Ugiansky, G. M., Skolnick, L. P., Stiefel, S. W., **Directional effects in the stress corrosion cracking of an aluminum alloy,** *Corrosion* **25,** *No. 2, 77–86 (February 1969).*

Key words: Aluminum alloy; corrosion; directional effects; grain morphology; preferred orientation; stress corrosion.

Studies of the relative effects of grain morphology and preferred orientation on the directional susceptibility to intergranular stress corrosion cracking of a 7075–T651 aluminum alloy plate have been conducted. The role of grain morphology was found to be of paramount importance in controlling crack propagation. It was found that a slow rate of propagation along grain boundaries parallel to the applied stress, and the fact that the intergranular crack must propagate primarily in this direction accounts for the low susceptibility of longitudinally stressed specimens. The results suggest that the threshold stress for short transverse specimens approximates the low stress necessary to crack grain boundaries normal to the applied stress, and the threshold stress for longitudinal specimens approximates the high stress needed to propagate cracks along boundaries parallel to the applied stress. Preferred orientation was found to be of secondary importance when compared to the effect of grain morphology. A high degree of preferred orientation, rather than any specific slip plane orientation, was found to increase the suceptibility of specimens with the same grain morphology. Pitting corrosion was found to occur to a much greater extent on unstressed than on stressed (undergoing stress corrosion cracking) specimens. This phenomenon is explained by what is termed an "internal cathodic protection mechanism."

Wall, L. A., Flynn, J. H., Strauss, S., **Rates of molecular vaporization of linear alkanes,** *J. Phys. Chem.* **74,** *17, 3237–3242 (1970).*

Key words: Alkanes; heats; *n*-hexatricontane; *n*-pristane; *n*-tetracosane; *n*-tetranonacontane; and vaporization.

The rates of molecular vaporization of four linear alkanes, *n*-pristane ($C_{19}$), *n*-tetracosane ($C_{24}$), *n*-hexatricontane ($C_{36}$), and *n*-tetranonacontane ($C_{94}$) was measured. By both isothermal and nonisothermal methods, the kinetics of the vaporization process showed essentially zero order behavior as a vaporization process proportional to the surface area should. The Arrhenius slope plus 3 RT/2 was compared to heats of vaporization of other *n*-alkanes in the literature. The old and new data show that the heat of vaporization is proportional to the two-thirds power of the number, *n*, of carbon atoms in the species and not to the first power. The majority of the known heats of vaporization were well fitted by the equation.

$$\Delta H_v = 13.43\, n^{2/3} - 0.08075\, T + /2.92, \text{KJ/mol}$$

The tetranonacontane vaporized without detection of hydrocarbon decomposition products by mass spectral monitoring. The results suggests a much higher limit to the size of species capable of molecular vaporization without decomposition, than previously assumed.

Wasik, S. P., Tsang, W., **Determination of trace amounts of contaminants in water by isotope dilution gas chromatography,** *Anal, Chem.* **42,** *No. 13, 1649–1651 (1970).*

Key words: gas chromatography; isotope dilution; olefins; and water analysis.

An isotope dilution technique using gas liquid chromatography is proposed for the quantitative analysis of trace organic pollutants in water supplies. The method was demonstrated using benzene with perdeuterated benzene as the isotope with both substances in the p.p. B. concentration range. Columns with aqueous silver nitrate as the stationary phase were used to determine the ratio of the concentration of benzene to perdeuterated benezene.

Wasik, S. P., Tsang, W., **Gas-liquid chromatography separations of hydrocarbons using columns with aqueous solutions of complexing metal ions as stationary phases,** *Anal Chem.* **42,** *No. 13, 1648–1649 (November 1970).*

Key words: Aliphatics; aromatics; complexing effects; gas chromatography; group separation; mercuric nitrate; olefins; silver nitrate; surface effect.

Interesting hydrocarbon selectivity was obtained in gas-liquid chromatography using aqueous solutions of $Ag^+$ and $Hg^{++}$ ions as the stationary phases. This was achieved by taking advantage of the complexing properties of these ions and the large surface effect of the solution. Columns may be designed to be specific for certain hydrocarbon groups using this technique.

Waxman, M., Hastings, J. R., Chen, W. T., **Nonlinear statistical analysis of Burnett PVT data,** *Proc. 5th Symp. Thermophysical Properties, Boston, Massachusetts, September 30-October 2, 1970, C. F. Bonilla, Ed., pp. 248–261 (American Society of Mechanical Engineers, New York, N. Y., 1970).*

Key words: Burnett; gas; model dependency; nonlinear; PVT; statistical.

The Burnett method, which requires only temperature and isothermal pressure measurements made before and after stepwise expansions between two volumes, is being used extensively for determining gas compressibilities and density or pressure virial coefficients. The measurements are simple, but the data reduction involves rather formidable nonlinear statistical analysis of relationships containing the compressibility factor, defined as a density or a pressure virial expansion, and optional constants. In this paper we compare the results of analyzing different Burnett relationships with independent parameters and no restrictions on the data, using two nonlinear statistical methods, due to Gauss and to Deming, and argon data at 25°C for pressures up to 250 atm. We discuss the computational difficulties and present background information on the experimental and analytical methods.

Weidman, M. P., Campbell, E., **A method for designing multiscrew waveguide tuners,** *Nat. Bur. Stand. (U.S.), Tech. Note 393, 20 pages (Oct. 1970) 30 cents, SD Catalog No. C13.46:393.*

Key words: Capacitive screw tuner; impedance transformer; waveguide tuner.

Capacitive screw, waveguide tuners are commonly used in microwave measurement systems and as devices for adjusting the impedance of various waveguide terminations. The design of a broadband tuner of this type has been a problem in the past.

This paper describes a method for designing tuners which will work effectively for relatively wide ranges of frequencies.

West, E. D., Churney, K. L., **Theory of isoperibol calorimetry for laser power and energy measurements,** *J. Appl. Phys.* **41,** *No. 6, 2705–2712 (May 1970).*

Key words: Calorimetry; laser calorimetry; lasers; thermadynamics.

Laser power and energy measurements are commonly made in calorimeters operating in a constant-temperature environment. These calorimeters are analyzed in terms of the first law of thermodynamics and the boundary value problem describing heat flow in the calorimeter. This theory of the measurement suggests design features of the calorimeter, sources of error to be avoided in design and operation, and tests to demonstrate experimentally the adequacy of the design. The analysis shows how time-temperature data can be used to allow for the temperature gradient on the calorimeter and the heat exchange due to transients in the temperature.

Wexler, A., **Measurement of humidity in the free atmosphere near surface of the earth,** *(Proc. American Meteorological Society Symp. on Meteorological Observations and Instrumentations, Washington, D. C., February 10–14, 1969) Meteorological Monographs 11, No. 33, 262–282 (October 1970).*

Key words: Dew point; hygrometry; meteorology; measurement in gases; psychrometry.

This paper is a survey of the state-of-the-art in hygrometry as applied to humidity measurement in gases near atmospheric pressure. Although not indicated specifically, many of the methods discussed are applicable to humidity measurements in gases at pressures higher or lower than atmospheric. Hygrometric methods, techniques and instruments are divided arbitrarily into the following six classes: (1) methods dependent upon the total removal of water vapor from a moist gas, (2) methods dependent upon the

addition of water vapor to produce a saturated gas, (3) methods dependent upon the reversible sorption of water vapor by a sensor, (4) methods dependent upon the measurement of a physical property of a gas, (5) condensation methods, that is, methods dependent upon the liquid-vapor or the solid-vapor equilibrium state of the water substance, and (6) methods dependent upon chemical reactions and procedures. The methods of each class are further subdivided by principles of operation and are examined to assess such characteristics as range, accuracy, sensitivity, speed of response, effect of environmental conditions, and limitations in behavior and utility.

White, H., Editor, **Vocabulary for Information Processing,** *Nat. Bur. Stand. (U.S.), Fed. Info. Process. Stand Publ. (FIPS Pub.) 11, 4 pages (1970) 15 cents, SD Catalog No. C13.52:11.*

Key words: Computers; data processing; definitions, Federal Information Processing Standards Publication; information processing; terms; vocabulary.

This publication provides an alphabetic listing of approximately 1200 entries, each consisting of a term and its definition, for use in information processing activities such as the description, representation, communication, interpretation, and processing of data by human or automatic means.

Multiple-word terms are listed in their natural order; terms with identical last words appear as "See references" under the common word. Other reference symbols indicate synonyms, preferred terms, contrasting meanings, and unabbreviated forms for defined terms which are acronyms or abbreviations.

Wiederhorn, S. M., Bolz, L. H., **Stress corrosion and static fatigue of glass,** *J. Am. Ceram. Soc.* **53,** *No. 10, 543–548 (October 1970).*

Key words: Crack propagation; fracture; glass; static fatigue; stress corrosion.

Stress corrosion cracking of six glasses was studied using fracture mechanics techniques. Crack velocities in water were measured as a function of applied stress intensity factor and temperature. Apparent activation energies for crack motion were obtained. Data were consistent with the universal fatigue curve for static fatigue of glass and it was found that the universal fatigue curves depended on glass composition. Of the glass compositions tested, silica glass exhibited most resistance to static fatigue followed by aluminosilicate and borosilicate glass. Sodium was found to be detrimental to stress corrosion resistance. The crack velocity data could be explained by the Charles and Hillig theory of stress corrosion and it is probable that stress corrosion of glass is normally caused and controlled by a chemical reaction between the glass and water.

Wiederhorn, S. M., Townsend, P. R., **Crack healing in glass,** *J. Am. Ceram. Soc.* **53,** *No. 9, 486–489 (September 1970).*

Key words: Crack healing; fracture; glass; strength; surface.

This paper discusses strength recovery in glass containing cracks that were observed to close spontaneously. Measurements of bonding across the surfaces of closed cracks were made on soda-lime glass, using fracture mechanics techniques. Approximately 80 percent strength recovery was observed on cracks formed by mechanical shock, while approximately 20 percent strength recovery was observed on cracks that closed after being held open to the atmosphere for several minutes. The high strength recovery during closure of cracks formed by mechanical shock is attributed to the very active nature of the surface formed during fracture. Reaction with air or dry nitrogen is believed to reduce the activity of the fracture surfaces because of oxygen and water adsorption.

Wilson, W. K., Fletcher, D. G., **Paper research at the National Bureau of Standards,** *Indian Pulp Paper* **24,** *No. 7, 325–329 (January 1970).*

Key words: Appearance properties; paper research; preservation of records; tear reference; testing program.

A brief history of paper research at the National Bureau of Standards is followed by a description of the current program. Work is in progress on the preservation of records, currency paper, and optical properties of paper. A collaborative testing program enables participating laboratories to compare their test results with the results obtained in other laboratories. A tear reference standard also has been maintained for several years. Several staff members participate in a number of committees in the Technical Association of the Pulp and Paper Industry, American Society for Testing and Materials, USA Standards Institute and International Organization for Standardization.

Yakowitz, H., **Some uses of color in metallography,** *Am. Soc. Testing Mater., Spec. Publ.* **480,** *pp. 49–66 (1970).*

Key words: Color photography; electron microscopy; electron probe microanalysis; metallography; microscopy; polarized light.

The application of various methods for using color in metallography is outlined. The methods include plane and circularly polarized light, color etching and color separation photography. Instruments used to obtain subjects for the color metallography examples shown in this paper include the optical microscope, the electron probe microanalyzer, the scanning electron microscope and the transmission electron microscope. A brief discussion of color films is given. The technique used to obtain color photographs is given in detail for each aspect of color metallography discussed.

Yokel, F. Y., Somes, N. F., **Proposed revision of ACI 318–63 Building Code Requirements for Reinforced Concrete,** *J. Am. Concrete Inst.* **67,** *No. 9, 723–725 (September 1970).*

Key words: Axial load (force); bending moment; building codes; end-fixity; reinforced concrete; slenderness; strength; structural analysis; walls.

This contribution discusses Chapters 10 and 14 of the Proposed Revision of ACI 318–63 Building Code Requirements for Reinforced Concrete Reported by ACI Committee 318 in the Journal of the American Concrete Institute, February 1970. It points out some inconsistencies in the respective ways in which these two Chapters cover bearing walls. Some changes are recommended which, if adopted, would extend the coverage of Chapter 10 to include those walls covered only by Chapter 14.

Young, J. P., Lamb, V. A., Reid, G. I., Berkeley, J. F., Ng, W., **Electroplated coatings on maraging steel for retarding catalytic decomposition of hydrazine rocket fuel,** *Plating* **57,** *No. 9, 921–926 (September 1970).*

Key words: Compatibility tests; electrolytic protection; hydrazine; maraging steel; metallic coatings; missiles; rocket-fuel tanks.

Hydrazine and methyl hydrazine are catalytically decomposed in contact with certain metals, e.g., Maraging steel, yielding gaseous decomposition products. As a result, dangerous pressure develops during prolonged storage of rockets that employ hydrazine-type fuels contained in Maraging steel tanks. The tanks therefore require a coating on their internal surfaces that will not be corroded by hydrazine nor cause it to decompose.

The work reported is a general survey of a variety of materials, most of them applied as plated coatings, to determine their suitability for this application. Cadmium and electroless nickel are the most practicable of a number of materials that were found to have low catalytic effect and that were not significantly corroded.

Younglove, B. A., Straty, G. C., **A capacitor for accurate wide range dielectric constant measurements on compressed fluids,** *Rev. Sci. Instr.* **41,** *No. 7, 1087–1089 (July 1970).*

Key words: Capacitance; dielectric constant; stable capacitance; temperature variation of capacitance.

A capacitor is described which has been used to make accurate measurements of the dielectric constant of liquid and gaseous oxygen over a wide temperature (55 to 300 K) and pressure (0.2 to 34 $MN/m^2$) range. The capacitor is simple to construct and

its stability is unaffected by large hydrostatic pressure variations. The temperature variation of the vacuum capacitance is small and remains reproducible even after repeated temperature and pressure cycling.

Zimmerman, J. E., **Low cost sensors with millikelvin temperatures and other virtues (Summary),** *Proc. Conf. Precision Electromagnetic Measurements, National Bureau of Standards, Boulder, Colorado, June 2–5, 1970, CPEM Digest, p. 1 (1970).*

Key words: Josephson effect; magnetometry; superconducting devices.

This paper is a 280-word summary of a talk to be given at the Conference on Precision Electrical Measurements. It summarizes the simple theory of the superconducting quantum devices known as weak links or Josephson junctions, and reviews some applications to magnetometry, high-frequency radiation sensing, and dc and rf current and voltage standards. The inherent low-noise, absolute calibration, versatility, and low-cost of the devices are emphasized.

## Other NBS Publications

### J. Res. Nat. Bur. Stand. (U. S.), 74B (Math. and Sci.), No. 4 (October-December 1970), SD Catalog No. C13.22/sec.B:74/4, $1.25

A property of the triangle groups. Joseph Lehner.
Some theorems on tensor composite graphs.
M. F. Capobianco.
The diophantine approximation of roots of positive integers.
C. F. Osgood.
The minimum number of problems to cover all subproblems.
H. J. Greenberg.
Error estimates for the solution of linear algebraic systems.
Brother K. E. Fitzgerald, F. S. C.
On the singular values of a product matrices.
W. Watkins
Contractifiable semigroups. P. R. Meyers.

Acquista, N., Abramowitz, S., Structure of the alkali hydroxides. V. The infrared spectra of matrix-isolated RbOH, RbOD, NaOH, and NaOD, J. Chem. Phys. **51,** No. 7, 2911–2914 (October 1, 1969).

Acquista, N., Schoen, L. J., Matrix isolation spectrum of the SH radical, J. Chem. Phys. **53,** No. 3, 1290–1291 (August 1, 1970).

Ausloos, P., Ion-molecule reactions and photoionization of hydrocarbons, Chapter in Progress in Reaction Kinetics, G. Porter, Ed., 5, 113–179 (March-April 1970).

Ausloos, P., Lias, S. G., Carbonium ions in radiation chemistry. Reactions of t-butyl ions with hydrocarbons, J. Am. Chem. Soc. **92,** No. 17, 5037–5045 (August 26, 1970).

Bates, R. D., Jr., Flynn, G. W., Ronn, A. M., Laser-induced vibrational fluorescence in nitrous oxide, J. Chem. Phys. **49,** No. 3, 1432–1433 (1968).

Bates, R. G., Staples, B. R., Robinson, R. A., Ionic hydration and single ion activities in unassociated chlorides at high ionic strengths, Anal. Chem. **42,** No. 8, 867–871 (July 1970).

Bennett, H. S., Two-electron F′ centers in the alkaline-earth oxides and in the alkali halides, Phys. Rev. B. **1,** No. 4, 1702–1715 (February 15, 1970).

Berger, M. J., Seltzer, S. M., Bremsstrahlung and photoneutrons from thick tungsten and tantalum targets, Phys. Rev. C, **2,** No. 2, 621–631 (August 1970).

Bergstrom, J. C., Bretozzi, W., Kowalski, S., Maruyama, X. K., Lightbody, Jr., J. W., Fivozinsky, S. P., Penner, S., Electroexcitation of the low-lying states of $O^{16}$, Phys. Rev. Letters **24,** No. 4, 152–155 (January 26, 1970).

Blandford, J. M., Gurel, L. M., Fibers and fabrics, Nat. Bur. Stand. (U.S.), Consumer Info. Series 1, 31 pages (Nov. 1970) 65 cents, SD Catalog No. C13.53:1.

Blaugher, R. D., Hein, R. E., Cox, J. E., Waterstrat, R. M., Atomic ordering and superconductivity in A–15 compounds, J. Low Temp. Phys. **1,** No. 6, 539–561 (December 1969).

Block, S., Weir, C. E., Piermarini, G. J., Polymorphism in benzene, napthalene, and anthracene at high pressure, Science **169,** 586–587 (August 7, 1970).

Bowen, R. L., Crystalline dimethacrylate monomers, J. Dental Res. **49,** No. 4, 810–815 (July-August 1970).

Brady, R. F., Jr., Cyclic acetals of ketoses. Part III. Re-investigation of the synthesis of the isomeric Di-*O*-isopropylidene-ß-D-fructopyranoses, Carbohydrate Res. **15,** No. 1, 35–40 (1970).

Brenner, F. C., Tires. Their selection and care, Nat. Bur. Stand. (U.S.), Consumer Info. Series 2, 32 pages (Nov. 1970) 65 cents, SD Catalog No. C13.53:2.

Bridges, J. M., Wiese, W. L., Transition probabilities for the prominent red lines of Ne I, Phys. Rev. A. **2,** No. 2, 285–293 (August 1970).

Brinckman, F. E., Wachtman, J. B., Jr., Editors, Research materials developed under the NBS inorganic materials program, Nat. Bur. Stand. (U.S.), Spec. Publ. 333, 71 pages (September 1970) 70 cents, SD Catalog No. C13.10:333.

Bullis, W. M., Baroody, A. J., Jr., Methods of measurement for semiconductor materials, process control, and devices, Quarterly Report—January 1 to March 31, 1970, Nat. Bur. Stand. (U.S.), Tech. Note 555, 63 pages (Sept. 1970) 65 cents, SD Catalog No. C13.46:555.

Candela, G. A., Spin relaxation process of chromium ion in potassium alum, J. Chem. Phys. **52,** No. 7, 3754–3757 (April 1, 1970).

Carrington, T., Garvin, D., The chemical production of excited states, Chapter 3 in Comprehensive Chemical Kinetics Volume **3.** The Formation and Decay of Excited Species, pp. 107–181 (1969).

Cezairliyan, A., Morse, M. S., Berman, H. A., Improvements in oscilloscopic measurements in high-speed experiments, Nat. Bur. Stand. (U.S.), Tech. Note 539, 20 pages (Oct. 1970) 30 cents, SD Catalog No. C13.46:539.

Christ, B. W., Smith, G. V., Effects of nitrogen in lattice solution on the yielding and flow of zone-refined iron polycrystals between 128° and 300°K, Trans. Met. Soc. AIME **1,** No. 4, 827–833 (April 1970).

Coriell, S. R., Jackson, J. L., Probability distribution of the radius of gyration for two statistical segments, J. Chem. Phys. **53,** No. 8, 3389 (October 15, 1970).

Coxon, B., The conformations of 1,2:4,6-Di-*O*-benzylidene-α-D-glucopyranose derivatives, Carbohydrate Res. **14,** 9–15 (October 1970).

Crissman, J. M., Passaglia, E., Eby, R. K., Colson, J. P., Crystal data on *n*-eicosane ($C_{20}H_{42}$), J. Appl. Cryst. **3,** 193–195 (1970).

Currie, L. A., Radioactivity monitors and accuracy in photonuclear experiments, (Summary), Trans. Am. Nucl. Soc. **13,** No. 1, 59 (1970).

Davis, M. M., Bronsted acid-base behavior in "inert" organic solvents, Chapter 1 in The Chemistry of Nonaqueous Solvents, III, 1–135 (Academic Press Inc., New York, N. Y., 1970).

Dehl, R. E., Collagen: Mobile water content of frozen fibers, Science **170,** 738–739 (November 13, 1970).

Dick, C. E., Lucas, A. C., K-shell fluorescence yields for light elements, Phys. Rev. A, **2,** No. 3, 580–586 (September 1970).

Dickens, B., Brown, W. E., The crystal structure of calcium carbonate hexahydrate at ∽ —120°, Inorg. Chem. **9,** No. 3, 480–486 (March 1970).

Dobbyn, R. C., Williams, M. L., Cuthill, J. R., McAlister, A. J., Occupied band structure of Cu: Soft-x-ray spectrum and comparison with other deep-band-probe studies, Phys. Rev. B. **2,** No. 6, 1563–1575 (September 15, 1970).

Douglas, T. B., New approach for evaluating lattice-configurational thermodynamic properties, J. Chem. Phys. **51,** No. 7, 2831–2839 (October 1, 1969).

Egelstaff, P. A., Cooperative rotation of spherical molecules, J. Chem. Phys. **53,** No. 7, 2590–2598 (October 1970).

Ensign, T. C., Chang, Te-Tse, Kahn, A. H., Hyperfine and nuclear quadrupole interactions in copper-doped $TiO_2$, Phys. Rev. **188,** No. 2, 703–709 (Dec. 10, 1969).

Ensign, T. C., Stokowski, S. E., Shared holes trapped by charge defects in $SrTiO_3$, Phys. Rev. B, **1,** No. 6, 2799–2810 (March 15, 1970).

Estin, A. J., Editor, Precision measurement and calibration. Selected NBS Papers on electricity-radio frequency, Nat. Bur. Stand. (U.S.), Spec. Publ. 300, Vol. 4, 456 pages (June 1970) $5.50, SD Catalog No. C13.10:300/v. 4.

Evans, W., Garvin, D., The evaluator versus the chemical literature, J. Chem. Doc. **10,** No. 3, 147–150 (1970).

Evenson, K. M., Wells, J. S., Radford, H. E., Infrared resonance of OH with the $H_2O$ laser: A galactic maser pump? Phys. Rev. Letters **25,** No. 4, 199–202 (July 27, 1970).

Feldman, A., Brower, W. S., Jr., Horowitz, D., Optical activity and Faraday rotation in bismuth oxide compounds, Appl. Phys. Letters **16,** No. 5, 201–202 (March 1, 1970).

Feldman, A., Kahn, A. H., Landau diamagnetism from the coherent states of an electron in a uniform magnetic field, Phys. Rev. B, **1,** No. 12, 4584–4589 (June 15, 1970).

Florin, R. E., Wall, L. A., Small and large radicals in thin-film polymer depolymerization, Macromolecules **3,** No. 5, 560–566 (September-October 1970).

Franklin, A. D., Marzullo, S., Orientation kinetics of $Gd^{3+}$-$F^-$ interstitial pairs in $CaF_2$, J. Phys. C. Solid State Phys. Letters to Editor **3,** L171–L174 (September 1970).

Frederikse, H. P. R., Comments on electronic transport in transition metal oxides, J. Res. Develop. **14,** No. 3, 295–300 (May 1970).

Freeman, D. H., Goldstein, S., Schmuckler, G., Homogeneous sulfonation of styrene-divinylbenzene copolymers with oleum in organic solvents, Israel J. Chem. **7,** No. 6, 741–749 (1969).

Freeman, D. H., Zielinski, W. L., Jr., Rittner, W. F., Recognition of crosslinking in the infrared spcetra of poly(styrene-divinylbenzene), Proc. Ion Exchange in the Process Industries Conf., Imperial College of Science and Technology, London, England, pp. 27–30 (1970).

Furcolow, W. H., Technical Standards Coordinator, Mosaic-parquet hardwood slat flooring, Nat. Bur. Stand. (U.S.), Prod. Stand. 27–70, 13 pages (Sept. 1970) 25 cents, SD Catalog No. C13.20/2:27–70.

Gibson, B. F., O'Connell, J. S., Angular distribution of the reaction $^1H(d, {}^3He)\gamma$, Physics Letters **32B,** No. 5, 331–332 (August 3, 1970).

Goldstein, J. I., Henderson, E. P., Yakowitz, H., Investigation of lunar metal particles, (Proc. Apollo 11 Lunar Science Conf., January 1970, Houston, Texas), Geochim. Cosmochim. Acta **1,** 499–512 (1970).

Greenberg, L., Newman, M., Some results on solvable groups, Arch. Math. **21,** No. 4, 349–352 (1970).

Groth, H. G., Wellmann, P., Editors, Spectrum formation in stars with steady-state extended atmospheres, Proceedings of the International Astronomical Union Colloquium No. 2, Commission 36, Munich, Germany, April 16–19, 1969, Nat. Bur. Stand. (U.S.), Spec. Publ. 332, 342 pages (August 1970) $1.75, SD Catalog No. C13.10:332.

Hardy, S. C., Coriell, S. R., Morphological stability of ice cylinders in aqueous solution, J. Crystal Growth **7,** No. 2, 147–154 (September-October 1970).

Hastie, J. W., Hauge, R. H., Margrave, J. L., High temperature chemistry: Stabilities and structures of high temperature species, Ann. Rev. Phys. Chem. **21,** 475–498 (1970).

Hayward, E., Photonuclear reactions, Nat. Bur. Stand. (U.S.), Monogr. 118, 46 pages (August 1970) 50 cents, SD Catalog No. C13.44:118.

Hayward, E., Schwartz, R. B., Murray, K. M., Comments on isospin of the $B^{11}$ giant resonance, Phys. Rev. **2,** No. 2, 761–762 (August 1970).

Hirshfeld, A. T., Hoppes, D. D., Transition mixing ratios determined from a study of the electron and gamma-ray distributions from oriented $^{192}Ir$ Phys. Rev. C **2,** No. 6, 2341–2349 (December 1970).

Hiza, M. J., Duncan, A. G., A correlation for the prediction of interaction energy parameters for mixtures of small molecules, AIChE J. **16,** No. 5, 733–738 (September 1970).

Hummer, D. G., Mihalas, D., Model atmospheres for the central stars of planetary nebulae, Monthly Notices Roy. Astron. Soc. **147,** No. 4, 339–354 (1970).

Jacox, M. E., Milligan, D. E., Matrix-isolation study of the vacuum-ultraviolet photolysis of methyl chloride and methylene chloride. Infrared and ultraviolet spectra of the free radicals CCl, $H_2CCl$, and $CCl_2$, J. Chem. Phys. **53,** 7, 2688–2701 (October 1, 1970).

Johannesen, R. B., Ferretti, J. A., Harris, R. K., UEAITR: A new computer program for analysis of NMR spectra analysis of the proton spectrum of triisopropylphosphine, J. Magnetic Resonance **3,** No. 1, 84–93 (July 1970).

Johnson, D. R., Powell, F. X., Microwave detection of thioformaldehyde, Science **169,** 679–680 (August 14, 1970).

Johnson, W. T. K., Chertok, B. T., Dick, C. E., Study of nuclear states of several odd-A nuclei $68 \leq Z \leq 79$ through electromagnetic excitation from 2.3 to 3.6 MeV, Phys. Rev. Letters **25,** No. 9, 599–602 (August 31, 1970).

Joiner, B. L., Laubscher, N. F., Brown, E. S., Levy, B., An author and permuted title index to selected statistical journals, Nat. Bur. Stand. (U.S.), Spec. Publ. 321, 510 pages (Sept. 1970) $5.75, SD Catalog No. C13.10:321.

Jordan, R. H., Stark, M. C., Bunn, C. O., Donaldson, J. L., Obright, W. J., Millie, H. R., Gilsinn, J., Goldman, A. J, Horn, W. A., Systems analysis of inland consolidation centers for marine cargo, Nat. Bur. Stand. (U.S.), Tech. Note 530, 162 pages (Nov. 1970) $1.25, SD Catalog No. C13.46:530.

Klein, R., A field emission study of carbon monoxide on hcp metals rhenium and ruthenium, Surface Sci. **20,** No. 1, 1–17 (March 1970).

Krauss, M., Potential energy surfaces, Ann. Rev. Phys. Chem. **21,** 39–46 (1970).

Krauss, M., Mies, F. H., Molecular-orbital calculation of the shape resonance in $N_2^-$, Phys. Rev. A. **1,** No. 6, 1592–1598 (June 1970).

Lafferty, W. J., Microwave spectrum, dipole moment, and conformation of cyclopentene oxide, J. Mol. Spectry. **36,** No. 1, 84–93 (October 1, 1970).

LaFleur, P. D., Becker, D. A., Editors, Activation analysis section: Summary of activities, July 1969 to June 1970, Nat. Bur. Stand. (U.S.), Tech. Note 548, 64 pages (Dec. 1970) $1.25, SD Catalog No. C13.46:548.

Lamb, V. A., Evidence for a complex chloromolybdate ion in a molten salt medium from transference experiments, J. Electrochem. Soc. **117,** No. 10, 1269–1270 (October 1970).

Lesclaux, R., Searles, S., Sieck, L. W., Ausloos, P., Irradiation of cyclohexene with 8.4, 10.0 and 11.6–11.8 eV photons. Dissociation of neutral excited cyclohexene and reactions of $C_6H_{10}^+$, J. Chem. Phys. **53,** No. 8, 3336–43 (October 15, 1970).

Levin, E. M., Liquid immiscibility in oxide systems, Chapter in Phase Diagrams Materials Science and Technology, Volume 3. The Use of Phase Diagrams in Ceramics, Glass and Metal Technology, pp. 143–236, (Academic Press, Inc., New York, N. Y., 1970).

Levin, E. M., Roth, R. S., The system niobium pentoxide-phosphorus pentoxide, J. Solid State Chem. **2,** No. 2, 250–261 (1970).

Lias, S. G., Collin, G. J., Rebbert, R. E., Ausloos, P., Photolysis of ethane at 11.6–11.8 eV, J. Chem. Phys. **52,** No. 4, 1841–1851 (February 15, 1970).

Lias, S. G., Rebbert, R. E., Ausloos, P., Irradiation of xenon-propane and argon-propane mixtures with gamma rays and 21.2 eV photons, J. Chem. Phys. **52,** No. 2, 773–783 (January 15, 1970).

Lide, D. R., Jr., Editor, Critical evaluation of data in the physical sciences—A status report on the National Standard Reference Data System—June 1970, Nat. Bur. Stand. (U.S.), Tech. Note 553, 77 pages (Sept. 1970) 70 cents, SD Catalog No. C13.46:553.

Maki, A. G., Hexter, R. M., Resonance interactions with $\nu_3$ of $CH_3I$; A method of determining $A_0$, J. Chem. Phys. **53,** No. 1, 453–454 (July 1, 1970).

Mandel, J., Paule, R. C., Interlaboratory evaluation of a material with unequal numbers of replicates, Anal. Chem. **42,** No. 11, 1194–1197 (September 1970).

Mann, D. B., Roder, H. M., Liquefied natural gas as a cryogenic fluid—instrumentation and properties, (Proc. Transmission Conf. American Gas Association Operation Section, New Orleans, La., May 26–27, 1969), pp. T-98-T-106 (American Gas Association, Arlington, Va., 1970).

Mann, W. B., Garfinkel, S. B., Editors, Radioactivity calibration standards, Nat. Bur. Stand. (U.S.), Spec. Publ. 331, 120 pages (August 1970) $1.25, SD Catalog No. C13.10:331.

Marshak, H., Langsford, A., Tamura, T., Wong, C. Y., Total neutron cross section of oriented $^{16n5}Ho$ from 2 to 135 MeV, Phys. Rev. C **2,** No. 5, 1862–1881 (November 1970).

Martin, W. C., Kaufman, V., $4p^2$ configuration in Neutral Zinc (Zn I), J. Opt. Soc. Am. **60,** No. 8, 1096–1099 (August 1970).

Mazur, J., Non-self-intersecting random walks in lattices with nearest-neighbor interactions, Chapter in Stochastic Processes in Chemical Physics, pp. 261–280 (John Wiley & Sons, Inc., New York, N. Y., 1969).

Meijer, P. H. E., The importance of dipole-dipole interactions in ultralow temperature physics, (Proc. 1970 Ultralow Temperature Symp. sponsored by Office of Naval Research and Naval Research Laboratory, April 23–24, 1970), R. A. Hein, D. U. Gubser, E. H. Takken, Ed., NRL Report 7133, pp. 123–128 (April 1970).

Meijer, P. H. E., O'Keeffe, D. J., Low-temperature behavior of a pure dipole-dipole system, Phys. Rev. B, **1,** No. 9, 3786–3800

(May 1, 1970).
Meinke, W. W., Analytical chemistry—a fading discipline? No!, Anal. Chem. **42,** 26A–38A (June 1970).
Menis, O., Shultz, J. I., Editors, Analytical coordination chemistry section: Summary of Activities July 1969–June 1970, Nat. Bur. Stand. (U.S.) Tech. Note 544, 151 pages (Sept. 1970) $1.25, SD Catalog No. C13.46:544.
Meshkov, S., Commentary on meson spectroscopy, Chapter in Experimental Meson Spectroscopy, C. Baltay and A. H. Rosenfeld, Ed., pp. 535–546 (Columbia Univ. Press, New York, N. Y., 1970).
Meshkov, S., Comments on baryon spectroscopy, Proc. Hyperon Resonances Conf., Duke University, Durham, N. C., pp. 471–500 (April 24–25, 1970).
Meshkov, S., How good are symmetry predictions?, Proc. Intern. Conf. on Symmetries and Quark Models, Wayne State University, Detroit, Michigan, June 18–20, 1969, Edited by Ramesh Chand, pp. 199–212 (November 1970).
Milligan, D. E., Jacox, M. E., Infrared spectrum of the ClHl–ion isolated in an argon matrix, J. Chem. Phys. **53,** No. 5, 2034–2040 (September 1, 1970).
Milligan, D. E., Jacox, M. E., Spectra of radicals in Physical Chemistry, 4, Chapter 5, 193–231 (Academic Press Inc., New York, N. Y., 1970).
Moore, C. E., Annual Report, July 1, 1968–June 30, 1969, The National Bureau of Standards, Washington, D. C., Bull. Am. Astron. Soc. **2,** No. 1, 99–100 (1970).
Moore, C. E., Ionization potentials and ionization limits derived from the analyses of optical spectra, Nat. Stand. Ref. Data Ser., Nat. Bur. Stand. (U.S.), 34, 22 pages (Sept. 1970) 75 cents, SD Catalog No. C13.48:34.
Moore-Sitterly, C. E., Fundamental spectroscopic data, IAU Commission 14, August 1967 Meeting, Trans. Intern. Astron. Union **13A,** 229–266 (1967).
Moore-Sitterly, C. E., Rare-earth spectra—the 1966 picture, Proc. First International Conf. Spectroscopy, Bombay, India, January 9–18, 1967, 1, 1–13 (1967).
Moore-Sitterly, C. E., Silicon in the sun, Chapter in Vistas in Astronomy (Commemoration of H. N. Russell) A. Beer, Ed., 12, 307–312 (Pergamon Press Inc., New York, N. Y., 1970).
Nargowalla, S. S., Suddueth, J. E., Rook, H. L., Determination of pulse pileup for nuclear interferences in 14-MeV neutron activation analysis for trace oxygen, (Summary), Trans. Am. Nucl. Soc. **13,** No. 1, 78–79 (1970).
Nimeroff, I., Deuteranopic convergence point, J. Opt. Soc. Am. **60,** No. 7, 966–969 (July 1970).
O'Connell, J. S., Electron scattering sum rule for $^2$H, $^3$H, $^3$He and $^4$He, Physics Letters **32B,** No. 5, 323–325 (August 3, 1970).
Oberholtzer, B. L., Publications of the National Bureau of Standards 1968–1969, Nat. Bur. Stand. (U.S.), Spec. Publ. 305 Suppl. 1, 497 pages (December 1970) $4.50, SD Catalog No. C13.10:305 Suppl.
Okabe, H., Photodissociation of HNCO in the vacuum ultraviolet; Production of NCO $A^2\Sigma$ and NH ($A^3\Pi$, $C^1\Pi$) J. Chem. Phys. **53,** No. 9, 3507–3515 (November 1, 1970).
Parker, H. S., Harding, C. A., Vapor growth of $Al_2O_3$ bicrystals, J. Am. Ceram. Soc. **53,** No. 11, 583–585 (November 11, 1970).
Parker, R. L., Crystal growth mechanisms: Energetics, kinetics, and transport, Solid State Phys. **25,** 151–299 (Academic Press, Inc., New York, N. Y., 1970).
Perel, J., Deslattes, R. D., Extended fine-structure in x-ray absorption spectra of certain perovskites, Phys. Rev. B. **2,** No. 5, 1317–1323 (September 1, 1970).
Perloff, A., The crystal structure of sodium hexamolybdochromate (III) octahydrate, $Na_3$ ($CrMo_6O_{24}H_6$) · $8H_2O$, Inorganic Chem. **9,** No. 10, 2228–2239 (1970).
Phucas, C. B., Technical Standards Coordinator, Glass stopcocks with polytetrafluoroethylene (PTFE) plugs, Nat. Bur. Stand. (U.S.), Voluntary Prod. Stand. 28–70, 10 pages (Sept. 1970) 25 cents, SD Catalog No. C13.20/2:28–70.
Plante, E. R., Paule, R. C., Explanation of the H° vs S° correlation, J. Chem. Phys. **53,** No. 9, 3770–3771 (November 1, 1970).
Plitt, K. F., Adhesives for everyday use, Nat. Bur. Stand. (U.S.), Consumer Info. Series 3, 17 pages (Nov. 1970) 40 cents, SD Catalog No. C13.53:3.
Powell, C. J., Comparison of optical data for sodium and potassium with interband-transition absorption theory, Optics Commun. **2,** No. 2, 87–89 (July 1970).
Powell, C. J., Validity of inelastic-electron-scattering data in determining the metallic or insulating properties of adsorbed atomic layers, Phys. Rev. **B-1,** No. 10, 4191–4192 (May 1970).
Raveche, H. J., Mountain, R. D., Three body correlations in simple dense fluids, J. Chem. Phys. **53,** No. 8, 3101–3107 (October 15, 1970).
Reader, J., Sugar, J., Ionization energies of CE I and Gd I, J. Opt. Soc. Am. Letter to Editor **60,** No. 10, 1421–1422 (October 1970).
Reimann, C. W., Santoro, A., Mighell, A. D., The crystal molecular structure of hexapyrazolenickel(II) nitrate, $Ni(C_3H_4N_2)_6(NO_3)_2$, Acta Cryst. **B26,** Part 5, 521–526 (May 1970).
Robertson, B., Quantum statistical mechanical derivation of generalized hydrodynamic equations, J. Math. Phys. **11,** No. 8, 2482–2488 (August 1970).
Roder, H. M., Diller, D. E., Thermal conductivity of gaseous and liquid hydrogen, J. Chem. Phys. **52,** No. 11, 5928–5949 (June 1, 1970).
Roth, R. S., Waring, J. L., Parker, H. S., Effect of oxide additions on the polymorphism of tantalum pentoxide. IV. The system $Ta_2O_5$-$Ta_2WO_8$, J. Solid State Chem. **2,** 445–461 (1970).
Rush, J. J., Schroeder, L. W., Melveger, A. J., Infrared and Raman spectra of sodium bifluoride: Isotope dilution studies, Chem. Phys. Letters **6,** No. 5, 533–536 (September 1, 1970).
Santone, L. C., Berlin, G., Location of fire stations, Proc. WORC Symp. Systems Analysis for Social Problems, National Bureau of Standards, Gaithersburg, Maryland, May 26–28, 1969, pp. 79–91 (December 3, 1970).
Saylor, C. P., Broken Virtue, Capital Chem. **20,** No. 6, 137–140 (September 1970).
Schooley, J. F., Soulen, R. J., Koonce, C. S., Surface potential barrier in $SrTiO_3$, Solid State Commun. **7,** 1077–1079 (1969).
Searles, S. K., Sieck, L. W., High pressure photoionization mass spectrometry, III. Reactions of $NO^+$ ($X'\ ^1\Sigma^+$) with $C_3$-$C_7$ hydrocarbons at thermal kinetic energies, J. Chem. Phys. **53,** No. 2, 794–797 (July 15, 1970).
Searles, S. K., Sieck, L. W., Ausloos, P., Reactions of $C_2H_6^+$. Formation of the $(C_2H_6)^+_2$ ion, J. Chem. Phys. **53,** No. 2, 849–850 (July 15, 1970).
Shields, W. R., Editor, Analytical mass spectrometry section: Summary of activities July 1969 to June 1970, Nat. Bur. Stand. (U.S.), Tech. Note 546, 120 pages (Nov. 1970) $1.25, SD Catalog No. C13.46:546.
Sieck, L. W., Searles, S. K., Rebbert, R. E., Ausloos, P., Reactivity of the cyclohexane Ion, J. Phys. Chem. **74,** No. 21, 3829–3831 (October 15, 1970).
Simmons, J. H., Macedo, P. B., Viscous relaxation above the liquid-liquid phase transition of some oxide mixtures, J. Chem. Phys. **53,** No. 7, 2914–2922 (October 1, 1970).
Simmons, J. H., Napolitano, A., Macedo, P. B., Supercritical viscosity anomaly in oxide mixtures, J. Chem. Phys. **53,** No. 3, 1165–1170 (August 1, 1970).
Sitterly, C. M., The present state of Atomic Spectra, J. Opt. Pura Aplicada **11,** No. 3, 103–113 (1969).
Sleater, G. A., Freeman, D. H., Rapid desorption of chromium (III) from cation exchanger with hydrogen peroxide solutions, Anal. Chem. **42,** No. 13, 1666–1668 (November 1970).
Staveley, L. A. K., Hard-sphere model applied to the solubility of gases in low-boiling liquids, J. Chem. Phys. **53,** No. 8, 3136–3138 (October 15, 1970).
Stevenson, D. R., Technical Standards Coordinator, Rigid poly (vinyl chloride) (PVC) profile extrusions, Nat. Bur. Stand. (U.S.), Voluntary Prod. Stand. 26–70, 7 pages (Oct. 1970) 10 cents, SD Catalog No. C13.20/2:26–70.
Sugar, J., Configuration $4f^{13}5f$ of doubly ionized ytterbium, J. Opt. Soc. Am. **60,** No. 4, 571–572 (April 1970).
Sugar, J., Spectrum of doubly ionized thulium (Tm III), J. Opt. Soc. Am. **69,** No. 4, 454–466 (April 1970).
Swanson, H. E., McMurdie, H. F., Morris, M. C., Evans, E. H., Standard x-ray diffraction powder patterns, Nat. Bur. Stand. (U.S.), Monogr. 25—Section 8, 171 pages (Sept. 1970) $1.50, SD Catalog No. C13.44:25/sec. 8.
Tsai, D. H., Bullough, R., Prerin, R. C., Molecular dynamical studies of the motion of point defects in a crystalline lattice, Proc. Phys. Soc. (London) C: Solid St. Phys. **3,** 2022–2036 (1970).
Weir, C. E., Block, S., Piermarini, G. J., Compressibility of inorganic azides, J. Chem. Phys. **53,** No. 1, 4265–4269 (December 1970).
Weisman, H. M., Sherwood, G. B., Annotated accession list of data compilations of the office of standard reference data, Nat.

Bur. Stand. (U.S.), Tech. Note 554, 196 pages (Sept. 1970) $1.50, SD Catalog No. C13.46:554.

White, H. J., Jr., Countries, dependencies and areas of special sovereignty, Nat. Bur. Stand. (U.S.), Fed. Info. Process. Stand. Publ. (FIPS Pub) 10, 23 pages (1970) 35 cents, SD Catalog No. C13.52:10.

Wolcott, N. M., Falge, R. L., Jr., Cluster specific heat in $Cu_{0.6}Ni_{0.4}$ Alloy, J. Low Temp. Phys. 2, No. 314, 329–331 (1970).

Younglove, B. A., Measurements of the dielectric constant of saturated liquid oxygen. (Proc. 1969 Cryogenic Engineering Conf., June 16–18, 1969, Univ. of California, Los Angeles, Calif.), Chapter in Advances in Cryogenic Engineering 15, Paper No. C-3, 70–75 (Plenum Press, Inc., New York, N. Y. 1970).

**Publications for which a price is indicated are available by purchase from the Superintendent of Documents, U. S. Government Printing Office, Washington, D. C. 20402 (foreign postage, one-fourth additional). The NBS non-periodical series are also available from the National Technical Information Service (NTIS), Springfield, Va. 22151, which was formerly the Clearinghouse. Reprints from outside journals and the NBS Journal of Research may often be obtained directly from the authors.*

☆U.S. GOVERNMENT PRINTING OFFICE: 1971 O - 428-104

UNITED STATES
GOVERNMENT PRINTING OFFICE
PUBLIC DOCUMENTS DEPARTMENT
WASHINGTON, D. C. 20402

OFFICIAL BUSINESS
PENALTY FOR PRIVATE USE, $300

POSTAGE AND FEES PAID
U.S. GOVERNMENT PRINTING OFFICE

JOURNAL OF RESEARCH of the National Bureau of Standards
C. Engineering and Instrumentation

Vol. 75C, No. 2 April-June 1971

# Contents

Page

Heated air adiabatic saturation psychrometer. Lewis Greenspan. 69

Computation of the temperature distribution in cylindrical high-pressure furnaces. Meyer Waxman and John R. Hastings. 79

Rotating adjustable transmission optical step attenuator. Ared Cezairliyan. 85

An improved method for microwave power calibration, with application to the evaluation of connectors. Glenn F. Engen. 89

Apparatus for impact-fatigue testing. R. E. Schramm, R. L. Durcholz, and R. F. Reed. 95

A program in refractory metal thermocouple research. G. W. Burns and W. S. Hurst. 99

Polarization measurements are related to the corrosion of underground steel piling. W. J. Schwerdtfeger. 107

Publications of the National Bureau of Standards. 123

Library of Congress Catalog Number: 62-3900

For sale by the Superintendent of Documents, U.S. Government Printing Office, Washington, D.C. 20402. (Order by SD Catalog No. C 12.22/sec. C: 75 (2). Price $1.25 (single copy). Subscription price: $5.00 a year; $1.25 additional or foreign mailing.

UNITED STATES GOVERNMENT PRINTING OFFICE, WASHINGTON: 1971